Test and Evaluation of the Piccolo II Autopilot System on a One-Third Scale Yak-54

BY

Rylan Jager

B.A.E. Auburn University, Auburn, Alabama, 2005

Submitted to the graduate degree program in Aerospace Engineering
and the Graduate Faculty of the University of Kansas
in partial fulfillment of the requirements of the degree of
Master's of Science.

_____
David Downing, Chairperson

Committee Members

_____
Richard Colgren

_____
Richard Hale

Date Defended: April 25th, 2008

The Thesis Committee of Rylan Jager certifies that this is the approved version of the following thesis:

Test and Evaluation of the Piccolo II Autopilot System on a One-Third Scale Yak-54

_____
David Downing, Chairperson

Committee Members

_____
Richard Colgren

_____
Richard Hale

Date Approved: April 29th, 2008

Abstract

To gain a better understanding of the dynamics of the great ice sheets the National Science Foundation established the Center for Remote Sensing of Ice Sheets (CReSIS) to develop technologies that would improve data gathering of said ice sheets. CReSIS was tasked with the development of an unmanned aerial vehicle, named the Meridian, which would have the ability to make use of advanced radar systems that could be used to gather data on the ice sheets of remote Polar Regions. CReSIS decided to use commercial-off-the-shelf autopilot systems on the Meridian, selecting the Cloud Cap Technologies Piccolo II UAV autopilot system as the initial system to be tested and evaluated.

A process for test and evaluation of modeling, simulation and control systems is presented. Three dynamic models for a one-third scale Yak-54 are developed. A deliberate and methodical flight test program is developed to evaluate the Piccolo II flight control system. Parameter identification flight tests are performed to evaluate the three modeling and simulation techniques. Closed loop flight testing is performed to evaluate the flight control system's ability to control an aircraft and the ability of the gains to be performance optimized. Finally flaws are found in the communication system architecture of the Piccolo II autopilot system which causes the system to go pilot-in-loop unstable and to be rejected from further consideration by the CReSIS team.

Acknowledgements

First I would like to thank Dr. Shah Keshmiri for giving me the inspiration to stick through all the rough times. Your support cannot be overstated. Thanks to Edmond Leong for being my partner through this project and teaching me a little bit about Chinese culture along the way.

Thanks to Dr. Dave Downing for giving some sage advice to a sometimes rash young engineer. Thanks to Dr. Richard Hale for believing we could pull off such a crazy feat like building our own airplane. Thanks to Dr. Richard Colgren for lending your years of experience in industry to young minds like I. Thanks to Dr. Ron Barrett for getting me to come out to a wonderful school like the University of Kansas.

Thanks to Lance Holly for helping us on all our questions about flying model airplanes. Thanks to Andy Pritchard for putting up with a bunch of know-it-all engineers, showing us how to use a wrench and brightening all of our days out at the airport.

Finally thanks to all my friends in the aerospace engineering community, this job is too hard to do without your camaraderie to make it all worth it.

Table of Contents

Abstract ii
Acknowledgements iii
Table of Contents iv
List of Figures vii
List of Tables x
List of Symbols xii
1 Introduction 1
2 Modeling, Simulation and Autopilot Test and Evaluation Process 7
2.1 Step 1: Select System 7
2.2 Step 2: Select Flight Test Platform 8
2.3 Step 3: Develop First Principles Aircraft Dynamic Models 9
2.4 Step 4: Integrate Dynamic Model into Simulation Platform 11
2.5 Step 5: Refine Dynamic Models using Flight Test Data 11
2.6 Step 6: Tune Flight Control System in Simulation 13
2.7 Step 7: Flight Test Tuned Control System 13
2.8 Step 8: Evaluate the Performance of the Control System and Reject or Certify 14
3 The Cloud Cap Piccolo II Autopilot System 15
3.1 Piccolo II Avionics Hardware 16
3.1.1 Gyros and Accelerometers 17
3.1.2 GPS 18
3.1.3 Pressure System 18
3.1.4 Kalman Filter 18
3.2 Communication System 18
3.3 Ground Station 19
3.3.1 Main Ground Station Electronics 19
3.3.2 Operator Interface PC 20
3.3.3 Futaba Console 21
3.4 Operator Interface 22
3.5 Piccolo II Flight Control Laws 24
3.6 Piccolo II Guidance and Navigation System 26
3.7 Piccolo II Modeling and Simulation Environment 26
3.7.1 Standard Cloud Cap Simulator 27
3.7.2 Athena Vortex Lattice Based Simulator 29
3.8 Hardware-in-Loop Simulation 30
4 Flight Test Platform 33
4.1 Yak-54 Geometry 34
4.2 Yak-54 Mass Properties 35
4.3 Yak-54 Engine and Propeller 35
4.3.1 Engine Calibration 36
4.4 Yak-54 Servos 36

4.5 Piccolo II Installation 37
4.6 Antennas 37
4.7 Batteries 37
4.8 Engine Kill Switch 38
5 Yak-54 Dynamic Model Development 39
5.1 Advance Aircraft Analysis Based Model 39
5.1.1 Lateral State Space Model and Analysis 40
5.1.2 Longitudinal State Space Model and Analysis 41
5.2 Athena Vortex Lattice Based Model 42
5.2.1 AVL Generated Stability Derivatives: Longitudinal 43
5.2.2 AVL Generated Stability Derivatives: Lateral-Directional 50
5.3 AVL-Piccolo Hardware-in-Loop Simulation and Dynamic Analysis 55
5.3.1 Modified Transient Peak Ratio Method 55
5.3.2 Maximum Slope Method 57
5.3.3 Open Loop Modal Analysis: Phugoid Mode 58
5.3.4 Open Loop Modal Analysis: Short Period Mode 59
5.3.5 Open Loop Modal Analysis: Dutch Roll Mode 60
5.4 Standard Cloud Cap Aircraft Modeling and Simulation 61
5.5 Simulation Model Dynamics Comparison 62
6 Flight Test Planning and Preparation 64
6.1 Preflight Checkout 64
6.2 Flight Test Team 65
6.2.1 Flight Test Engineer (FTE)/Command and Control Engineer 65
6.2.2 Flight Test Pilot in Command (PIC) 66
6.2.3 Vehicle Engineer (VE) 66
6.2.4 Safety Officer (SO) 66
6.2.5 Data Processing Engineer (DPE) 67
6.2.6 Pilot Assistant (PA) 67
6.2.7 Video Operator (VO) 67
6.2.8 Flight Test Organizational and Communications Flow Charts 68
6.3 Emergency Procedures 69
6.4 Flight Test Area 70
7 Manual Control Flight Test 71
7.1 Manual Control Tests Results 72
8 Parameter Identification Flight Testing 75
8.1 Dutch Roll Mode Flight Test 75
8.1.1 Dutch Roll Mode Flight Test Results 76
8.2 Short Period Mode Flight Test 78
8.2.1 Short Period Mode Flight Test Results 78
8.2.2 Short Period Data Processing Using the Time-Ratio Method 80
8.3 Phugoid Mode Flight Test 82
8.4 Flight Test vs. Simulation Model Dynamics 83
8.5 Open-Loop Flight Test Conclusions and Recommendations 87
9 Closed-Loop Piccolo II Flight Control System Tuning Using Simulation 89

9.1 Closed-Loop Gain Tuning Using AVL Hardware-in-Loop Simulation 89
9.2 Lateral-Directional Response with Default Gains 91
9.3 Longitudinal Command Performance with Default Gains 95
9.4 Lateral Gain Tuning Using AVL-Piccolo HIL Simulation..... 97
9.5 Longitudinal Gain Tuning Using AVL-Piccolo HIL Simulation 101
9.6 Closed Loop Gain Margins..... 105
9.7 Closed Loop Phase Margins 106
10 Closed Loop Piccolo II Gain Tuning in Flight Test 108
10.1 Bank Angle Control Flight Test..... 108
10.2 Heading Angle Control Flight Test..... 112
10.3 Tuned Gains for the Lateral-Directional Control System..... 115
10.4 Airspeed Control Flight Test 115
10.5 Piccolo II Closed Loop Flight Test Conclusions 119
11 Yak-54 Flight Incident and Investigation 121
11.1 First Flight..... 121
11.2 Second Flight 122
11.3 Third Flight..... 123
11.4 Accident Investigation 126
11.5 Communication System Laboratory Test 130
11.6 Effect of Discrete Drop of Pilot Commands on Handling Qualities 137
11.7 Incident Investigation Conclusions..... 139
12 Conclusions, Recommendations and Future Work..... 140
12.1 Piccolo II Flight Control System Test and Evaluation Conclusions..... 140
12.2 Piccolo II Flight Control System Test and Evaluation Recommendations141
12.3 Future Work..... 142
13 References..... 143
Appendix A: SCCS Yak-54 Model (ASCII Format)..... 147
Appendix B: SCCS Wing File (ASCII Format) 153
Appendix C: SCCS Horizontal Tail File (ASCII Format)..... 154
Appendix D: SCCS Vertical Tail File (ASCII Format)..... 155
Appendix E: SCCS Engine File (ASCII Format) 156
Appendix F: SCCS Propeller File (ASCII Format) 157
Appendix G: AVL Input Geometry File (ASCII Format) 161
Appendix H: AVL Simulator File (ASCII Format)..... 166
Appendix I: AVL Modal Data Reduction..... 169
Appendix J: Yak-54/Piccolo Ground Testing Procedures..... 170
Appendix K: Yak-54/Piccolo Pre-Flight Checklist 172
Appendix L: Handling Qualities Flight Test Dance Card 175
Appendix M: Open Loop Dynamics Flight Test Dance Card 176
Appendix N: Dutch Roll Flight Test Data Reduction..... 178
Appendix O: Bank Angle Control Flight Test Dance Card..... 179
Appendix P: Heading Angle Control Flight Test Dance Card 181
Appendix Q: Airspeed Control Flight Test Dance Card..... 183
Appendix R: Longitudinal Gain Change Log Sheet..... 185

List of Figures

Figure 1: Meridian Three View 6
Figure 2: Modeling, Simulation and Autopilot Test and Evaluation Process 8
Figure 3: Aircraft Dynamic Model Development Flow Chart 9
Figure 4: Flight Control Tuning Flow Chart 10
Figure 5: Piccolo II System Block Diagram 16
Figure 6: Cloud Cap Piccolo II Autopilot [26] 16
Figure 7: Piccolo Hardware Block Diagram [26] 17
Figure 8: Ground Station Unit Front Panel [26] 20
Figure 9: Ground Station Unit Back Panel [26] 20
Figure 10: Itronix GOBook II [27] 21
Figure 11: Futaba Pilot Console [26] 22
Figure 12: Operator Interface Telemetry Page [26] 23
Figure 13: Piccolo Navigation Screen [26] 24
Figure 14: Aerosonde AVL Model [30] 30
Figure 15: Hardware-in-Loop Simulation [29] 31
Figure 16: Flight Gear Visualization [29] 32
Figure 17: Aero-Works 75cc Yak-54 [31] 33
Figure 18: 3W-80 XI CS Engine [34] 35
Figure 19: Normalized Thrust and RPM Curves for Engine Calibration 36
Figure 20: Engine Kill Switch Schematic [35] 38
Figure 21: Yak-54 AVL Model 43
Figure 22: Modified Transient Peak Ratio [14] 55
Figure 23: Transient Peak Ratio vs. Damping Ratio [14] 56
Figure 24: Maximum Slope Method [14] 57
Figure 25: Maximum Slope Method for Determining ζ and ω_n [14] 58
Figure 26: AVL-Piccolo HIL Phugoid Simulation Response 59
Figure 27: AVL-Piccolo HIL Short Period Simulation Response 60
Figure 28: AVL-Piccolo HIL Dutch Roll Mode Simulation Response 61
Figure 29: Flight Test Organizational Chart 68
Figure 30: Flight Test Communication Flow Chart 69
Figure 31: Foley Airfield and Flight Test Area 70
Figure 32: Race Track Pattern 72
Figure 33: Pilot-in-loop Pitch Instability 73
Figure 34: Stabilized Pilot-in-Loop Pitch Control 74
Figure 35: Flight Test Dutch Roll Excitation #1 [33] 76
Figure 36: Flight Test Dutch Roll Excitation #2 [33] 77
Figure 37: Flight Test Dutch Roll Excitation #3 [33] 77
Figure 38: Flight Test Short Period Excitation #1 [33] 79
Figure 39: Flight Test Short Period Excitation #2 [33] 79
Figure 40: Flight Test Short Period Excitation #3 [33] 80
Figure 41: Time-Ratio Method [14] 80

Figure 42: Time-Ratio Method Data Reduction Plot [14] 81
Figure 43: Flight Test Excitation of the Phugoid Mode #1 [33] 82
Figure 44: Flight Test Excitation of the Phugoid Mode #2 [33] 83
Figure 45: AAA Yak-54 Phugoid Simulation 85
Figure 46: AVL-HIL Yak-54 Phugoid Simulation 86
Figure 47: AVL-HIL Bank Angle Response with Default Gains 93
Figure 48: AVL-HIL Heading Angle Response with Default Gains: 94
Figure 49: AVL-HIL Airspeed Response with Default Gains 95
Figure 50: AVL-HIL Altitude Response with Default Gains 96
Figure 51: AVL-HIL Bank Angle Control Response with Simulator Tuned Gains ... 99
Figure 52: AVL-HIL Heading Angle Control Loop Performance with Simulator Tuned Gains 100
Figure 53: AVL-HIL Airspeed Control Response with Simulator Tuned Gains 103
Figure 54: AVL-HIL Altitude Control Response with Simulator Tuned Gains 104
Figure 55: Initial Bank Angle Control Flight Test with AVL-HIL Tuned Gains 110
Figure 56: 20 Degree Bank Angle Command Flight Test with Simulator Tuned Gains 110
Figure 57: Final Roll Control Flight Test with Tuned Gains 111
Figure 58: Initial Heading Command Flight Test with Simulator Tuned Gains 113
Figure 59: Final Heading Angle Command Flight Test with Tuned Gains 114
Figure 60: Initial Airspeed Regulator Flight Test with Simulator Tuned Gains 116
Figure 61: Second Airspeed Command Flight Test Response with Simulator Tuned Gains 117
Figure 62: Final Airspeed Command Flight Test Response with Tuned Gains 118
Figure 63: RSSI Levels during First Flight Pilot Control Loss 121
Figure 64: RSSI during First Flight Test 122
Figure 65: RSSI during Second Flight Test Pilot Control Loss 123
Figure 66: RSSI during Second Flight Test 123
Figure 67: RSSI during Third Flight Pilot Control Loss 124
Figure 68: RSSI during Crash 125
Figure 69: Engine Data during Crash 125
Figure 70: RSSI and Time between Packets during Ground Testing 127
Figure 71: RSSI during Uncommanded Autopilot Activation 128
Figure 72: RSSI Signal Strength Levels and Percentage of Data Lost 128
Figure 73: Data Loss Magnitudes 129
Figure 74: Data Dropout Rates during All Flight Tests 130
Figure 75: RSSI Signal Strength and Percentage of Data Loss during Laboratory Test 131
Figure 76: RSSI and Packet Time at Autopilot Activation during Lab Test 132
Figure 77: RSSI Signal Strength and Percentage of Data Loss during Autopilot ON Lab Test 133
Figure 78: RSSI Levels and Data Dropouts during Various Lab Tests 134
Figure 79: Autopilot Activation during Laboratory Test 134
Figure 80: Dropout Rates for Laboratory Tests 135

Figure 81: Autopilot Activation during Flight and Lab Test Activities 135
Figure 82: RSSI and Data Dropout Times during 900 MHz Lab Tests..... 136
Figure 83: Poor Pilot-in-loop Pitch Stability Due to Time-Lag and Data Drop..... 137

List of Tables

Table 1: Piccolo Gain Scaling Parameters 25
Table 2: 75cc Yak-54 Lifting Surfaces [33] 34
Table 3: Vehicle Mass Properties [33] 35
Table 4: Trim Conditions [33] 39
Table 5: Yak-54 Stability Derivatives Generated Using AAA 40
Table 6: AAA Steady State Coefficients 40
Table 7: AAA Yak-54 Lateral Modal Analysis [33] 41
Table 8: AAA Yak-54 Longitudinal Modal Analysis [33] 42
Table 9: AAA vs. AVL Longitudinal Stability Derivatives 43
Table 10: AVL Steady State Coefficients 44
Table 11: AAA vs. AVL Longitudinal Gain Scaling Terms 44
Table 12: AAA vs. AVL Lateral-Directional Derivatives 51
Table 13: AAA vs. AVL Lateral-Directional Gain Scaling Terms 52
Table 14: AVL Generated Lateral-Directional Dimensional Stability Derivatives 53
Table 15: AVL Yak-54 Modal Analysis 54
Table 16: SCCS Modal Analysis [33] 62
Table 17: Simulator Model Modal Comparison 62
Table 18: Dutch Roll Flight Test Results 78
Table 19: Short Period Mode Flight Test Results 81
Table 20: Flight Test vs. Simulation Model Dynamics 84
Table 21: Yak-54/Piccolo Gain Scaling Terms 90
Table 22: Piccolo Default Lateral-Directional Gains 91
Table 23: Piccolo Default Longitudinal Gains 91
Table 24: Bank Angle Control Loop Performance with Default Gains 93
Table 25: Heading Angle Control Loop Performance with Default Gains 94
Table 26: Airspeed Control Loop Performance with Default Gains 95
Table 27: Altitude Control Loop Performance with Default Gains 96
Table 28: AVL-HIL Tuned Lateral-Directional Gains 98
Table 29: AVL-HIL Bank Angle Control Loop Performance with Simulator Tuned Gains 98
Table 30: Heading Angle Control Loop Performance with AVL-HIL Tuned Gains 100
Table 31: AVL-HIL Tuned Longitudinal Gains 101
Table 32: AVL-HIL Airspeed Control Performance with Simulator Tuned Gains 103
Table 33: AVL-HIL Altitude Control Performance with Simulator Tuned Gains 104
Table 34: Piccolo II AVL-HIL Lateral-Directional Gain Margins 106
Table 35: Piccolo II AVL-HIL Longitudinal Gain Margins 107
Table 36: Roll Control Loop Performance with Simulator Tuned Gains 111
Table 37: Final Roll Control Performance 112
Table 38: Final Heading Angle Control Performance with Tuned Gains 114
Table 39: Final Lateral-Directional Gains 115

Table 40: Second Airspeed Command Flight Test Performance with Simulator Tuned Gains 117
Table 41: Final Airspeed Command Response Performance with Tuned Gains..... 118
Table 42: Final Longitudinal Gains 119

List of Symbols

Symbol	Definition	Units
a	Acceleration	ft/sec^2
AR	Aspect ratio	~
b	Span	ft
c	Chord	ft
$\bar{c}$	Mean geometric chord	ft
C_D	Airplane drag coefficient	~
C_{D_1}	Airplane trim drag coefficient	~
C_{l_β}	Variation of airplane rolling moment coefficient with angle of sideslip	~
$C_{l_{\delta_a}}$	Variation of airplane rolling moment coefficient with aileron deflection angle	1/rad
$C_{l_{\delta_r}}$	Variation of airplane rolling moment coefficient with rudder deflection angle	1/rad
C_{l_p}	Variation of airplane rolling moment coefficient with dimensionless rate of change of roll rate	1/rad
C_{l_r}	Variation of airplane rolling moment coefficient with dimensionless rate of change of yaw rate	1/rad
C_L	Lift coefficient	~

Symbols (cont.)

C_{L_α}	Variation of airplane lift coefficient with angle of attack	1/rad
$C_{L_{\dot{\alpha}}}$	Variation of airplane lift coefficient with dimensionless rate of change of angle of attack	1/rad
$C_{L_{\delta_e}}$	Variation of airplane lift coefficient with elevator deflection angle	1/rad
C_{L_q}	Variation of airplane lift coefficient with dimensionless pitch rate	1/rad
C_{L_u}	Variation of airplane lift coefficient with dimensionless speed	~
C_m	Pitching moment coefficient	~
C_{m_1}	Airplane trim pitching moment coefficient	~
C_{m_α}	Variation of airplane pitching moment coefficient with angle of attack	1/rad
$C_{m_{\dot{\alpha}}}$	Variation of airplane pitching moment coefficient with dimensionless rate of change of angle of attack	1/rad
$C_{m_{\delta_e}}$	Variation of airplane pitching moment coefficient with elevator deflection angle	1/rad
C_{m_T}	Pitching moment due to thrust	~
$C_{m_{T_1}}$	Trim pitching moment due to thrust	~

Symbols (cont.)

C_{m_q}	Variation of airplane pitching moment coefficient with pitch rate	1/rad
C_{m_u}	Variation of airplane pitching moment coefficient with dimensionless speed	~
$C_{m_{T_\alpha}}$	Variation of airplane pitching moment coefficient due to thrust with angle of attack	1/rad
$C_{m_{T_u}}$	Variation of airplane pitching moment coefficient due to thrust with dimensionless speed	1/rad
C_{n_β}	Variation of airplane yawing moment coefficient with angle of sideslip	1/rad
$C_{n_{\delta_a}}$	Variation of airplane yawing moment coefficient with aileron deflection	1/rad
$C_{n_{\delta_r}}$	Variation of airplane yawing moment coefficient with rudder deflection	1/rad
C_{n_p}	Variation of airplane yawing moment coefficient with dimensionless rate of change of roll rate	1/rad
C_{n_r}	Variation of airplane yawing moment coefficient with dimensionless rate of change of yaw rate	1/rad
$C_{n_{T_\beta}}$	Variation of airplane yawing moment coefficient due to thrust with sideslip angle	1/rad
C_P	Power coefficient	~

Symbols (cont.)

C_T	Thrust coefficient	~
$C_{T x_1}$	Trim thrust coefficient in the X-axis direction	~
$C_{T x_u}$	Variation of airplane thrust coefficient in the X-axis direction with dimensionless speed	~
$C_{T \alpha}$	Variation of airplane thrust coefficient in the X-axis direction with angle of attack	1/rad
C_y	Airplane side force coefficient	~
C_{y_β}	Variation of airplane side force coefficient with sideslip angle	1/rad
$C_{y_{\delta_a}}$	Variation of airplane side force coefficient with aileron angle	1/rad
$C_{y_{\delta_r}}$	Variation of airplane side force coefficient with rudder angle	1/rad
C_{y_p}	Variation of airplane side force coefficient with dimensionless rate of change of roll rate	1/rad
C_{y_r}	Variation of airplane side force coefficient with dimensionless rate of change of yaw rate	1/rad
d	Propeller diameter	ft
D	Airplane drag	lbs
e	Error	varies

Symbols (cont.)

h	Altitude	ft
g	Acceleration due to gravity	ft/sec^2
I_{xx} , I_{yy} , I_{zz}	Airplane moments of inertia about XYZ	slug ft^2
J	Propeller advance ratio	~
K	Gain	varies
L	Lift	lbs
L_β	Roll angular acceleration per unit sideslip angle	rad/sec^2/rad
L_p	Roll angular acceleration per unit roll rate	1/sec
L_r	Roll angular acceleration per unit yaw rate	1/sec
L_{δ_a}	Roll angular acceleration per unit aileron angle	rad/sec^2/rad
L_{δ_r}	Roll angular acceleration per unit rudder angle	rad/sec^2/rad
M_α	Pitch angular acceleration per unit angle of attack	1/sec^2
M_{T_α}	Pitch angular acceleration per unit angle of attack due to thrust	1/sec^2
M_u	Pitch angular acceleration per unit change in speed	rad/sec/ft
M_{T_u}	Pitch angular acceleration per unit change in speed due to thrust	rad/sec/ft
$M_{\dot{\alpha}}$	Pitch angular acceleration per unit change of angle of attack rate	1/sec

Symbols (cont.)

n	Propeller RPM	rev/min
n also:	Load factor	~
N_β	Yaw angular acceleration per unit sideslip angle	rad/sec^2/rad
N_{T_β}	Yaw angular acceleration per unit sideslip angle due to thrust	rad/sec^2/rad
N_p	Yaw angular acceleration per unit roll rate	1/sec
N_r	Yaw angular acceleration per unit yaw rate	1/sec
N_{δ_a}	Yaw angular acceleration per unit aileron deflection	rad/sec^2/rad
N_{δ_r}	Yaw angular acceleration per unit rudder angle	rad/sec^2/rad
p, q, r	Perturbed values of P, Q and R	rad/sec
P, Q, R	Airplane angular velocity components about XYZ	rad/sec
P also:	Power	hp
$\bar{q}$	Dynamic pressure	lbs/ft^2
s	Laplace domain variable	rad/sec
S	Area	ft^2
t	Thickness	ft
t also:	Time	sec
t_r	Rise time	sec
t_s	Settling time	sec

Symbols (cont.)

T	Thrust	lbs
T_{lag}	Pilot lag time constant	sec
T_{lead}	Pilot lead time constant	sec
T_n	Pilot neuromuscular time constant	sec
u, v, w	Perturbed values of U, V, and W	ft/sec
U, V, W	Components of V_a along XYZ	ft/sec
V_a	True airspeed	ft/sec
V_g	Ground speed	ft/sec
W	Weight	lbs
x_{ac}	Airplane aerodynamic center location along the X axis	ft
x_{cg}	Airplane center of gravity location along the X axis	ft
X_α	Forward acceleration per unit angle of attack	ft/sec^2/rad
X_u	Forward acceleration per unit change in speed	1/sec
X_{T_u}	Forward acceleration per unit change in speed due to thrust	1/sec
X_{δ_e}	Forward acceleration per unit elevator angle	ft/sec^2/rad
Y_β	Lateral acceleration per unit sideslip angle	ft/sec^2/rad
Y_p	Lateral acceleration per unit roll rate	ft/sec/rad

Symbols (cont.)

Y_p also:	Human pilot transfer function	~
Y_r	Lateral acceleration per unit yaw rate	ft/sec/rad
Y_{δ_a}	Lateral acceleration per unit aileron angle	ft/sec^2/rad
Y_{δ_r}	Lateral acceleration per unit rudder angle	ft/sec^2/rad
Z_α	Vertical acceleration per unit angle of attack	ft/sec^2/rad
Z_u	Vertical acceleration per unit change in speed	1/sec
$Z_{\dot{\alpha}}$	Vertical acceleration per unit rate change of angle of attack	ft/sec/rad
Z_q	Vertical acceleration per unit pitch rate	ft/sec/rad
Z_{δ_a}	Vertical acceleration per unit elevator angle	ft/sec^2/rad

Greek

α	Angle of attack	deg or rad
$\dot{\alpha}$	Rate of change of angle of attack	rad/sec
α_1	Trim angle of attack	deg or rad
β	Angle of sideslip	deg or rad
γ	Flight path angle	deg
χ	Ground track heading	deg or rad
δ	Control surface deflection angle	deg or rad

Greek (cont.)

Δ	Increment of a parameter	~
θ	Perturbed value of Θ	rad
Θ	Airplane pitch attitude angle	rad
Λ	Sweep angle	~
ζ	Damping ratio	slugs/ft^2
ρ	Air density	sec
τ	Pilot reaction time delay constant	rad
ϕ	Perturbed value of Φ	rad
Φ	Airplane bank angle	rad
ψ	Perturbed value of Ψ	rad
Ψ	Airplane heading angle	rad/sec
ω_n	Natural frequency	rad/sec
ω_d	Damped frequency	

Subscripts

a	Aileron
aero	Aerodynamic
alt	Altitude
cg	Center of gravity
cmd	Command

Subscripts (cont.)

Cr	Critical
c/4	Relative to the quarter chord
D	Damping
dr	Dutch roll
e	Elevator
h	Horizontal tail
I	Integrator
max	Maximum
min	Minimum
p	Peak
ph	Phugoid
pred	Predicted
r	Rudder
req	Required
sp	Spiral
ss	Steady State
t	Throttle
vt	Vertical tail
w	Wing
wf	Wing + fuselage
x, y or z	In the x, y or z direction

Acronyms

ac	Aerodynamic center
AGL	Above ground level
ASL	Above sea level
AVL	Athena Vortex Lattice
c.g.	Center of gravity
CReSIS	Center for Remote Sensing of Ice Sheets
DPE	Data Processing Engineer
FTE	Flight Test Engineer
GPS	Global positioning system
HIL	Hardware-in-loop
IAS	Indicated airspeed
IPCC	Intergovernmental Panel on Climate Change
PA	Pilot Assistant
PIC	Pilot in Command
SCCS	Standard Cloud Cap Simulator
SFC	Specific fuel consumption
SO	Safety Officer
UAS	Unmanned aerial system
UAV	Unmanned aerial vehicle
VO	Video Operator

1 Introduction

In November of 2007 the Intergovernmental Panel on Climate Change (IPCC) released a summary of their findings with regard to climate change [1]. In this summary the IPCC states that the average sea level change has risen to a rate of 3.1 mm/yr (the average from 1961 is 1.8 mm/yr). The report also stated that the average sea ice extent in the Arctic has shrunk by 2.7% per decade and a correlation is clearly drawn between these two events. The IPCC predicted that the Earth's sea level will rise 18 to 59 centimeters due to climate change but does not include in these predictions changes in the mass balance of the great ice sheets, only the thermal expansion of the oceans. Currently glacial data sets do not exist to such an extent that the dynamics of the glaciers under rapidly warming conditions can be understood with any high level of certainty.

To combat this lack of knowledge the National Science Foundation, in 2005, established the Center for Remote Sensing of Ice Sheets (CReSIS). CReSIS is a multi-university organization headquartered at the University of Kansas (KU). The main goal of CReSIS is to conduct and foster multi-disciplinary research that will result in technology, new datasets, and models necessary to achieve a better understanding of the mass balance of the polar ice sheets (e.g., Greenland and Antarctica) and their contributions to sea level rise.

For some years the Electrical Engineering Department at KU has been developing radar systems that allow data on the great ice sheets to be collected. The radar gives scientists the ability to measure the depth, surface elevation, and

accumulation rate of the great ice sheets and determine their basal conditions. Knowing the basal conditions of the glaciers allows modelers to better predict their dynamic behavior. The radar has been carried by both ground based and manned air based vehicles and part of the initial goals of the center was to develop an autonomous aerial platform on which to carry the radar sensors.

The Aerospace Engineering Department at the University of Kansas was given the primary task of developing an unmanned aerial vehicle (UAV) to carry the radar system. The final design, named the Meridian, is a low wing, V-tail, 1,000 lb, diesel driven, tail dragger airplane that will operate autonomously during its data collecting missions (Figure 1). The aircraft has been designed to carry up to eight radar antennas along the wing that will be used to collect the data on the glaciers. A detailed discussion of the design of the Meridian can be found in Reference [2] and a detailed discussion of the Meridian's avionics systems can be found in Reference [3].

For the Meridian to operate autonomously during its missions an autopilot must be selected that can safely and effectively control the aircraft within the mission parameters. The Meridian development team at CReSIS chose to use a commercial off-the-shelf (COTS) autopilot system rather than developing a system in-house because of a short time to flight schedule. The initial autopilot of choice was the Cloud Cap Technologies Piccolo II flight control system. To determine if the Piccolo could safely control the aircraft and successfully perform the science mission a detailed development, test and evaluation process was needed. The Piccolo requires user-end modeling and simulation of the aircraft for user-end gain tuning. These

modeling and simulation packages were included with the Piccolo system and their accuracy is unknown and their validity must be determined. A one-third scale Yak-54 was chosen as the platform to develop and verify modeling and simulation tools, test the system's ability to perform the desired mission and also establish a flight test program structure that could be easily transitioned to Meridian or other UAV flight testing.

The research presented in this thesis was a team effort and proper recognition should be performed before proceeding. Hou In "Edmond" Leong and Shariar Keshmiri were the primary collaborators to the work presented herein. The direct contributions of each team with regards to this thesis were be broken down as follows.

1. **Rylan Jager**
    - Developed flight test plans for all flight test activities
    - Lead flight test engineer for all flight test activities
    - Setup the Piccolo system in the Yak-54
    - Developed Standard Cloud Cap Simulation models
    - Developed Athena Vortex Lattice models
    - Analyzed piloted responses
    - Performed some parameter identification data processing
    - Analyzed parameter identification flight test data
    - Analyzed simulation models
    - Performed gain tuning activities in simulation and flight test

- Analyzed closed-loop performance
- Developed communications lab tests and performed tests
- Analyzed processed communications data

2. **Edmond Leong**
    - Estimated Yak-54 moments of inertia
    - Developed telemetry plotting software
    - Performed open-loop analysis of the Standard Cloud Cap Simulator
    - Assisted in the construction of the Yak-54 Advanced Aircraft Analysis dynamic model
    - Developed Bolly 26” x 10” propeller model
    - Performed some parameter identification data processing
    - Plotted open-loop response flight test data
    - Developed communications data loss analysis techniques
    - Processed and plotted communications data
3. **Shahriar Keshmirir**
    - Primary developer of Yak-54 Advanced Aircraft Analysis dynamic model

Chapter 2 of this document presents the high level test and evaluation process that was developed for modeling, simulation and control system development, test and evaluation. Chapter 3 details the Piccolo II UAS autoflight system that was tested and evaluated. Chapter 4 presents the Yak-54 flight test platform for the Piccolo II test and evaluation program. Chapter 5 presents modeling and simulation platforms

that were used with the Piccolo II system. Chapter 6 details the flight test planning and preparation process. Chapter 7 presents the manual control flight test of the Yak-54/Piccolo system. Chapter 8 details the parameter identification flight testing and the evaluation of the various modeling and simulation platforms using the data gathered in those flight tests. Chapter 9 presents the gain tuning of the Piccolo II flight control system using hardware-in-loop simulation. Chapter 10 details the closed-loop Piccolo II flight control system test and evaluation. Chapter 11 presents a flight incident caused by a poor communication system setup in the Piccolo II system that was revealed during the test and evaluation process. Finally Chapter 12 presents the conclusions and recommendations of the Piccolo II test and evaluation process.

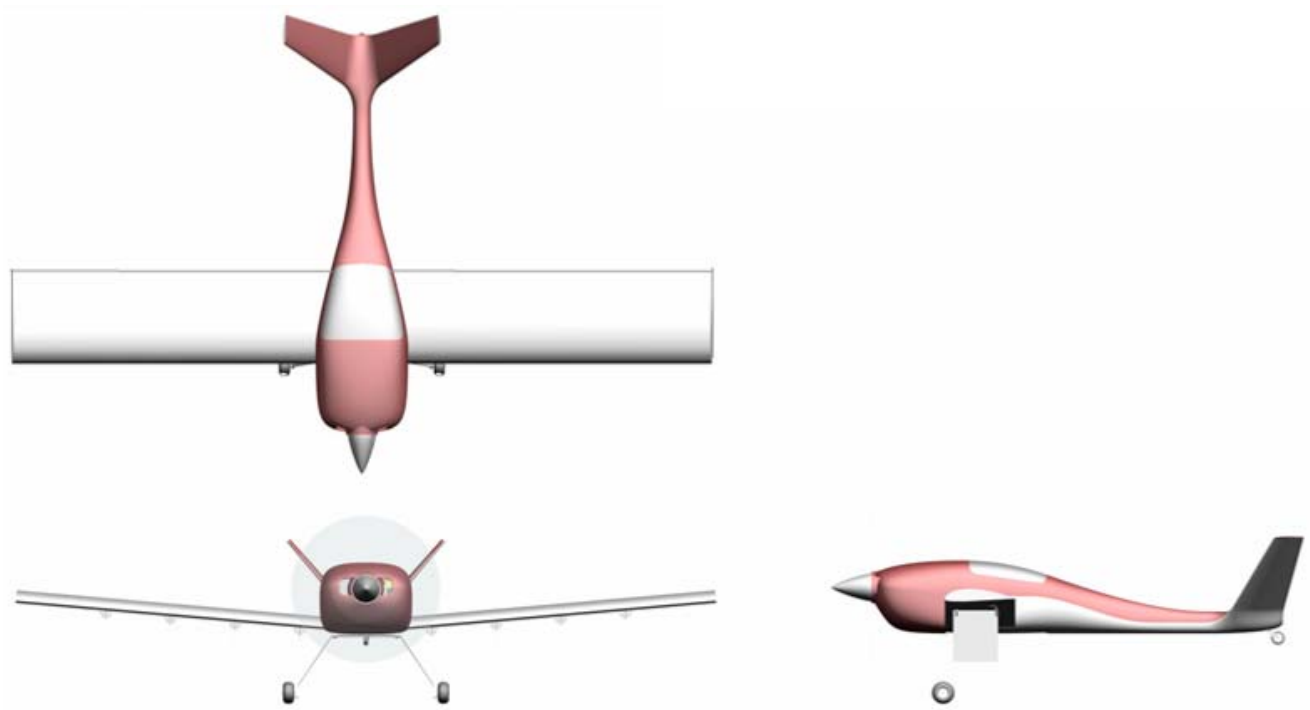

Figure 1: Meridian Three View

2 Modeling, Simulation and Autopilot Test and Evaluation Process

As mentioned in the introduction the CReSIS UAV development team chose to use commercial-off-the-shelf avionics systems. A thorough and deliberate process was developed to test and evaluate COTS UAV flight control systems. This process can also be used in the in-house development and test of flight control systems.

Figure 2 shows a detailed block diagram of how these development, test and evaluation processes were laid out. The figure shows the test and evaluation process is an iterative one. The steps in the modeling, simulation and autopilot development, test and evaluation process and the options available to the test and evaluation engineer are presented in this chapter.

2.1 Step 1: Select System

Currently there are only a few low-cost commercial-off-the-shelf autopilot systems available for purchase. The Cloud Cap Piccolo, the Micropilot series of autopilots and the WeControl WePilot are currently the standards in the small, low-cost UAV autopilot market. More expensive off-the-shelf systems for UAVs are available from Athena Control. Reference [4] presented some detailed information on the current state of the art in small, low-cost UAV autopilots.

Always an option is to develop a flight control system in-house, which requires a significant amount of development time and money.

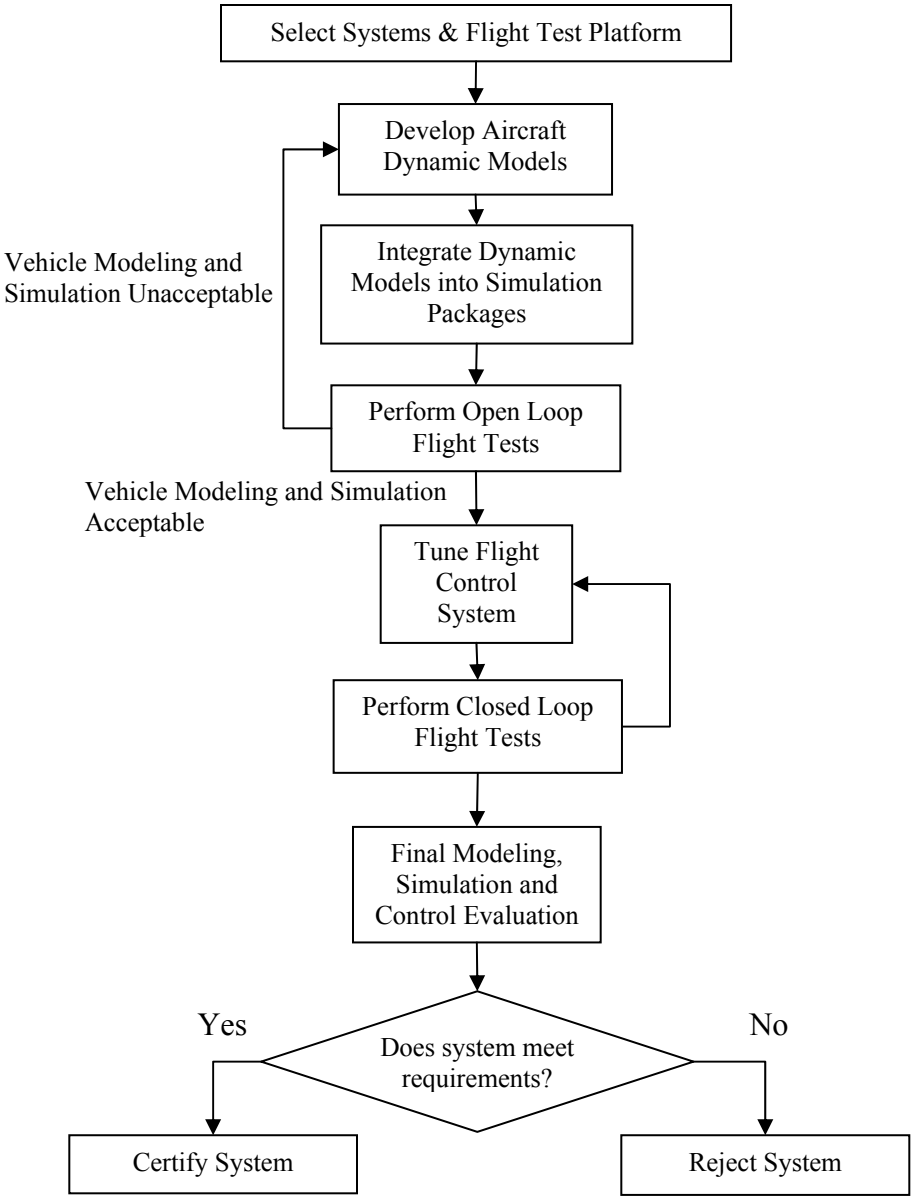

Figure 2: Modeling, Simulation and Autopilot Test and Evaluation Process

2.2 Step 2: Select Flight Test Platform

Almost ready to fly (ARF) remote control aircraft are ideal for flight testing autopilot systems. They provide a rapidly built, low-cost platform for testing of UAV autopilots. Important considerations when selecting an RC platform is the internal

payload capacity for mounting autopilot avionics and the structural integrity of the platform to handle the increased weight of the avionics.

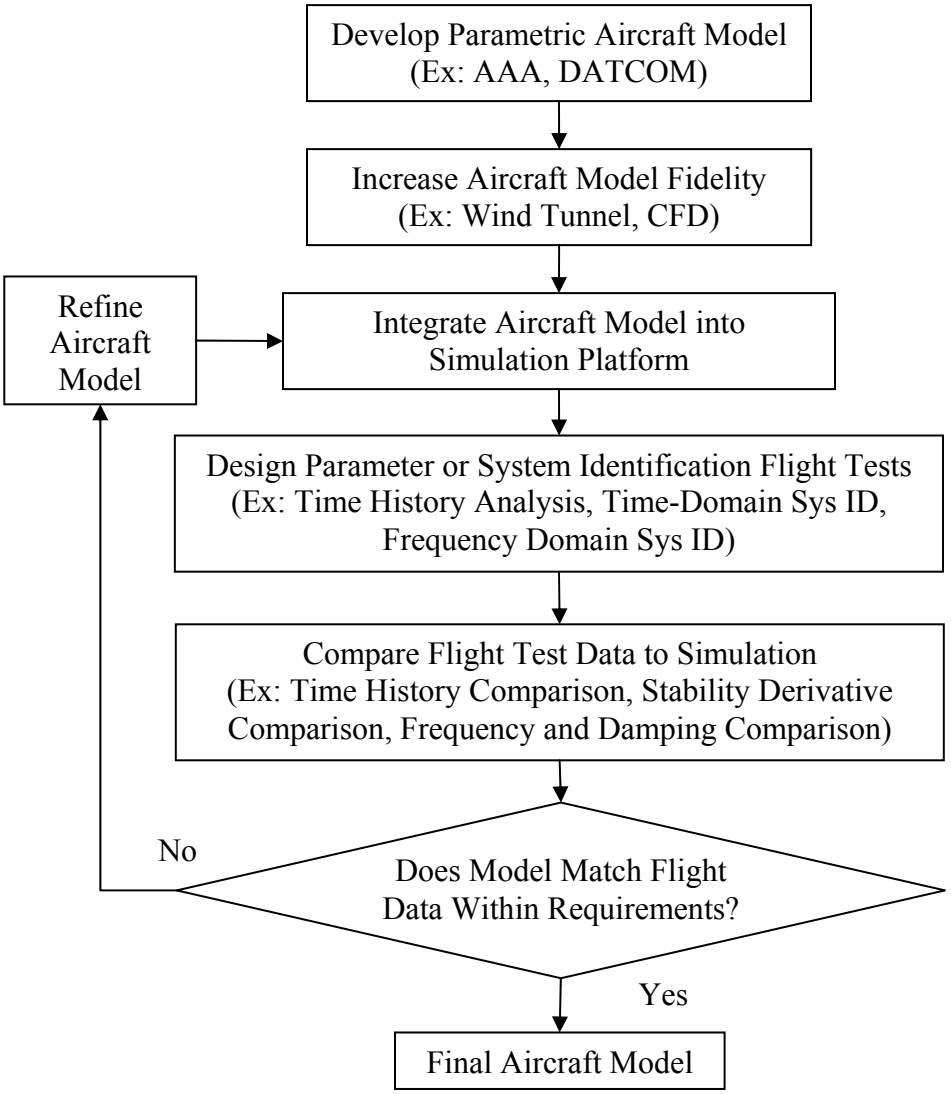

Figure 3: Aircraft Dynamic Model Development Flow Chart

2.3 Step 3: Develop First Principles Aircraft Dynamic Models

Figure 3 shows the modeling and simulation development process. Developing a good flight control system requires a good aircraft dynamic model. The

simplest method for developing an initial first principles parametric aircraft dynamic model is to use geometric information. These parameters are used to approximate the aircraft stability derivatives using past aircraft information databases, such as the US Air Force's digital DATCOM or DARcorporation's Advanced Aircraft Analysis. References [5], [6] and [7] used geometric techniques to estimate UAV stability derivatives. These techniques tend to be low fidelity.

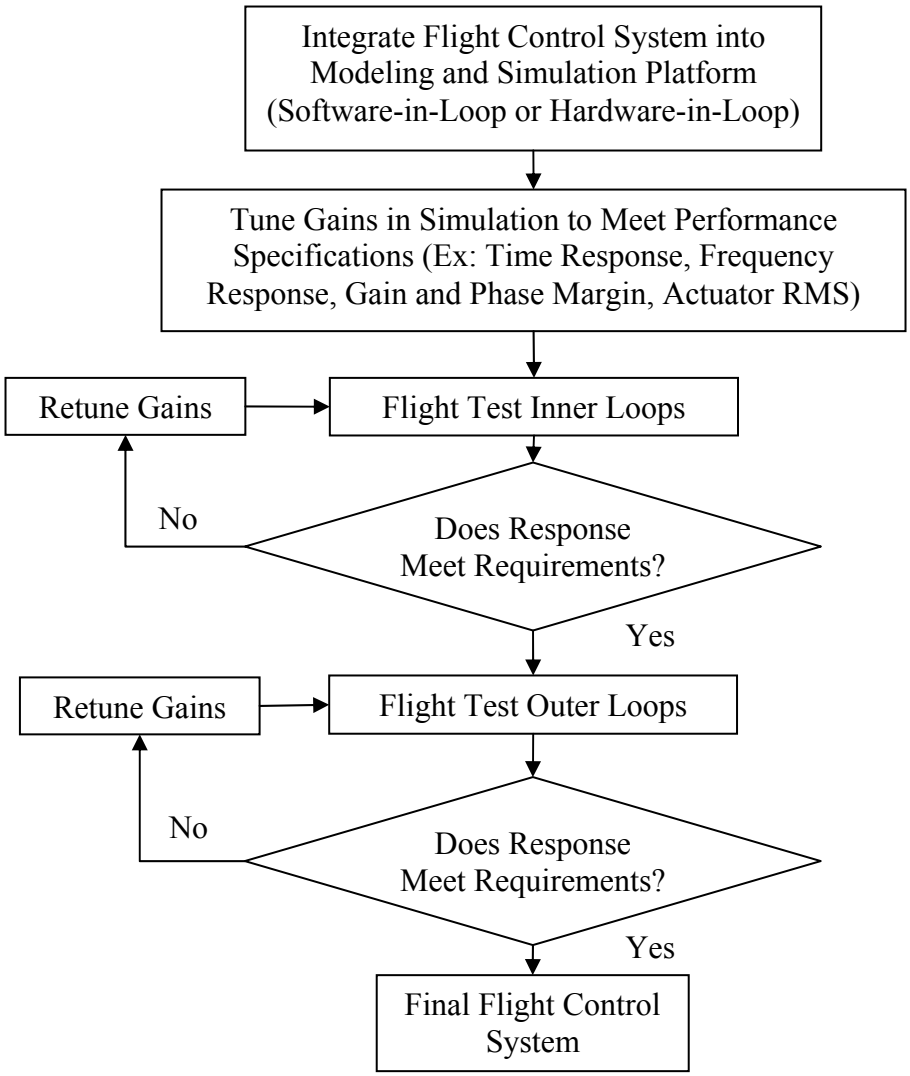

Figure 4: Flight Control Tuning Flow Chart

Wind tunnel data can also be used to determine a UAV's stability derivatives, as presented in Reference [8]. Wind tunnel testing is more expensive and labor intensive than geometric techniques but will produce a more accurate model. Computational fluid dynamics can also be used to develop aerodynamic parameters.

2.4 Step 4: Integrate Dynamic Model into Simulation Platform

A variety of simulation platforms exist for integration with aircraft dynamic models. 3 DoF linear and 6 DoF nonlinear models can be simulated software-in-loop in platforms like MATLAB/Simulink. 3 DoF techniques are presented thoroughly in References [9], [10] and [11]. The more advanced 6 DoF techniques a used in References [12] and [13]. Reference [6] provides a nice comparison between the various simulation techniques.

Hardware-in-loop (HIL) simulation is the ideal as it is the closest to reality. HIL simulation is often platform specific, as with the Piccolo II autopilot system, or is performed using real-time C code generated from MATLAB/Simulink using Real-Time Workshop. This is because HIL simulation has to be performed real-time and MATLAB/Simulink does not operate in real-time. The test and evaluation engineer should select the most appropriate simulator for his or her platform.

2.5 Step 5: Refine Dynamic Models using Flight Test Data

The only way to truly evaluate an aircrafts dynamics are in flight test. Classical flight test data reduction techniques (References [14] and [15]) can be used to evaluate dynamic models in terms of frequency and damping and can be used to

estimate static stability derivatives. Flight data can also be placed directly into simulator to give side by side comparison of responses.

More modern system identification techniques are gaining popularity in enhancing UAV dynamic models. This is because wind tunnel and CFD analysis are time consuming and expensive and classical flight test techniques tend to be less accurate at estimating specific stability derivatives. Several methods exist for developing aircraft dynamic models from flight test data.

Time domain system identification methods were developed at the German Aerospace Research Establishment (References [16] and [17]). These methods utilize the 3-2-1-1 input to excite the aircraft dynamics. 3-2-1-1 refers to step inputs lasting, in sequence, three seconds, two seconds, one second and one second. These techniques require an initial parametric model, such as a digital DATCOM model, to work. Reference [18] used these techniques to model a UAV.

Frequency domain system identification can be utilized as well. Reference [19] provides detailed information on how dynamic models can be developed using frequency domain methods. Reference [20] used frequency domain system identification on a UAV helicopter and Reference [21] presents how frequency domain techniques can be used to enhance UAV flight controllers. Frequency domain techniques can be used without parametric models of the system dynamics, can determine high frequency structural modes, and can identify unstable dynamics. They do, however, require more flight time to complete (30 seconds to a few minutes per maneuver). This makes them well suited to helicopters but also makes them

difficult to perform on fixed wing UAVs using a remote pilot as the aircraft will leave visual range before the sweep can be finished. Automated frequency sweeps should be used if frequency domain techniques are used on fixed wing UAVs.

2.6 Step 6: Tune Flight Control System in Simulation

There are several options available for tuning a control system. Requirements can be set using classical parameters (rise time, percent overshoot, settling time, damping ratio, gain margin, phase margin, actuator RMS, etc.). Reference [22] is an excellent text in the area of control system requirements definition.

From these requirements the control system gains should are tuned in simulation with the dynamic model previously developed. For more complicated systems gains may have to be tuned iteratively until an ideal system can be reached. If the exact structure of the system is known useful tools exist to find ideal gains based on performance specifications. CONDUIT, a program for the optimization of control system gains developed by the Army Aeroflightdynamics Directorate at Ames Research Center, was used in Reference [23] to find optimal gains for various control methodologies. Reference [24] used stochastic methods to find optimal gains of a control system for an unmanned spacecraft. It is important to remember that these "optimal" gains are only "optimal" for the dynamic model used in the optimization. Thus the better the dynamic model the better performance the flight system has.

2.7 Step 7: Flight Test Tuned Control System

When flight testing a control system it is important to develop efficient and

safe flight test plans prior to first flight. References [9], [10] and [24] provide solid foundations on how to setup a flight test program.

Tuning a UAV flight control system in flight should be performed loop by loop if possible. It is important to isolate which each parameter so that problems can be isolated. Starting with the lateral-directional system can be useful as it allows for roll and heading stabilization during longitudinal control testing. Gain tuning can be performed in flight to meet performance specifications but it is important to remember that gain tuning in flight can be expensive, difficult, stressful and dangerous and should be avoided as much as is possible.

2.8 Step 8: Evaluate the Performance of the Control System and Reject or Certify

After flight test of the control system is complete the system should be analyzed to determine of the closed loop performance meets the requirements. If the system meets the requirements and can safely be used then the system can be certified. If not, problem areas can be addressed or the system can be rejected.

3 The Cloud Cap Piccolo II Autopilot System

The Piccolo autopilot system is a complete integrated avionics system for unmanned aerial vehicles. The system includes hardware and software for the avionics, hardware and software for the ground station and a flight model development and simulation environment. Piccolo has been widely chosen for UAV flight control systems and flight tests have been conducted by several university and industry research programs, Reference [26], such as:

Government Customers
Air Force Research Laboratory (AFRL), Eglin
Idaho National Engineering Laboratory (INEL)
NASA, Ames, Dryden and Langley Research Centers
NAVAIR
Naval Post Graduate School
Naval Research Lab (NRL)
Naval Surface Warfare Center, Carderock
Office of Naval Research (ONR)

University Customers:
Idaho State University
Massachusetts Institute of Technology (MIT)
Oklahoma State University
Penn State University
UC Berkeley
UCLA
University of Arizona Aerial Robotics Club
University of Colorado at Boulder
University of Illinois
University of Pennsylvania
US Air Force Academy
US Naval Academy
Texas A+M

Industry Customers:
Advanced Ceramic Research (ACR)
Aerosonde Robotic Aircraft
Aero Mech
Alion Science and Technology
Arcturus Inc.
BAI Aerosystems
Griffon Aerospace
Georgia Tech Research Institute (GTRI)
Johns Hopkins Applied Physics Lab
KalScott Engineering
Lockheed Martin
Meggitt Defense Systems
Navmar Applied Sciences
Northrop Grumman PRB Systems
Raytheon, Tucson
Rockwell
UAV Applications Center

The basic Piccolo II system architecture is shown in Figure 5.

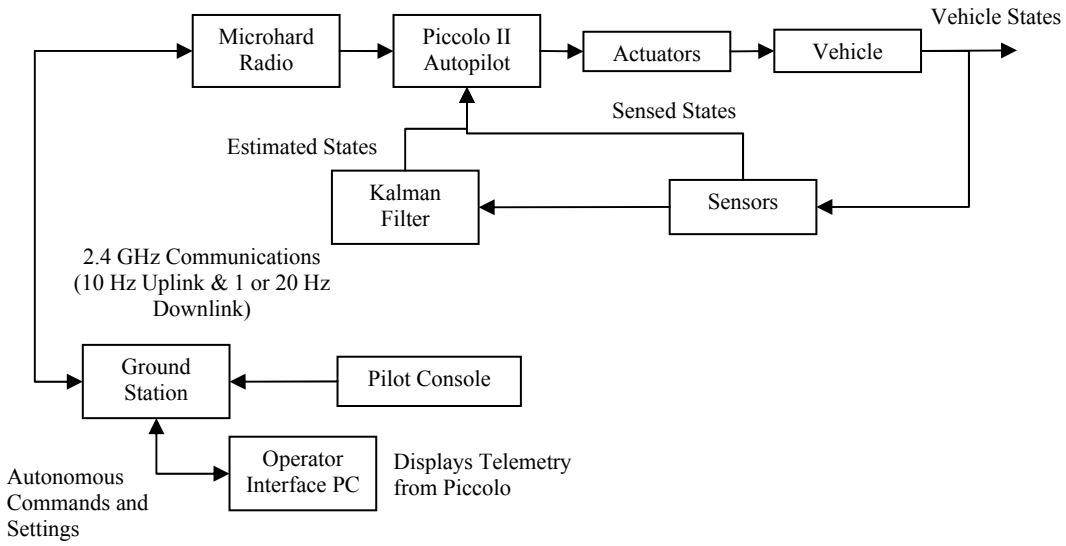

Figure 5: Piccolo II System Block Diagram

3.1 Piccolo II Avionics Hardware

The Piccolo II, shown in Figure 6 and detailed in Reference [26], is a near fully self-contained autopilot system, with the only external equipment needed being pitot and static tubes and an optional magnetometer. The Piccolo is driven by a 40 MHz core MPC-555 microprocessor. A block diagram of the Piccolo II system hardware is given in Figure 7.

Figure 6: Cloud Cap Piccolo II Autopilot [26]

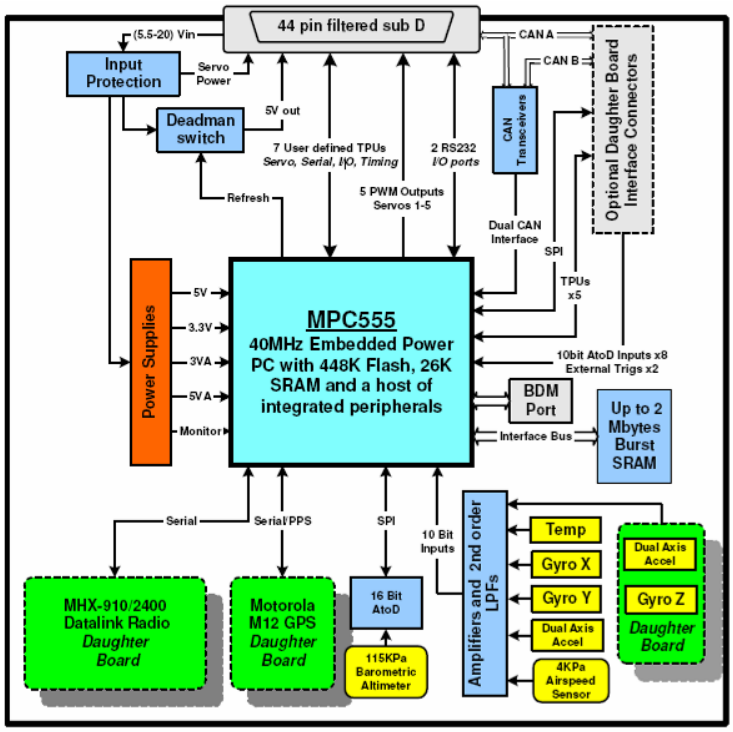

Figure 7: Piccolo Hardware Block Diagram [26]

The Piccolo II has sixteen digital I/O lines, five serial ports and four analog inputs. The digital I/O lines are used both for payload I/O and servo actuation. A 44-pin connector and a 24-pin microdot connector are used to connect the I/O, serial, analog and power lines to the Piccolo.

3.1.1 Gyros and Accelerometers

The Piccolo II uses three Analog Devices, Inc. ADXRS300 MEMS rate gyros and two two-axis ADXL210e MEMS accelerometers to determine the rates and accelerations in all three axes. The rate gyros give 300 °/sec resolution rate measurements.

3.1.2 GPS

An uBlox TIM-LP GPS receiver is used to provide position data as well as groundspeed determination. The system has an update rate of 4 Hz.

3.1.3 Pressure System

A Freescale Semiconductor 115 KPa mpx4115 barometric pressure sensor, a Freescale Semiconductor 20 KPa differential pressure sensor and a board temperature sensor are used to determine the true airspeed and altitude. The system compares the true airspeed to GPS ground speed to determine winds aloft.

3.1.4 Kalman Filter

The Piccolo uses a Kalman filter to estimate the aircraft attitude in flight as well as determine the sensor biases.

3.2 Communication System

The Piccolo II uses either a 910 MHz or 2.4 GHz transceiver built by Microhard Systems, Inc. In the current research program the 2.4 GHz transceiver was used. The system provides 40K baud of throughput and transfers autopilot command functions, telemetry, payload data, differential GPS corrections and pilot control to and from the autopilot and ground station. Downlink data is updated at either 1 Hz or 20 Hz and uplink data is 10 Hz.

3.3 Ground Station

The ground station includes the following items:

- Main ground station electronics unit
- 2.4 GHz antenna
- Operator Interface PC
- Futaba console for manual pilot control

3.3.1 Main Ground Station Electronics

The main Piccolo ground station electronics unit manages communication with the avionics, interfaces with the pilot console and streams telemetry and command and control data to and from the operator interface PC. The ground station interface connects to the operator interface using a 9-pin serial connection.

To communicate with the avionics the ground station interface utilizes a 1 Watt 2.4 GHz transceiver. This gives a maximum communication range of approximately 6 miles [3].

Figure 8 and Figure 9 give a front and back views of the Piccolo ground station unit.

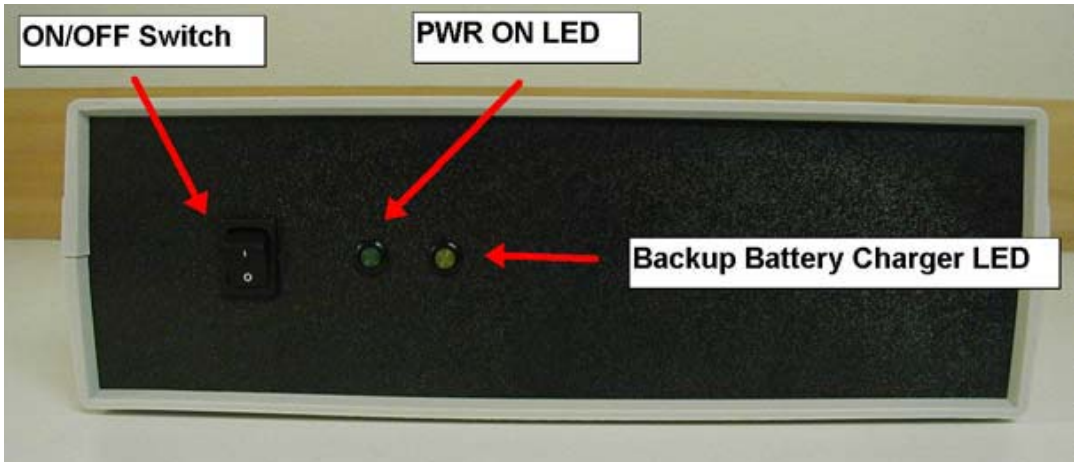

Figure 8: Ground Station Unit Front Panel [26]

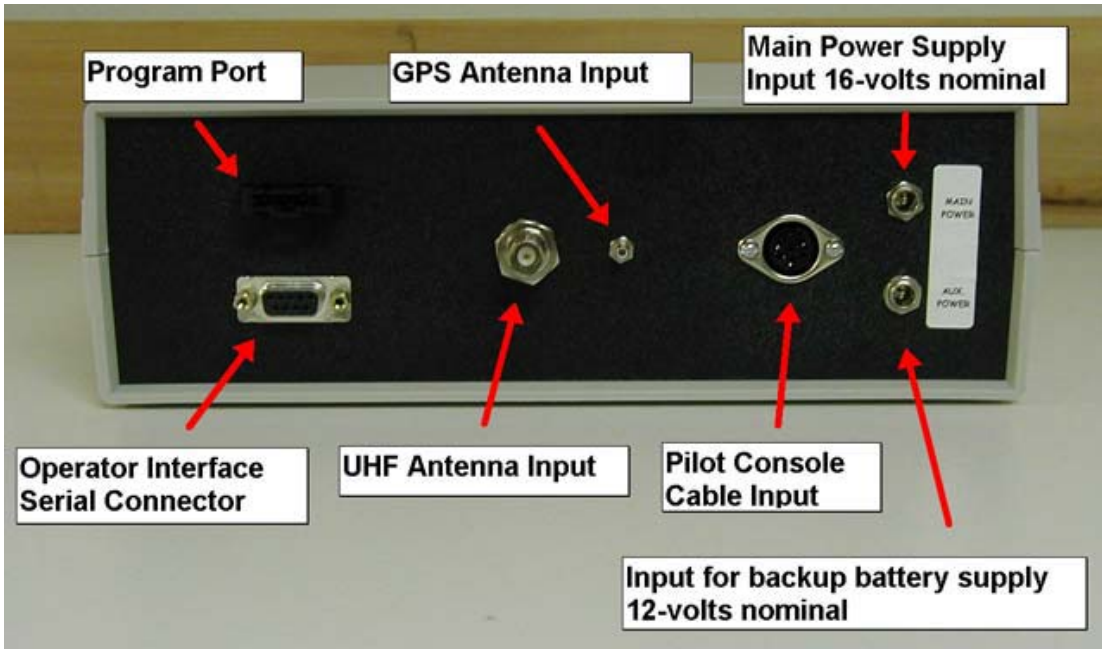

Figure 9: Ground Station Unit Back Panel [26]

3.3.2 Operator Interface PC

The command and control interface functions from a PC using the Piccolo operator interface. For this research program the computer of choice is an Itronix GOBook III rugged notebook PC of the following specifications:

- 1.8 GHz Intel Centrino Pentium M 745
- 1 GB SDRAM
- Integrated GPS and Wireless Communication
- Fully-Rugged to Mil-STD 810F
- Cold Tested to -30 °C
- Heated Hard Drive
- Water-Proofed Keyboard

Figure 10: Itronix GOBook II [27]

3.3.3 Futaba Console

Pilot commands are relayed to the aircraft when in manual mode using a Futaba T9CAP Super Console. The console is connected to the ground station interface unit using the Futaba compatible buddy-box 6 pin DIN connector. Using the pilot console

the pilot is able to activate or deactivate the autopilot and has full control authority over the aircraft including trim settings.

Figure 11: Futaba Pilot Console [26]

3.4 Operator Interface

The operator interface environment software allows for monitoring of the aircraft health status, including attitudes, rates, accelerations, airspeed, ground speed, GPS location, winds aloft and communication signal strength, as shown in Figure 12. Outer-loop commands are also issued to the aircraft through the operator interface, including waypoint data. The limits of the control surfaces as well as airspeed are inputted into the aircraft through this system as well.

In addition the position of the aircraft can be real-time monitored on the navigation page, where a map can be used for geographic referencing to the GPS coordinates (Figure 13). Flight plans are displayed on the maps and can be updated at any time from the operator interface.

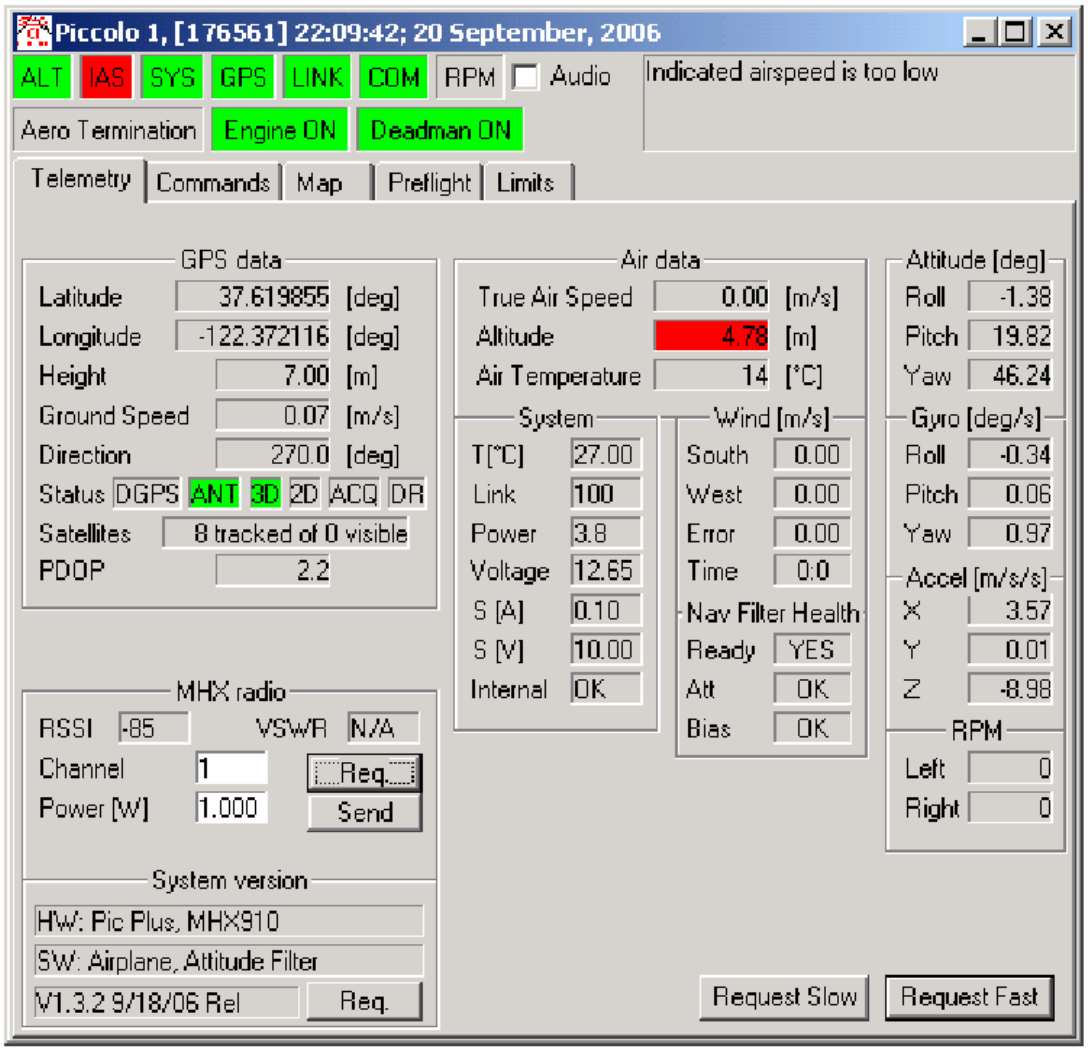

Figure 12: Operator Interface Telemetry Page [26]

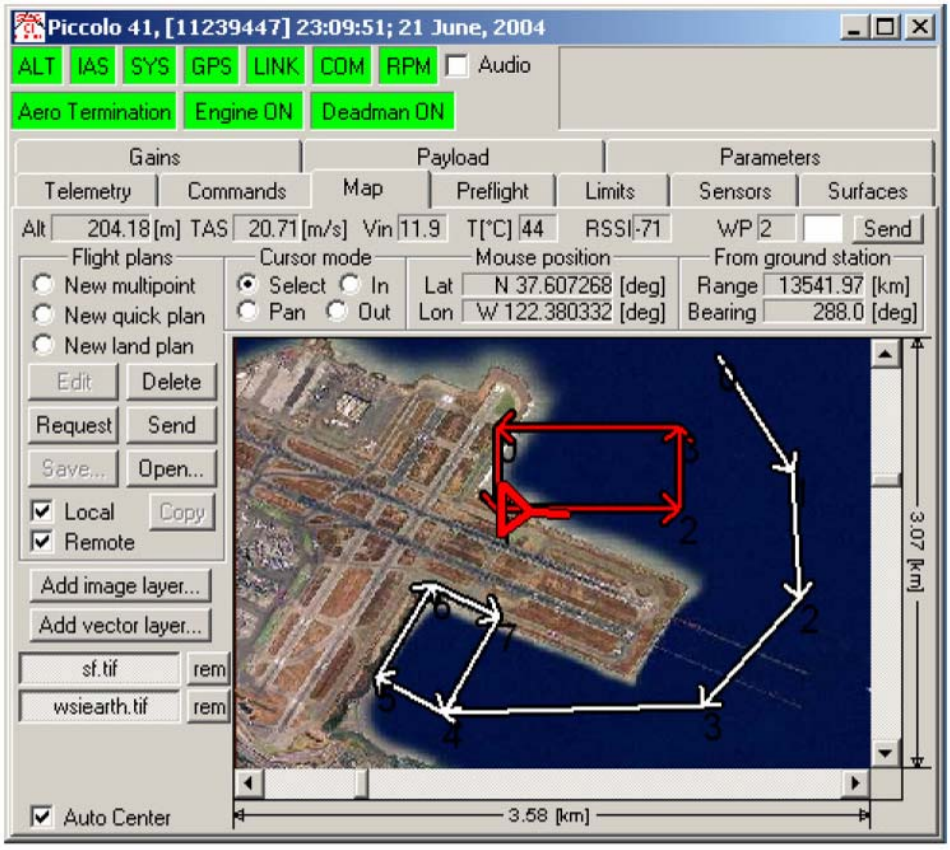

Figure 13: Piccolo Navigation Screen [26]

3.5 Piccolo II Flight Control Laws

The Piccolo uses a so-called physics based control scheme. This system makes use of the gain scaling parameters which are presented in Table 1. There are then 20 gains in the system that can be tuned by the user. References [26] and [28] provide some more thorough presentation of the Piccolo control laws but the exact control algorithms are not publicly available.

The Piccolo allows for the direct control of the following states:

1. Bank Angle
2. Heading

3. Altitude
4. Airspeed
5. Vertical Rate
6. Waypoint Navigation

The Piccolo uses total energy methods to control altitude and airspeed. This means that both elevator and aileron are used simultaneously to control altitude and airspeed.

Table 1: Piccolo Gain Scaling Parameters

Geometry
Wing Area (S_w)
Wing Span (b_w)
Vertical Tail Arm ($x_{ac_{vt}} - x_{cg}$)
Mass
Gross Mass
Empty Mass
I_{XX}
I_{YY}
I_{ZZ}
Longitudinal Aerodynamics
Elevator Power ($C_{m_{\delta_e}}$)
C_{L_0}
Elevator Effectiveness ($\frac{dC_L}{d\delta_e}$)
Lateral Aerodynamics
Aileron Effectiveness ($\frac{\partial \overline{p}}{\partial \delta_a}$)
Rudder Power ($C_{n_{\delta_r}}$)
Rudder Effectiveness ($\frac{\partial \beta}{\partial \delta_r}$)
Sideslip Effect (C_{y_β})
Engine
Power

3.6 Piccolo II Guidance and Navigation System

The Piccolo used waypoints defined by latitude, longitude and altitude the guidance and navigation outer loops. Ground tracks are defined by a straight line vector between the waypoints and the Piccolo performs a decision making computation to determine whether to converge on the ground track or fly straight to the waypoint commanded. The aircraft contains a pre-turn algorithm that estimates when the aircraft should begin the turn onto the next waypoint defined ground track as to not overshoot the ground track. Thus the aircraft does not fly directly over the waypoint (this feature can be disabled if waypoint flyover is desired). The Piccolo has a "tracker convergence" term that can be used to make the aircraft perform more aggressive ground course tracking. Orbiting waypoints of a fixed time and radius may also be input to the Piccolo system. The exact guidance and navigation algorithms are not publicly available. The waypoint monitoring and entry screen on the operator interface is presented in Figure 13.

3.7 Piccolo II Modeling and Simulation Environment

The Piccolo II has two options for modeling and simulation of the aircraft and guidance navigation and control system: 1) the standard Cloud Cap Simulator, which makes use of look-up tables for the main lifting surfaces (i.e. wing and tail), and 2) Athena Vortex Lattice based simulator that uses vortex lattice code to produce the aerodynamic derivatives for simulation. Both modeling techniques can be simulated in a hardware-in-loop environment, including open loop pilot control. In this section

both simulation techniques will be discussed.

3.7.1 Standard Cloud Cap Simulator

The foundation of the Standard Cloud Cap Simulator (SCCS) resides in ASCII look- up tables for the various lifting surfaces of the aircraft to be modeled. For each lifting surface an ASCII table containing lift coefficient (C_L), drag coefficient (C_D) and pitching moment coefficient (C_M) for various angles of attack was created (or various sideslip angles for the vertical stabilizer). The aerodynamic parameters were generated internally in the simulator using geometric data for the lifting surfaces (span, incidence, dihedral, area, span efficiency, etc). Control surfaces were modeled by declaring the inboard and outboard control surface locations as well as the average chord length of the control surface.

Fuselage information was also declared, including pitching moment coefficient with respect to angle of attack, yawing moment with respect to sideslip, parasite drag, etc.

The propulsion model used a simple power vs. RPM look up table to determine the engine power. The simulator assumes a linear relationship between throttle movement and power generation. From the table the current engine RPM was determined. The advance ratio of the aircraft was then determined as:

$$J = \frac{V_a}{n\,d} \tag{3.2}$$

A propeller model input by the user was then used to lookup the thrust coefficient for the propeller in question and calculates the aircraft thrust. The thrust was determined as:

$$T = \rho n^2 d^4 C_T \tag{3.3}$$

The power absorbed by the propeller is calculated from the same lookup table as:

$$P_{absorbed} = \rho n^3 d^5 C_p \tag{3.4}$$

The mismatch between the propeller power and the engine power causes a change in the propeller RPM based on the moment of inertia of the propeller. The RPM will change until the power absorbed and the power generated match.

The final set of items in the SCCS are the mass properties of the aircraft. The empty mass, gross mass, and moments of inertia are input to generate the dimensional stability derivatives. As with the other items this data is provided by the user.

Reference [29] gives a detailed description of the SCCS and Appendices A through F can be referenced for the SCCS models used during this research program.

There are several negatives associated with the Standard Cloud Cap Simulator. Probably the most significant negative is the extreme black box nature of the simulator. It is very difficult to troubleshoot any mistakes in the modeling as only a few stability derivatives are output by the simulator. The other problem is that modeling of a V-Tail cannot be done directly, but must be done using the projected surface on the vertical and horizontal planes. This is not an especially accurate representation, especially as no vortex interactions are taken into account. Another slight disadvantage of the simulator is the lack of a graphical projection of the tabular

surface data that would assist in troubleshooting errors in the geometry input to the simulator file.

3.7.2 Athena Vortex Lattice Based Simulator

Cloud Cap Technology offers a second modeling technique that addresses some of the issues associated with the SCCS. This simulator makes use of Athena Vortex Lattice (AVL), a vortex lattice code developed by Mark Drela and Harold Youngren at the Massachusetts Institute of Technology. The basic logic behind AVL is that the aircraft stability derivatives generated by its lifting surfaces can be estimated based on the steady vortex shedding of the surfaces at small angles of attack and sideslip. In AVL the fuselage effects are ignored.

In the model each major airfoil section can be defined. Using an aircraft's wing as an example, the center airfoil section, the airfoil section where the flap or aileron starts and ends, the airfoil section where the sweep angle changes, or the airfoil section where the dihedral changes, can all be defined so the geometry will exactly match the actual aircraft. This also allows for the creation of v-tail geometry models directly.

A significant advantage of AVL is that the geometry can be graphically represented in three dimensions, allowing for increased troubleshooting ability. Figure 14 shows a 3-D model of the Aerosonde that was included with the simulator.

The stability derivatives about the center of gravity are then calculated using the lifting surface geometry. The angle of attack of the aircraft is varied based on intervals set by the user and the stability derivatives are determined for each angular

position. The stability derivatives are output to an .XML file for use by the Cloud Cap Simulator. The simulator uses the same propulsion and inertia models as the SCCS, substituting in the AVL aerodynamics for the lifting surface tables. The .XML file allows greater insight into what goes into the Cloud Cap Simulator, allowing for better troubleshooting of the dynamics model. Reference [30] contains a more detailed discussion of the AVL simulator.

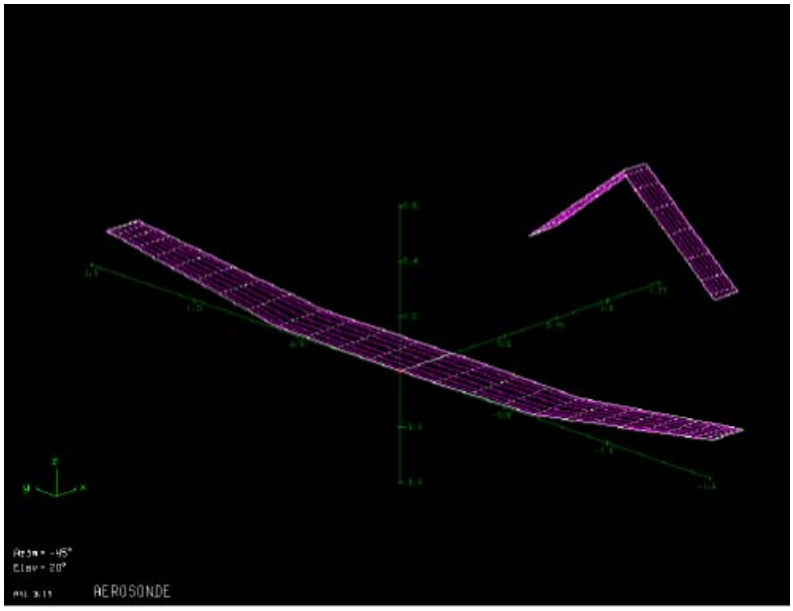

Figure 14: Aerosonde AVL Model [30]

3.8 Hardware-in-Loop Simulation

Using either of the two models hardware-in-loop simulations can be performed using the Piccolo II (Figure 15). The Cloud Cap Simulation software takes the aerodynamic data either from the SCCS or the AVL simulator as well as the propulsion and inertial models and simulates the dynamics of the aircraft modeled. The simulator PC communicates to the Piccolo II hardware using a CAN bus,

simulating the sensor data that would be generated by the Piccolo in flight. The Piccolo then calculates the control surface positions using its control algorithms. These control surface commands are sent back to the simulator and the system recalculates the dynamics.

The hardware-in-loop simulation can also be performed pilot-in-loop using the Futaba console, allowing for manual piloting to be performed and static stability to be analyzed. Visualization of the aircraft can be performed using a second PC using Flight Gear. A UDP network is created that sends the simulation data to the PC running the flight gear software. This allows for better understanding of the aircraft states.

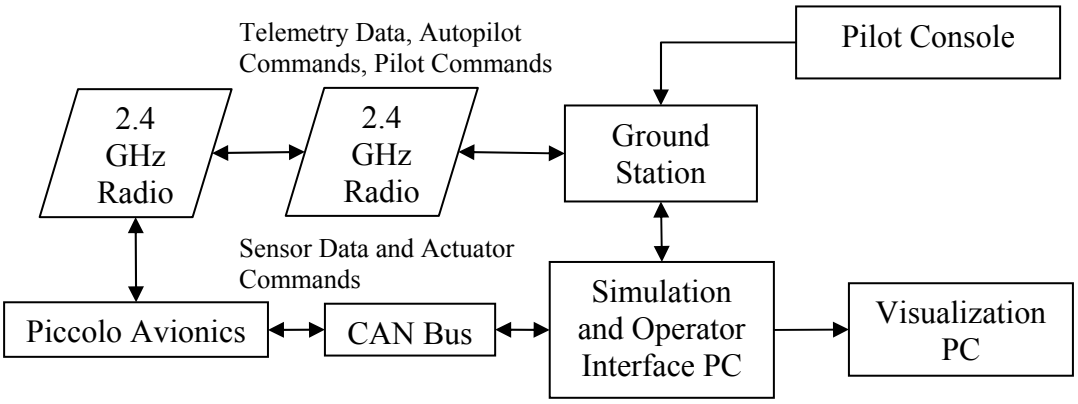

Figure 15: Hardware-in-Loop Simulation [29]

Figure 16: Flight Gear Visualization [29]

4 Flight Test Platform

To evaluate the performance of the Piccolo II flight control system and its simulation platforms, flight tests were conducted. The flight test platform for Piccolo II flight control system test and evaluation was the Aero-Works 1/3 scale Yak-54 (Figure 17). The Yak-54 was selected as it is a highly aerobatic aircraft, thus the structural layout is designed for high load factors. This allows some confidence that loading the aircraft with the Piccolo II avionics will not affect structural integrity.

Figure 17: Aero-Works 75cc Yak-54 [31]

4.1 Yak-54 Geometry

The Yak-54's lifting surface geometry was measured directly and is listed in Table 2:

Table 2: 75cc Yak-54 Lifting Surfaces [33]

Wing		
Area (S_w)	10.90	ft^2
Span (b_w)	7.90	ft
Mean Aerodynamics Chord ($\bar{c}_w$)	1.45	ft
Aileron Mean Aerodynamic Chord ($\bar{c}_a$)	4.90	in
Quarter Chord Sweep Angle ($\Lambda_{(c/4)_w}$)	-2.00	deg
Aspect Ratio (AR_w)	5.77	~
Taper Ratio (λ_w)	0.46	~
Root Airfoil	NACA 0016	~
Tip Airfoil	NACA 0017	~
Horizontal Tail		
Area (S_{ht})	2.30	ft^2
Span (b_{ht})	3.00	ft
Mean Aerodynamics Chord ($\bar{c}_{ht}$)	9.20	in
Elevator Mean Aerodynamic Chord ($\bar{c}_e$)	4.20	in
Quarter Chord Sweep Angle ($\Lambda_{(c/4)_{ht}}$)	12.60	deg
Aspect Ratio (AR_{ht})	3.91	~
Taper Ratio (λ_{ht})	0.81	~
Root Airfoil	NACA 0015	~
Tip Airfoil	NACA 0012	~
Vertical Tail		
Area (S_{vt})	1.60	ft^2
Span (b_{vt})	1.42	ft
Mean Aerodynamics Chord ($\bar{c}_{vt}$)	14.56	in
Rudder Mean Aerodynamic Chord ($\bar{c}_r$)	8.50	in
Quarter Chord Sweep Angle ($\Lambda_{(c/4)_{vt}}$)	12.70	deg
Aspect Ratio (AR_{vt})	1.25	~
Taper Ratio (λ_{vt})	0.35	~
Root Airfoil	NACA 0009	~
Tip Airfoil	NACA 0010	~

4.2 Yak-54 Mass Properties

The Yak-54's weight was measured directly. The moments of inertia were estimated by weighing each part that could be disassembled off the Yak-54 and approximating the dimensions of each part as either a cylinder or a box. The distance from the reference point, the engine firewall in this case, was measured and the moment of inertia for each component calculated. The sum of these measurements yielded the vehicle moments of inertia in the X, Y and Z body axes. The details of the moment of inertia calculations can be found in Reference [33].

Table 3: Vehicle Mass Properties [33]

Parameter		*Value*	*Units*
W	Takeoff Weight	28.1	lbs
I_{XX}	Moment of Inertia About the X Axis	1.0886	Slug ft^2
I_{YY}	Moment of Inertia About the Y Axis	2.1068	Slug ft^2
I_{ZZ}	Moment of Inertia About the Z Axis	3.0382	Slug ft^2
I_{XZ}	Moment of Inertia About the X-Z Axis	0.0000	Slug ft^2

4.3 Yak-54 Engine and Propeller

The Yak-54 used a gas powered, single piston 3W 80cc XI CS engine. This engine produces 9 Hp at a maximum RPM of 8500. The engine drives a Bolly 26" x 10" wood propeller.

Figure 18: 3W-80 XI CS Engine [34]

4.3.1 Engine Calibration

The Piccolo issues throttle commands as a percentage of maximum power. Thus it was important to calibrate the throttle servo position based on that positions output power. A power measuring device was not available for the engine and thus an approximation was used that assumed thrust varied linearly with power. Thrust was linearized as:

$$\overline{T} = \frac{T}{T_{\max}} \tag{3.1}$$

This revealed the throttle arm position pulse curve shown in Figure 19.

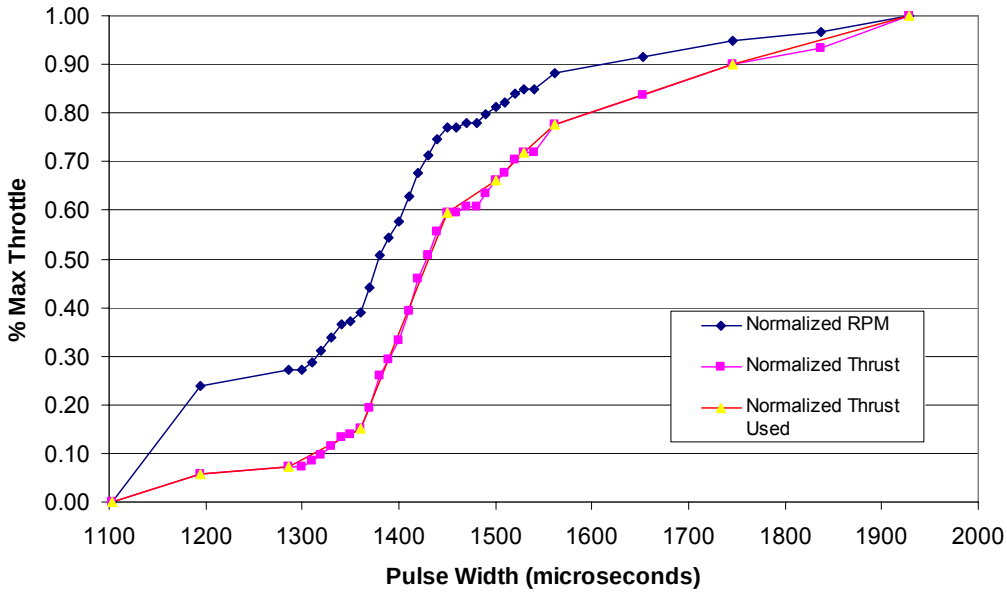

Figure 19: Normalized Thrust and RPM Curves for Engine Calibration

4.4 Yak-54 Servos

The Yak-54 control surfaces used Hitec HS-5985MG digital servos for actuation and the throttle was driven by a Hitec HS-525MG analog servo.

4.5 Piccolo II Installation

The Piccolo II was mounted just to the rear of the wing spar upon a foam mount that was provided by Cloud Cap Technologies. The foam mount was used to reduce vibration during flight.

4.6 Antennas

The Yak-54/Piccolo system requires two antennas for flight operations. The first was a Maxrad low profile 2.4 GHz antenna that was used for UHF communications with the ground station and pilot console. The 2.4 GHz antenna was mounted to a 3.25" x 4" aluminum ground plane to the rear of the aircraft.

The second antenna was a MK-4 GPS antenna used for guidance and position information. The MK-4 was mounted in the Yak-54 canopy on a small 2.5" x 2.5" aluminum ground plane.

4.7 Batteries

Five batteries were used on the Yak-54:

1. Two *Fromeco* "Relion" 5200 mAh 7.4 Volt lithium ion Batteries with two Fromeco "The Regulator" 7.4 Volt to 6 Volt regulators for servo power. The Piccolo had two servo power inputs so no external wiring was required.
2. Two *Thunder Power* "Pro Lite" 2100 mAh 11.1 Volt lithium polymer batteries for Piccolo II main power. These batteries were wired in parallel to provide 4200 mAh of capacity.

4.8 Engine Kill Switch

Due to the inherent risks in testing a new unmanned flight control system, it was important to equip the Yak-54/Piccolo system with a secondary flight termination device that could be used in the event that the aircraft became uncontrollable. An *Electrodynamics* "EDR-107" fiber optic engine kill switch was used for this purpose (Figure 20).

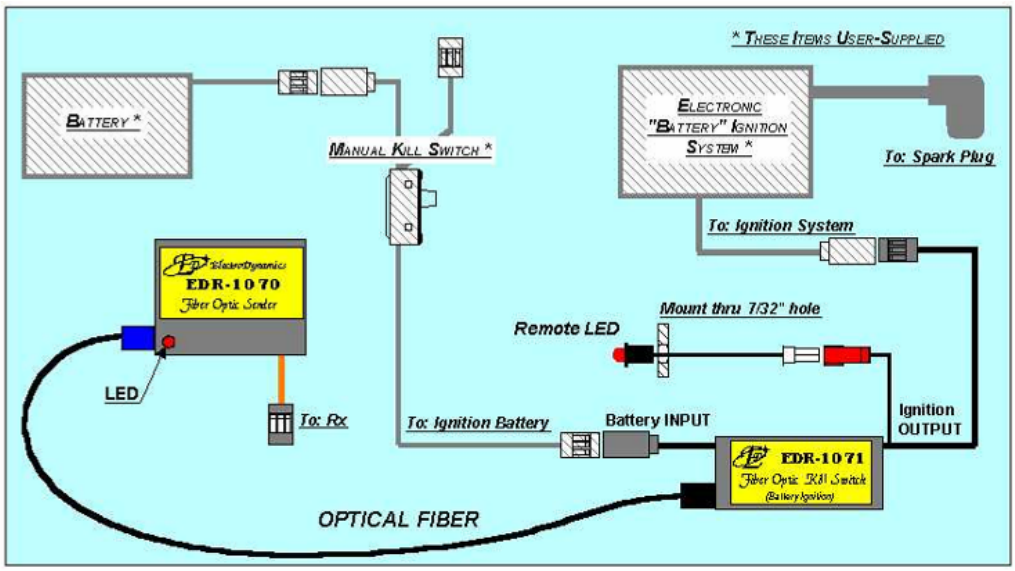

Figure 20: Engine Kill Switch Schematic [35]

The kill switch operates with a standard RC receiver (72 MHz) and a second Futaba pilot console. Should the Yak-54 become uncontrollable and communication cannot be reestablished the kill switch can be triggered only by the secondary pilot console, thus eliminating the possibility of a powered and careening aircraft. The engine kill switch can NOT be triggered because of a power loss to any part of the system. The use of a fiber optic system also greatly reduced the possibility of interference causing the engine to be killed inadvertently.

5 Yak-54 Dynamic Model Development

As mentioned in Chapter 2 the development of a dynamic model is crucial in the development, test and evaluation of a flight control system. Without a good dynamic model the system cannot be tuned pre-flight test with any level of confidence, which can have a significant negative effect on safety of flight. The traditional development techniques used to develop a dynamic aircraft model (parametric models, wind tunnel, CFD, system identification) are not available for use with the Piccolo system. Instead the Piccolo makes use of one of two modeling techniques: the Standard Cloud Cap Simulation model (SCCS) or an Athena Vortex Lattice based aircraft modeling tool. This chapter will detail the development of these two models and compare them to a more traditional parametric technique that made use of Advanced Aircraft Analysis (AAA).

5.1 Advance Aircraft Analysis Based Model

An Advanced Aircraft Analysis Model (AAA) model of the Yak-54 was developed (Reference [33]) using the geometric data listed previously for the straight and level trim condition described in Table 4.

Table 4: Trim Conditions [33]

h	Altitude (Above Sea Level)	400	ft
M	Mach Number	0.106	~
V_a	True Airspeed	70	knots
$\bar{q}$	Dynamic Pressure	16.394	lbs/ft^2
α_1	Angle of Attack	1.95	deg

The dimensionless derivatives calculated by AAA for these trim conditions are shown in Table 5.

Table 5: Yak-54 Stability Derivatives Generated Using AAA

Longitudinal Derivatives			*Lateral Derivatives*		
C_{D_u}	0.0011	rad^{-1}	C_{y_β}	-0.3462	rad^{-1}
C_{D_α}	0.0863	rad^{-1}	C_{y_p}	0.0080	rad^{-1}
$C_{T_{X_u}}$	-0.1546	rad^{-1}	C_{y_r}	0.2324	rad^{-1}
C_{L_u}	0.0017	rad^{-1}	C_{l_β}	-0.0255	rad^{-1}
C_{L_α}	4.5465	rad^{-1}	C_{l_p}	-0.3819	rad^{-1}
$C_{L_{\dot{\alpha}}}$	1.8918	rad^{-1}	C_{l_r}	0.0504	rad^{-1}
C_{L_q}	5.5046	rad^{-1}	C_{n_β}	0.0955	rad^{-1}
C_{m_u}	0.0002	rad^{-1}	$C_{n_{T\beta}}$	-0.0041	rad^{-1}
C_{m_α}	-0.3937	rad^{-1}	C_{n_p}	-0.0171	rad^{-1}
$C_{m_{\dot{\alpha}}}$	-4.3787	rad^{-1}	C_{n_r}	-0.1161	rad^{-1}
C_{m_q}	-8.7532	rad^{-1}	$C_{y_{\delta_a}}$	0.0000	rad^{-1}
$C_{m_{T_u}}$	0.0000	rad^{-1}	$C_{y_{\delta_r}}$	0.2189	rad^{-1}
$C_{m_{T_\alpha}}$	0.0275	rad^{-1}	$C_{l_{\delta_a}}$	0.3490	rad^{-1}
$C_{D_{\delta_e}}$	0.0000	rad^{-1}	$C_{l_{\delta_r}}$	0.0178	rad^{-1}
$C_{L_{\delta_e}}$	0.3762	rad^{-1}	$C_{n_{\delta_a}}$	-0.0080	rad^{-1}
$C_{m_{\delta_e}}$	-0.8778	rad^{-1}	$C_{n_{\delta_r}}$	-0.1129	rad^{-1}

The trim coefficients are presented in Table 6:

Table 6: AAA Steady State Coefficients

C_{L_1}	0.1496
C_{D_1}	0.0528
$C_{T_{X1}}$	0.0515
C_{m_1}	0.0002
$C_{m_{T1}}$	0.0009

5.1.1 Lateral State Space Model and Analysis

From the lateral dimensionless stability derivatives and the trim conditions the

lateral state space model was constructed. Please see Reference [33] for the details of the state space model construction.

$$\begin{bmatrix} \dot{p} \\ \dot{\phi} \\ \dot{\beta} \\ \dot{r} \end{bmatrix} = \begin{bmatrix} -16.6423 & 0.0000 & -35.7516 & 2.3092 \\ 1.0000 & 0.0000 & 0.0000 & 0.0000 \\ 0.0004 & 0.2722 & -0.6017 & -0.9865 \\ 0.0958 & 0.0000 & 43.4267 & -1.8709 \end{bmatrix} \begin{bmatrix} p \\ \phi \\ \beta \\ r \end{bmatrix} + \begin{bmatrix} 454.0359 & 22.8520 \\ 0.0000 & 0.0000 \\ 0.0000 & 0.3353 \\ -14.0214 & -46.9710 \end{bmatrix} \begin{bmatrix} \delta_a \\ \delta_r \end{bmatrix}$$

From the state space models the eigenvalues were used to analyze the modes of the Yak-54.

Table 7: AAA Yak-54 Lateral Modal Analysis [33]

Eigenvalues	*Damping Ratio, ζ*	*Natural Frequency, ω_n (rad/sec)*	*Period, T (sec)*	*Time Constant, τ (sec)*	*Mode*
0.0123	~	~	~	81.3	Spiral
-16.7	~	~	~	0.06	Roll
-1.22 ± 6.54i	0.18	6.64	0.95	~	Dutch Roll

From the eigenvalue analysis it can be seen that the Yak-54 model exhibited the standard three lateral dynamic modes. The spiral mode was slightly unstable, which was to be expected as the Yak-54 wing has no dihedral. The roll mode was quite fast, which would be typical of a very small aerobatic aircraft. The Dutch Roll mode was lower damped than is typical.

5.1.2 Longitudinal State Space Model and Analysis

As with the lateral modes, the longitudinal state space model was formed from the trim conditions and the dimensionless stability derivatives. The details of this calculation can also be found in Reference [33].

$$\begin{bmatrix} \dot{u} \\ \dot{\alpha} \\ \dot{q} \\ \dot{\theta} \end{bmatrix} = \begin{bmatrix} -0.2751 & 12.9976 & 0.0000 & -32.1554 \\ -0.0043 & -7.8357 & 0.9229 & -0.0091 \\ 0.0167 & -19.1618 & -9.6043 & 0.0299 \\ 0.0000 & 0.0000 & 1.0000 & 0.0000 \end{bmatrix} \begin{bmatrix} u \\ \alpha \\ q \\ \theta \end{bmatrix} + \begin{bmatrix} 0.0000 \\ -0.6409 \\ -105.5632 \\ 0.0000 \end{bmatrix} [\delta_e]$$

From the state space model the eigenvalues of the A matrix can be found and a modal analysis performed.

Table 8: AAA Yak-54 Longitudinal Modal Analysis [33]

Eigenvalues	*Damping Ratio ζ*	*Natural Frequency ω_n (rad/sec)*	*Period T (sec)*	*Mode*
-0.133 ± 0.235i	0.49	0.27	23.27	Phugoid
-8.720 ± 4.11i	0.90	9.65	0.65	Short Period

The Yak-54 longitudinal dynamic analysis showed somewhat atypical behavior. The Phugoid mode has higher damping than is typical and the short period mode is very highly damped.

5.2 Athena Vortex Lattice Based Model

The Athena Vortex Lattice modeling tool was the second method used. The first major advantage was that AVL assists the programmer with a graphical representation of the lifting surfaces. Figure 21 shows the geometry for the Yak-54 used in the vortex analysis. Appendix G can be referenced for the AVL simulation model.

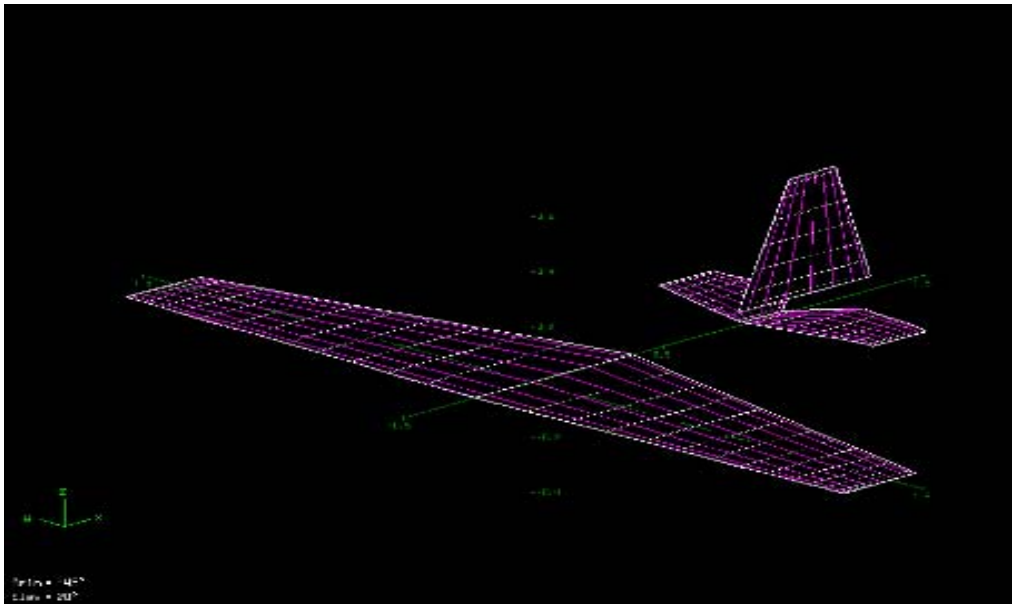

Figure 21: Yak-54 AVL Model

5.2.1 AVL Generated Stability Derivatives: Longitudinal

Table 9 shows the stability derivatives generated by the vortex lattice simulation.

Table 9: AAA vs. AVL Longitudinal Stability Derivatives

Stability Derivative	*AAA*	*AVL*	*% Difference*	*AAA Margin of Error (%)*
C_{L_α}	4.5465 rad^{-1}	3.7007 rad^{-1}	18.60	5
C_{m_α}	-0.3937 rad^{-1}	-0.2850 rad^{-1}	27.61	10
C_{L_q}	5.5046 rad^{-1}	3.5927 rad^{-1}	34.73	20
C_{m_q}	-8.7532 rad^{-1}	-4.3732 rad^{-1}	50.04	20
$C_{L_{\delta_e}}$	0.3762 rad^{-1}	0.3976 rad^{-1}	-5.68	~
$C_{m_{\delta_e}}$	-0.8778 rad^{-1}	-0.7572 rad^{-1}	13.74	~

As can be seen in the table the percentage difference between the two derivative predictions was about twice as large as the margin of error given for AAA. Some of this may be due to the lack of good fuselage modeling in AVL.

The AVL model trimmed at an angle of attack of $\alpha = 1^\circ$ and the trim

coefficients are shown in Table 10.

Table 10: AVL Steady State Coefficients

C_{L_1}	0.1426
C_{D_1}	0.03245
C_{m_1}	0.00974

Another modeling comparison item is the gain scaling terms. The two longitudinal gain scaling terms were $C_{m_{\delta_e}}$ (elevator power) and $\frac{dC_L}{d\delta_e}$ (elevator effectiveness). Elevator effectiveness describes a steady state change in lift with a trim change in elevator and can be calculated as:

$$\frac{dC_L}{d\delta_e} = -\frac{C_{L_\alpha} C_{m_{\delta_e}} - C_{L_{\delta_e}} C_{m_\alpha}}{C_{m_\alpha}} \qquad 5.1$$

Table 11 shows a comparison of these terms as calculated by AAA and AVL.

Table 11: AAA vs. AVL Longitudinal Gain Scaling Terms

Scaling Term	*AAA*	*AVL*	*% Difference*
$C_{m_{\delta_e}}$	-0.8778 rad^{-1}	-0.7570 rad^{-1}	13.70
$\frac{dC_L}{d\delta_e}$	-9.7608 rad^{-1}	-9.3782 rad^{-1}	3.92

The AVL generated gain scaling terms, especially elevator effectiveness, show a fairly good match with the AAA model.

5.2.1.1 Phugoid Approximation

From the derivatives output by the AVL simulator a modal analysis was performed using the Phugoid and short period approximations given in Reference [10]. The Phugoid mode was approximated as motion involving a constant angle of

attack and constant pitching moment. Thus these terms can be neglected in a modal analysis. The linearized longitudinal equations of motion can then be approximated as:

$$\begin{bmatrix} (s - X_u - X_{T_u}) & (g\cos\theta_1) \\ -Z_u & -(Z_q + U_1)s + g\sin\theta_1 \end{bmatrix} \begin{bmatrix} \frac{u(s)}{\delta_e(s)} \\ \frac{\theta(s)}{\delta_e(s)} \end{bmatrix} = \begin{bmatrix} X_{\delta_e} \\ Z_{\delta_e} \end{bmatrix} \tag{5.2}$$

Further approximation were performed by assuming that $Z_q << U_1$ and $\theta_1 \approx 0$. Roskam [10] states that it is appropriate to consider the thrust contribution to the speed damping term as part of the total speed damping effect of the aircraft and thus $X_u \mapsto X_u + X_{T_u}$. This was a useful approximation for our purposes as AVL does not take into account thrust effects, however with such a high thrust to weight ratio this approximation may be inappropriate which will be elaborated on further later on in this section. These approximations yielded a new system of equations:

$$\begin{bmatrix} (s - X_u) & g \\ -Z_u & -U_1 s \end{bmatrix} \begin{bmatrix} \frac{u(s)}{\delta_e(s)} \\ \frac{\theta(s)}{\delta_e(s)} \end{bmatrix} = \begin{bmatrix} X_{\delta_e} \\ Z_{\delta_e} \end{bmatrix} \tag{5.3}$$

The speed and pitch transfer functions were then approximated as:

$$\frac{u(s)}{\delta_e(s)} = \frac{(X_{\delta_e} U_1 s + g Z_{\delta_e})}{U_1(s^2 - X_u s - \frac{g Z_u}{U_1})} \tag{5.4}$$

$$\frac{\theta(s)}{\delta_e(s)} = \frac{(Z_{\delta_e} s - X_u Z_{\delta_e} - X_{\delta_e} Z_u)}{U_1(s^2 - X_u s - \frac{g Z_u}{U_1})} \tag{5.5}$$

The denominator of these two transfer functions were used as the approximate quadratic of the Phugoid mode, with the damping ratio and frequency being written as:

$$\omega_{n_{ph}} \approx \sqrt{\frac{-gZ_u}{U_1}} \tag{5.6}$$

$$\zeta_{ph} \approx \frac{-X_u}{2\omega_{n_{ph}}} \tag{5.7}$$

The speed dimensional derivatives were found from the AVL generated derivatives:

$$Z_u = \frac{-\bar{q}_1 S_w (C_{L_u} + 2C_{L_1})}{mU_1} \tag{5.8}$$

$$X_u = \frac{-\bar{q}_1 S_w \bar{c} (C_{D_u} + 2C_{D_1})}{mU_1} \tag{5.9}$$

Neglecting the dimensionless speed derivatives at low Mach number ($C_{L_u} \approx C_{D_u} \approx C_{m_u} \approx 0$) the dimensional speed derivatives were calculated as:

$$Z_u = -0.4938 \; rad/sec$$

$$X_u = -0.1124 \; rad/sec$$

Finally with these derivatives the Phugoid mode damping and frequency were calculated:

$$\omega_{n_{ph}} \approx 0.367 rad/sec$$

$$\zeta_{ph} \approx 0.15$$

Comparing these to the values in Table 8 it was seen that there is a significant

difference in natural frequency and a significant difference in the damping ratio of the Phugoid mode. One reason for this discrepancy was the removal of X_{T_u} from the Phugoid approximation. If the Phugoid approximation is used on the AAA based data it was seen that the Phugoid mode damping ratio and natural frequency are approximated as:

$$\omega_{n_{ph}} \approx 0.377 rad/sec$$

$$\zeta_{ph} \approx 0.15$$

However, if the X_{T_u} term is added to the Phugoid approximation such that:

$$\zeta_{ph} \approx \frac{-(X_u + X_{Tu})}{2\omega_{n_{ph}}} \qquad 5.10$$

The Phugoid mode damping ratio was recalculated taking into account the propulsion system:

$$\zeta_{ph} \approx 0.365$$

While this approximation of the Phugoid damping ratio is closer to the eigenvalue analysis, it is still off by greater than 40%. The frequency is also not corrected by the addition of X_{T_u} to the analysis.

Clearly the use of conventional analytical techniques did allow a correct analysis of the Phugoid mode using only the aerodynamic data derived from AVL. Additionally the Phugoid approximation only yields accurate representations of the vehicle dynamics in a limited number of cases. The lack of a good thrust model to produce the thrust data significantly degrades our ability to perform any analytical

analysis on the Phugoid mode and thus another way to analyze the Cloud Cap simulator must be used.

5.2.1.2 Short Period Approximation

In order to better understand the short period motion described by the AVL analysis it was useful to perform a short period approximation, as described in Reference [10]. In the short period approximation the speed degree-of-freedom terms in the longitudinal state space model were neglected, as short period motions occur at constant speed. Thus the new equations of motion were approximated as:

$$\begin{bmatrix} s(U_1 - Z_{\dot{\alpha}}) - Z_{\alpha} & -U_1 s \\ -(M_{\dot{\alpha}} s + M_{\alpha}) & (s^2 - M_q s) \end{bmatrix} \begin{bmatrix} \dfrac{\alpha(s)}{\delta_e(s)} \\ \dfrac{\theta(s)}{\delta_e(s)} \end{bmatrix} = \begin{bmatrix} Z_{\delta_e} \\ M_{\delta_e} \end{bmatrix} \tag{5.11}$$

The following additional approximations were made: $Z_{\dot{\alpha}} << U_1$, $Z_q << U_1$ and $\theta_1 \approx 0$. Additionally the thrust contribution were neglected as part of the total static longitudinal stability of the aircraft such that $X_u \mapsto X_u + X_{T_u}$. These approximations yielded the following angle of attack and pitch attitude transfer functions:

$$\frac{\alpha(s)}{\delta_e(s)} = \frac{Z_{\delta_e} + M_{\delta_e} U_1 - M_q Z_{\delta_e}}{U_1 \left\{ s^2 - \left(M_q + \dfrac{Z_{\alpha}}{U_1} + M_{\dot{\alpha}} \right) s + \left(\dfrac{Z_{\alpha} M_q}{U_1} - M_{\alpha} \right) \right\}} \tag{5.12}$$

$$\frac{\theta(s)}{\delta_e(s)} = \frac{\left(U_1 M_{\delta_e} + Z_{\delta_e} M_{\dot{\alpha}} \right) s + \left(M_{\alpha} Z_{\delta_e} - Z_{\alpha} M_{\delta_e} \right)}{s U_1 \left\{ s^2 - \left(M_q + \dfrac{Z_{\alpha}}{U_1} + M_{\dot{\alpha}} \right) s + \left(\dfrac{Z_{\alpha} M_q}{U_1} - M_{\alpha} \right) \right\}} \tag{5.13}$$

From the denominator quadratic the short period mode damping ratio and frequency were found as:

$$\omega_{n_{sp}} \approx \sqrt{\frac{Z_\alpha M_q}{U_1} - M_\alpha} \tag{5.14}$$

$$\zeta_{sp} \approx \frac{-\left(M_q + \frac{Z_\alpha}{U_1} + M_{\dot{\alpha}}\right)}{2\omega_{n_{sp}}} \tag{5.15}$$

The dimensional derivatives were calculated as:

$$Z_\alpha = \frac{-\bar{q}_1 S_w (C_{L_\alpha} + C_{D_1})}{m} \tag{5.16}$$

$$M_q = \frac{\bar{q}_1 S_w \bar{c}^2 (C_{m_q})}{2 I_{yy} U_1} \tag{5.17}$$

$$M_\alpha = \frac{-\bar{q}_1 S_w \bar{c} (C_{m_\alpha})}{I_{yy}} \tag{5.18}$$

$$M_{\dot{\alpha}} = \frac{-\bar{q}_1 S_w \bar{c} (C_{m_{\dot{\alpha}}})}{2 I_{yy} U_1} \tag{5.19}$$

AVL does not compute angular rate terms, $C_{m_{\dot{\alpha}}} = 0$, and thus $M_{\dot{\alpha}} = 0$. The rest of the dimensional derivatives are calculated as:

$$Z_\alpha = -766.5399 \qquad M_\alpha = -34.9539$$

$$M_q = -3.2816 \qquad M_{\dot{\alpha}} = 0$$

From the stability derivatives the short period approximation was used to determine the AVL determined short period mode natural frequency and damping:

$$\omega_{n_{sp}} \approx 7.5\, rad/sec$$

$$\zeta_{sp} \approx 0.6513$$

Using these same approximations with the AAA derivatives the short period mode damping and frequency are:

$$\omega_{n_{sp}} \approx 10.0406\, rad/sec$$

$$\zeta_{sp} \approx 0.89$$

This shows that the use of the short period approximation was a valid assumption in this case. It is interesting to note the effect of neglecting the angular rate term from the short period damping approximation:

$$\zeta_{sp}(M_{\dot{\alpha}} = 0) \approx 0.7253$$

Neglecting the rate damping terms had a significant effect on short period damping, reducing it by 0.165.

5.2.2 AVL Generated Stability Derivatives: Lateral-Directional

Table 12 shows the stability derivative comparison for the lateral-directional terms. The analyses showed that the sideslip and yaw rate associated derivatives were near or within the margin of error. The AAA roll rate derivatives showed much less coupling between lateral and directional motion than does the AVL model. This was also the case in the $C_{l_{\delta_r}}$ term, which shows more rolling moment magnitude with a rudder deflection.

Table 12: AAA vs. AVL Lateral-Directional Derivatives

Stability Derivative	*AAA*	*AVL*	*% Difference*	*AAA Margin of Error (%)*
C_{l_β}	-0.0255 rad^{-1}	-0.0314 rad^{-1}	-23.23	20
C_{n_β}	0.0955 rad^{-1}	0.1052 rad^{-1}	-10.19	15
C_{y_β}	-0.3462 rad^{-1}	-0.2727 rad^{-1}	21.24	20
C_{l_r}	0.0504 rad^{-1}	0.07427 rad^{-1}	-47.37	60
C_{n_r}	-0.1153 rad^{-1}	-0.1156 rad^{-1}	0.57	60
C_{y_r}	0.2324 rad^{-1}	0.2531 rad^{-1}	-8.91	60
C_{l_p}	-0.3819 rad^{-1}	-0.5858 rad^{-1}	-53.38	40
C_{n_p}	-0.0171 rad^{-1}	-0.03874 rad^{-1}	-126.57	25
C_{y_p}	0.0080 rad^{-1}	0.0194 rad^{-1}	-142.98	30
$C_{l_{\delta_a}}$	0.3490 rad^{-1}	0.3707 rad^{-1}	-6.05	~
$C_{l_{\delta_r}}$	0.0154 rad^{-1}	0.02194 rad^{-1}	-43.96	~
$C_{n_{\delta_r}}$	-0.0996 rad^{-1}	-0.1003 rad^{-1}	-0.70	~
$C_{y_{\delta_r}}$	0.1929 *rad^{-1}*	0.2228 rad^{-1}	-15.5	~

The important gain scaling terms in the lateral-directional control system were: aileron effectiveness ($\frac{\partial \overline{p}}{\partial \delta_a}$), rudder power ($C_{n_{\delta_r}}$), rudder effectiveness ($\frac{\partial \beta}{\partial \delta_r}$) and sideslip effect ($C_{y_\beta}$). The effectiveness terms can be determined as:

$$\frac{\partial \overline{p}}{\partial \delta_A} = \frac{C_{l_{\delta_A}}}{C_{l_p}} \tag{5.20}$$

$$\frac{\partial \beta}{\partial \delta_R} = \frac{C_{n_{\delta_R}}}{C_{n_\beta}} \tag{5.21}$$

Table 13 shows the gain scaling terms produced by AAA and AVL.

Table 13: AAA vs. AVL Lateral-Directional Gain Scaling Terms

Scaling Term	*AAA*	*AVL*	*% Difference*
$\frac{\partial \overline{p}}{\partial \delta_a}$	-0.9138 $\left(\frac{rad/sec}{rad}\right)$	-0.6328 $\left(\frac{rad/sec}{rad}\right)$	30.83
$C_{n_{\delta_r}}$	-0.1003 rad^{-1}	-0.0996 rad^{-1}	-0.70
$\frac{\partial \beta}{\partial \delta_r}$	-1.0429 $\left(\frac{rad}{rad}\right)$	-0.9467 $\left(\frac{rad}{rad}\right)$	9.22
C_{y_β}	-0.3462 rad^{-1}	-0.2727 rad^{-1}	21.24

As the table shows, AAA predicts greater rolling and yawing performance with aileron and rudder deflections than does AVL. This would result in a lower gain on the respective feedforward and feedback terms.

5.2.2.1 AVL Based State Space Model Generation and Lateral-Directional Modal Analysis

AVL generated all the necessary derivatives, save N_{T_β}, to generate a complete linear state space of the lateral-directional dynamics. Prior to generating a state space model the lateral-directional dimensional derivatives were constructed. Using the definitions found in Reference [10], the lateral-directional derivatives are shown in Table 14.

Table 14: AVL Generated Lateral-Directional Dimensional Stability Derivatives

Y_β	-55.9849	$\left(\frac{ft/sec^2}{rad}\right)$	L_{δ_a}	481.3165	$\left(\frac{rad/sec^2}{rad}\right)$
Y_p	0.1339	$\left(\frac{ft/sec^2}{rad/sec}\right)$	L_{δ_r}	28.8322	$\left(\frac{rad/sec^2}{rad}\right)$
Y_r	1.7435	$\left(\frac{ft/sec^2}{rad/sec}\right)$	N_β	49.0742	$\left(\frac{rad/sec^2}{rad}\right)$
Y_{δ_a}	0.0	$\left(\frac{ft/sec^2}{rad}\right)$	N_{T_β}	0.0	$\left(\frac{rad/sec^2}{rad}\right)$
Y_{δ_r}	45.7483	$\left(\frac{ft/sec^2}{rad}\right)$	N_p	-0.6061	$\left(\frac{rad/sec^2}{rad/sec}\right)$
L_β	-40.8657	$\left(\frac{rad/sec^2}{rad}\right)$	N_r	-1.8091	$\left(\frac{rad/sec^2}{rad/sec}\right)$
L_p	-25.5565	$\left(\frac{rad/sec^2}{rad/sec}\right)$	N_{δ_a}	0.0	$\left(\frac{rad/sec^2}{rad}\right)$
L_r	3.2405	$\left(\frac{rad/sec^2}{rad/sec}\right)$	N_{δ_r}	-46.7729	$\left(\frac{rad/sec^2}{rad}\right)$

The lateral-directional state space model was constructed using the linearized equations of motion:

$$U_1\dot{\beta} + U_1\dot{\psi} = g\phi\cos\Theta_1 + Y_\beta\beta + Y_p\dot{\phi} + Y_r\dot{\psi} + Y_{\delta_a}\delta_a + Y_{\delta_r}\delta_r \qquad 5.22$$

$$\ddot{\phi} - \overline{A}_1\ddot{\psi} = L_\beta\beta + L_p\dot{\phi} + L_r\dot{\psi} + L_{\delta_a}\delta_a + L_{\delta_r}\delta_r \qquad 5.23$$

$$\ddot{\psi} - \overline{B}_1\ddot{\phi} = N_\beta\beta + N_{T_\beta}\beta + N_p\dot{\phi} + N_r\dot{\psi} + N_{\delta_a}\delta_a + N_{\delta_r}\delta_r \qquad 5.24$$

$$\overline{A}_1 = \frac{I_{xz}}{I_{xx}} \quad \overline{B}_1 = \frac{I_{xz}}{I_{zz}} \qquad 5.25$$

In straight and level flight ($p = \dot{\phi}$, $\dot{p} = \ddot{\phi}$, $r = \dot{\psi}$ and $\dot{r} = \ddot{\psi}$) the equations of motion were written in matrix form as:

$$\begin{bmatrix} 1 & 0 & 0 & -\overline{A}_1 \\ 0 & 1 & 0 & 0 \\ 0 & 0 & U_1 & 0 \\ -\overline{B}_1 & 0 & 0 & 1 \end{bmatrix} \begin{bmatrix} \dot{p} \\ \dot{\phi} \\ \dot{\beta} \\ \dot{r} \end{bmatrix} = \begin{bmatrix} L_p & 0 & L_\beta & L_r \\ 1 & 0 & 0 & 0 \\ Y_p & g\cos\Theta_1 & Y_\beta & (Y_r - U_1) \\ N_p & 0 & (N_\beta + N_{T_\beta}) & N_r \end{bmatrix} \begin{bmatrix} p \\ \phi \\ \beta \\ r \end{bmatrix} + \begin{bmatrix} L_{\delta_a} & L_{\delta_r} \\ 0 & 0 \\ Y_{\delta_a} & Y_{\delta_r} \\ N_{\delta_a} & N_{\delta_r} \end{bmatrix} \begin{bmatrix} \delta_a \\ \delta_r \end{bmatrix} \quad 5.26$$

Using the values given in Table 14 and performing the necessary matrix algebra the lateral-directional state space model was constructed:

$$\begin{bmatrix} \dot{p} \\ \dot{\phi} \\ \dot{\beta} \\ \dot{r} \end{bmatrix} = \begin{bmatrix} -25.5465 & 0.0000 & -42.4133 & 3.2982 \\ 1.0000 & 0.0000 & 0.0000 & 0.0000 \\ 0.0011 & 0.2723 & -0.4739 & -0.9852 \\ -0.3200 & 0.0000 & 49.5492 & -1.8461 \end{bmatrix} \begin{bmatrix} p \\ \phi \\ \beta \\ r \end{bmatrix} + \begin{bmatrix} 481.4849 & 30.2026 \\ 0.0000 & 0.0000 \\ 0.0000 & 0.3872 \\ -5.3924 & -47.1123 \end{bmatrix} \begin{bmatrix} \delta_a \\ \delta_r \end{bmatrix}$$

An eigenvalue analysis was performed on the lateral-directional state space model in order to characterize the lateral-directional dynamics described by the AVL modeling. These results are given in Table 15.

Table 15: AVL Yak-54 Modal Analysis

Eigenvalues	***Damping Ratio***	***Frequency (rad/sec)***	***Period (sec)***	***Time Constant (sec)***	***Mode***
0.0179	~	~	~	55.87	Spiral
-25.5	~	~	~	0.04	Roll
-1.17 ± 7.03i	0.16	7.13	0.88	~	Dutch Roll

This eigenvalue analysis shows similar dynamics to the AAA model, with the biggest difference being in the spiral mode dynamics. A more thorough comparison will be made at the end of this chapter.

5.3 AVL-Piccolo Hardware-in-Loop Simulation and Dynamic Analysis

As stated before there were no inclusion of power or fuselage effects in the AVL model. To get a true description of the dynamics described by the model flight test type data reduction was performed on the open loop dynamics described by the AVL-Piccolo hardware-in-loop simulation. Several data analysis techniques were available that will give an estimation of the damping ratio and frequency of the various modes in flight simulation. For the lowly damped modes the modified transient peak ratio method was used and for the higher damped short period mode the maximum slope method was used. The spiral mode and roll mode were not estimated, the spiral mode because of the very slow time constant that is difficult to confirm in flight test and the roll mode because of a time constant so fast that the dynamics cannot be evaluated at the Piccolo's 20 Hz sampling rate.

5.3.1 Modified Transient Peak Ratio Method

The modified transient peak ratio method (MTPR), as described in Reference [14], was a convenient way to estimate the frequency and damping of an oscillatory response with a damping ratio range of $-0.5 < \zeta < 0.5$. Figure 22 shows the parameters of interest for the MTPR.

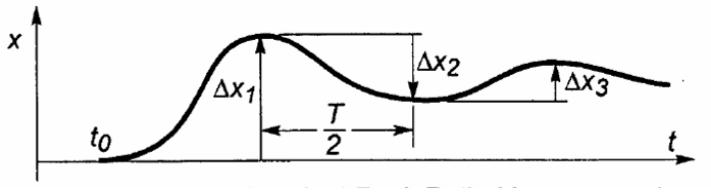

Figure 22: Modified Transient Peak Ratio [14]

The damped frequency was determined as:

$$\omega_d = \frac{2\pi}{T} \tag{5.27}$$

The transient peak ratios were measured as:

$$\frac{\Delta x_2}{\Delta x_1} = \frac{\Delta x_3}{\Delta x_2} = \frac{\Delta x_4}{\Delta x_3} = ... = \frac{\Delta x_{i+1}}{\Delta x_i} \tag{5.28}$$

Typically these ratios do not match exactly so an average was used. Figure 23 was used to determine the damping ratio of the oscillatory response. From the damping ratio the natural frequency was calculated as:

$$\omega_n = \frac{\omega_d}{\sqrt{1-\zeta^2}} \tag{5.29}$$

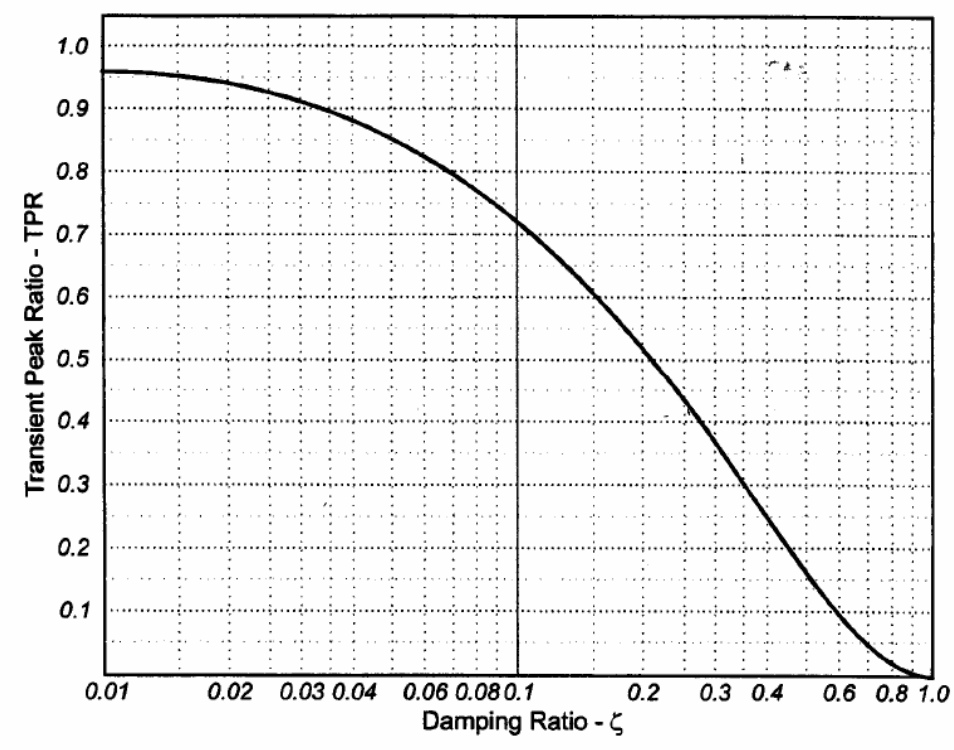

Figure 23: Transient Peak Ratio vs. Damping Ratio [14]

5.3.2 Maximum Slope Method

The maximum slope method (MS), as described in References [14] and [15], was a useful approach for determining the natural frequency and damping ratio when the damping ratio of a time response is between $0.5 < \zeta < 1.2$. Figure 24 shows the parameters used in the MS method.

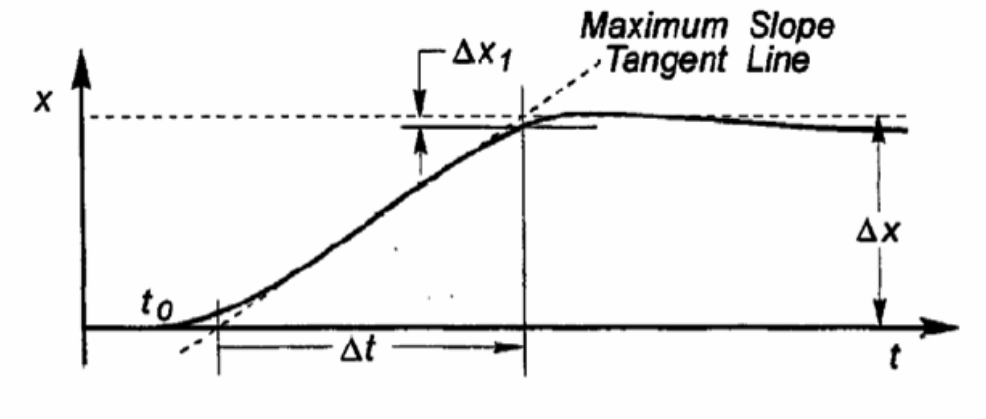

Figure 24: Maximum Slope Method [14]

In the MS method the maximum slope tangent line and the half-cycle peak lines were drawn and from there the intersection of the maximum slope tangent line and the horizontal half-cycle peaks Δt is defined. The second vertical line's intersection with the response curve defines Δx_1. Δx was defined by the distance between the half-cycle peaks. Finally the damping ratio and natural frequency were determined using Figure 25.

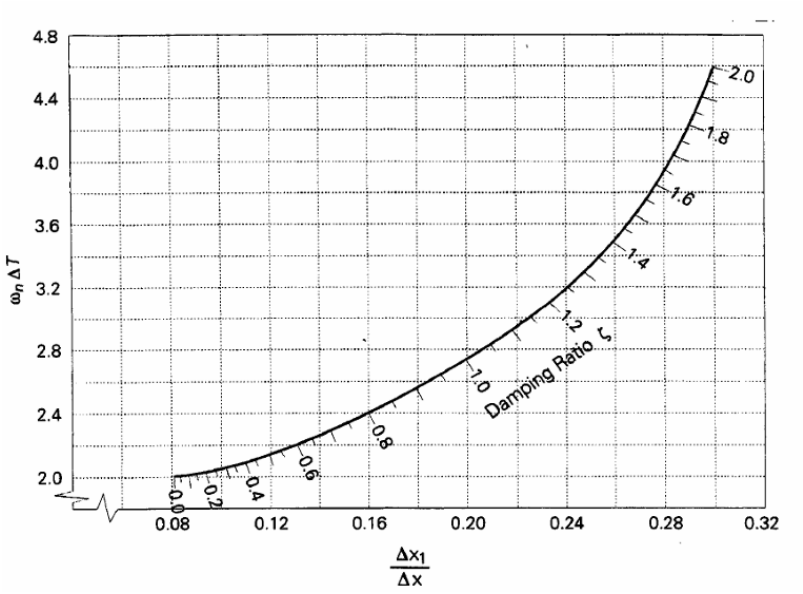

Figure 25: Maximum Slope Method for Determining ζ and ω_n [14]

The natural frequency was computed as:

$$\omega_n = \frac{\omega_n \Delta T}{\Delta T} \tag{5.30}$$

5.3.3 Open Loop Modal Analysis: Phugoid Mode

Using the AVL-Piccolo hardware-in-loop simulation the Phugoid mode dynamics were analyzed using the modified transient peak ratio method. The Phugoid mode dynamics were excited using a step elevator input that lasted until the airspeed had left trim (≈ 70 knots) by approximately 5 knots. At that point the elevator is released and the aircraft is allowed to oscillate freely. Figure 26 shows a time history of this test.

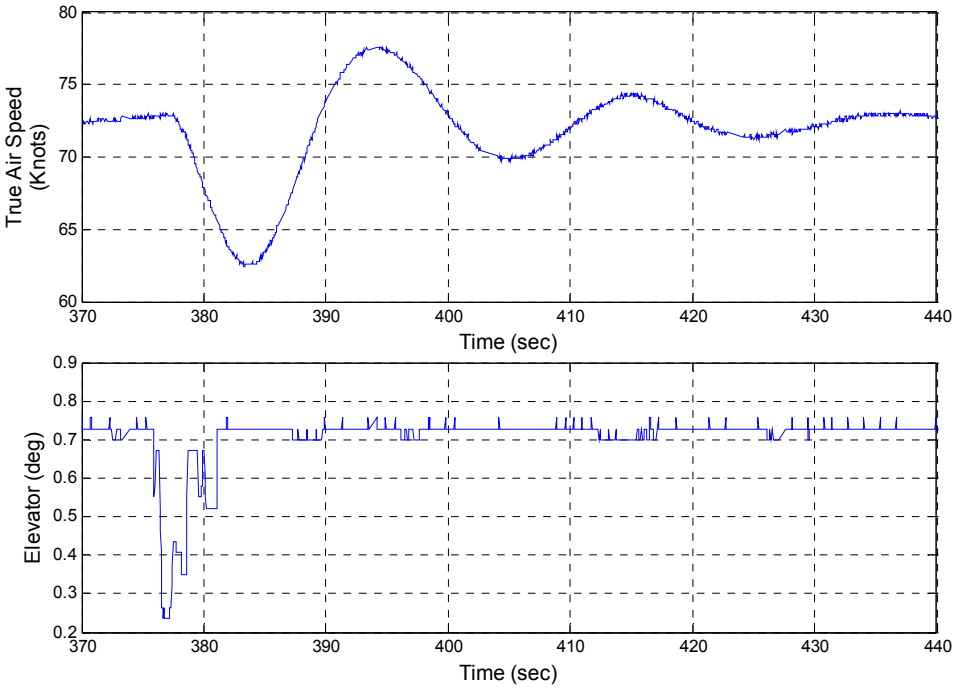

Figure 26: AVL-Piccolo HIL Phugoid Simulation Response

The reader is referenced to Appendix H for the calculation tables used to determine the damping and frequency which yielded the following results:

$$\omega_{n_{ph}} = 0.3 \; rad/sec$$

$$\zeta_{ph} = 0.17$$

5.3.4 Open Loop Modal Analysis: Short Period Mode

Using the AVL-Piccolo hardware-in-loop simulation the short period mode dynamics were analyzed using the maximum slope method. The short period mode was excited using an elevator doublet. Figure 27 shows the short period time response.

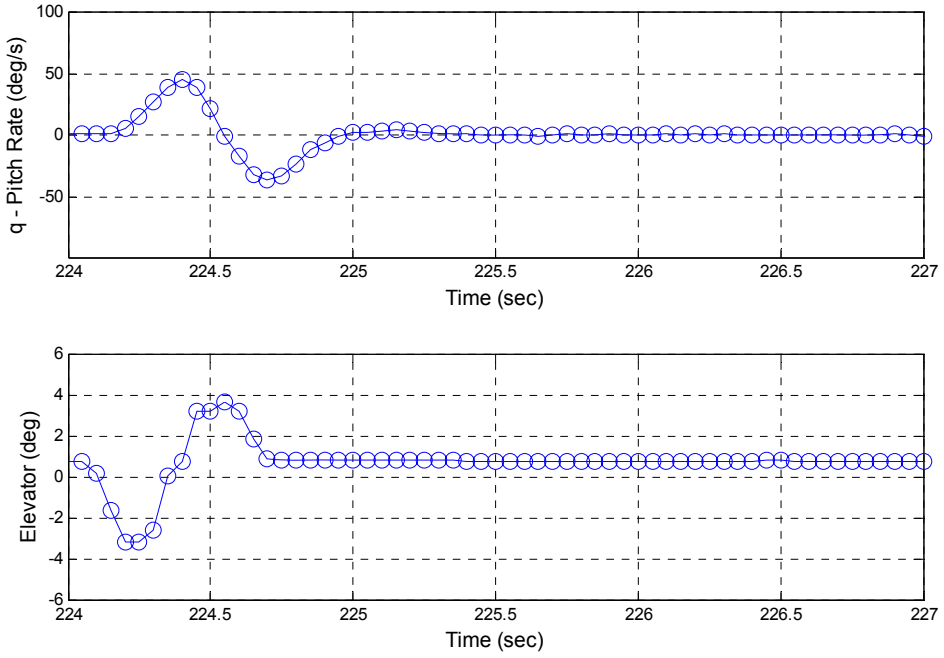

Figure 27: AVL-Piccolo HIL Short Period Simulation Response

The reader is referenced to Appendix I for the calculation tables used to determine the damping and frequency of the short period response which yielded the following results:

$$\omega_{n_{sp}} = 12.89 \; rad/sec$$

$$\zeta_{sp} = 0.85$$

5.3.5 Open Loop Modal Analysis: Dutch Roll Mode

Using the AVL-Piccolo hardware-in-loop simulation the Dutch roll mode dynamics were analyzed using the maximum slope method. The Dutch roll mode was excited using a rudder doublet. Figure 28 shows the Dutch roll time response.

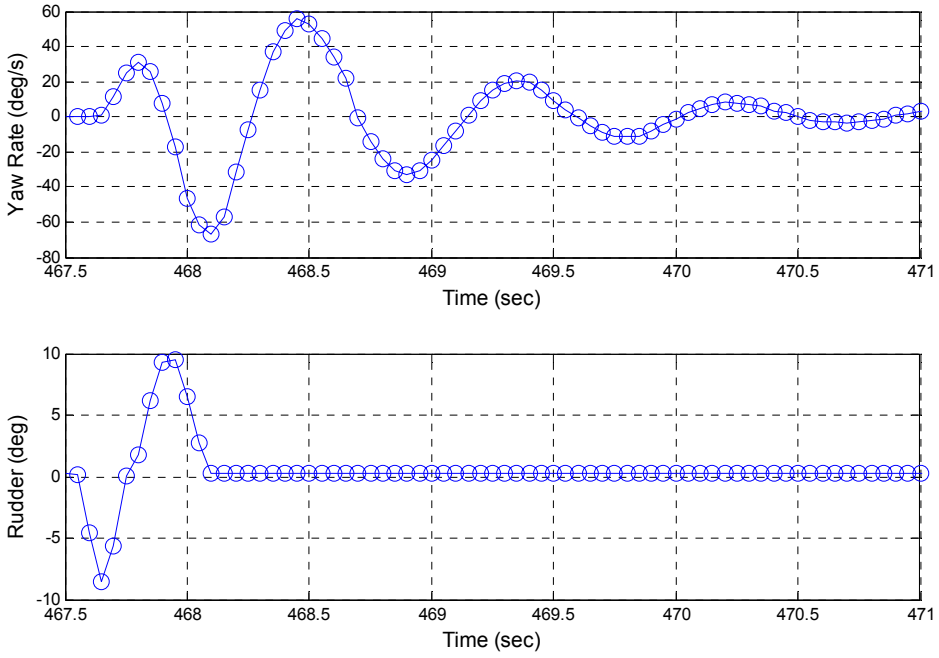

Figure 28: AVL-Piccolo HIL Dutch Roll Mode Simulation Response

The reader is referenced to Appendix I for the calculation tables used to determine the damping and frequency of the Dutch roll response which yielded the following results:

$$\omega_{n_{dr}} = 7.06\ rad/sec$$

$$\zeta_{dr} = 0.15$$

5.4 Standard Cloud Cap Aircraft Modeling and Simulation

The major disadvantage of the Standard Cloud Cap Simulator is that the only stability derivatives output by the system that the engineer can use to analyze the simulator and troubleshoot changes are the gain scaling parameters. The best way to

analyze the validity of the simulator therefore was to perform time response modal excitation and then reduce the data to approximate the damping ratio and natural frequency of the oscillatory modes and the time constant of the first order modes. Using the same data analysis techniques used in the AVL-HIL model the SCCS simulation model can be analyzed. From Reference [33] we see that the modes exhibited the characteristics shown in Table 16.

Table 16: SCCS Modal Analysis [33]

Mode	*Damping Ratio ζ*	*Natural Frequency ω_n (rad/sec)*	*Period T (sec)*	*Time Constant (sec)*
Dutch Roll	0.15	9.08	0.69	~
Short Period	0.67	12.67	0.50	~
Phugoid	0.16	0.36	17.45	~

5.5 Simulation Model Dynamics Comparison

Three methods of modeling and simulation have been discussed as well as two methods for the evaluation of the AVL simulation model. It is appropriate now to make a comparison between the various methods. Table 17 shows the dynamic parameters for the various modes.

Table 17: Simulator Model Modal Comparison

	Spiral	*Roll*	*Dutch Roll*		*Short Period*		*Phugoid*	
Source	*τ (sec)*	*τ (sec)*	*ω_n (rad/sec)*	*ζ*	*ω_n (rad/sec)*	*ζ*	*ω_n (rad/sec)*	*ζ*
AAA	81.3	0.06	6.64	0.18	9.65	0.90	0.27	0.49
SCCS	~	~	9.08	0.15	12.67	0.67	0.36	0.16
AVL	55.87	0.04	7.13	0.16	7.50	0.65	0.37	0.15
AVL-HIL	~	~	7.06	0.15	12.89	0.85	0.30	0.17

Table 17 shows the Dutch roll dynamics were fairly similar between the AVL

and AAA simulators, with the most variation being in frequency. It was interesting to note that the AVL-HIL model shows a large difference in the short period mode as opposed to using the short period approximation in the AVL aerodynamics only model. This is most likely due to some power effects in the Cloud Cap simulator, but this cannot be known for certain as the simulator acts as a "black box" with the input data. The accuracy of the frequency estimation from simulation for a highly damped mode like the short period mode is not especially accurate and thus the short period frequency data was not reliable.

The Phugoid mode showed the biggest variation among the modeling techniques. The AVL vs. SCCS show minimal differences, and the AVL-HIL showed slightly higher damping and lower frequency than the Phugoid approximated AVL terms. The AAA model showed significant differences in Phugoid from the other models. The question remained, which model is closest to the truth? To determine this open-loop flight tests were performed to compare to the modeling techniques. Chapter 8 will present this evaluation.

6 Flight Test Planning and Preparation

Prior to any flight test program thorough flight test planning is required. The lead flight test engineer must decide how many and what type of personnel to include in the test program and define their responsibilities. He or she must also define the airfield location, instrumentation required, weather limitations, develop thorough pre-flight checklists, ensure thorough ground testing has been performed, and finally lead a team of engineers in a dynamic flight test environment. This section will detail the flight planning and pre-flight operations that took place before any Yak-54 flight test.

6.1 Preflight Checkout

Prior to flight testing thorough ground testing of the Piccolo II flight control system and Yak-54 was performed. It was important before any flight activity to verify that all systems to be used were operating as expected. The aircraft was thoroughly tested to ensure that the servos and control surfaces were calibrated appropriately, telemetry (GPS, air data, rates, accelerations, Euler attitude angles, signal strength) was being received accurately, the engine was running properly, etc. Taxi tests were performed as well, to ensure steering was working appropriately, that the UHF signal strength was strong, and that vibration did not cause any items on the aircraft to come loose. Appendix J contains a detailed description of the ground testing procedures followed.

Immediately prior to every flight a thorough pre-flight check list was followed. This checklist, which requires dual signatures of the Flight Test Engineer

and the Vehicle Engineer, ensures that the vehicle and ground station are ready for flight. Appendix K can be referenced for the pre-flight checklist in its entirety.

6.2 Flight Test Team

In order for the flight test to run smoothly the flight test team members and their respective responsibilities must be explicitly defined.

6.2.1 Flight Test Engineer (FTE)/Command and Control Engineer

The FTE was responsible for the following:

1. Responsible for overall test and crew members
2. Briefed crew and pilot on responsibilities
3. Hade go/no-go decision
4. Performed pre-flight checks with the Vehicle Engineer
5. Communicated with the pilot during flight test
6. Communicated with engineering team during flight test
7. Instructed the pilot on which flight test point to follow
8. Responsible for managing the Piccolo ground station
9. Relayed all gain changes determined by the engineering team to the Piccolo
10. Ensured ground station is in proper working order
11. Responsible for all autonomous flight commands to the Piccolo
12. Made Piccolo autopilot activation/deactivation calls
13. Made gain tuning decisions

6.2.2 Flight Test Pilot in Command (PIC)

The PIC had the following responsibilities:

1. Safety was the PIC's highest responsibility
2. Made independent per-flight checks
3. Performed all manual flight activities
4. Activated/Deactivated autopilot
5. Deactivated the autopilot if the PIC judged the aircraft to be entering an unsafe flight condition
6. Assisted engineers with aircraft performance evaluation

6.2.3 Vehicle Engineer (VE)

The VE had the following responsibilities:

1. Ensured aircraft is in proper working order
2. Performed Weight and Balance
3. Confirmed avionics and power systems were installed appropriately and are in working order
4. Ensured all control surface actuators are properly installed and calibrated
5. Performed pre-flight checks with the FTE
6. Ensured engine is tuned and in working order

6.2.4 Safety Officer (SO)

The SO had the following responsibilities:

1. Ensured all procedures detailed in this document are followed

2. Ensured only maneuvers specified in the dance cards are performed
3. Had go/no-go authority with regards to safety
4. Observed that general safe practices are followed
5. Made 5, 10 and 15 minute engine ON time calls
6. Checked FTE gain entries

6.2.5 Data Processing Engineer (DPE)

The DPE had the following responsibilities

1. Evaluated in flight data
2. Evaluated maneuver performance acceptability
3. Communicated flight test point maneuver that is desired to the FTE
4. Made go/no-go recommendations to the FTE with regards to flight data quality

6.2.6 Pilot Assistant (PA)

The PA had responsible for the following:

1. Assisted the PIC in intra-team communications
2. Read test card points to the PIC
3. Assisted the PIC in vehicle trimming
4. Performed air traffic scanning for the pilot
5. Generally assisted the PIC during the entire test phase

6.2.7 Video Operator (VO)

The VO was responsible for filming all flight activities during the test.

6.2.8 Flight Test Organizational and Communications Flow Charts

The flight test communications and organizational charts are displayed in Figures 34 and 35. It was important that communications and decision making flow in the order dictated by the flow charts, minimizing confusion that could have resulted in longer testing times, poor data, or at worse loss of the aircraft.

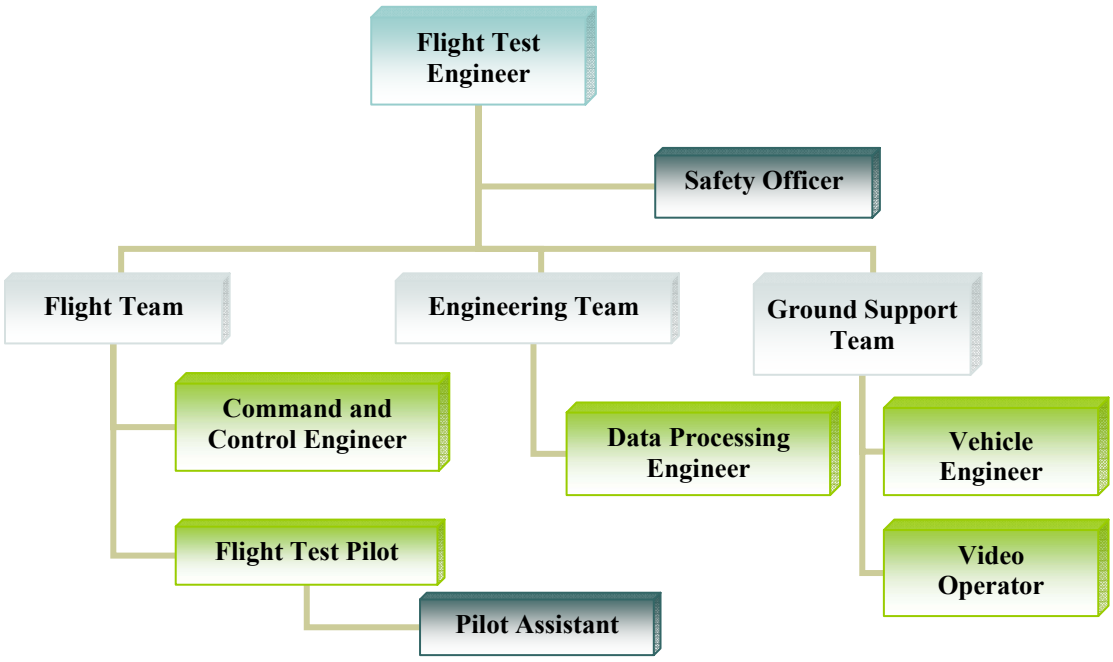

Figure 29: Flight Test Organizational Chart

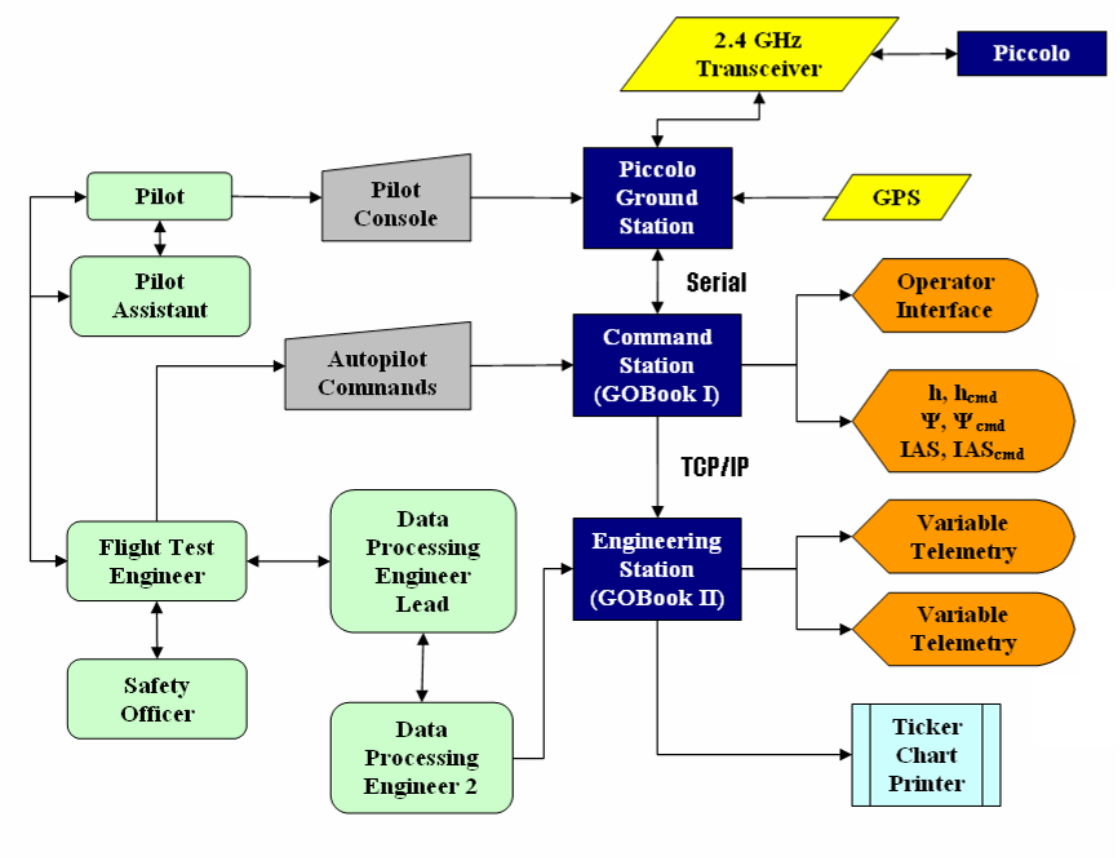

Figure 30: Flight Test Communication Flow Chart

6.3 Emergency Procedures

An emergency procedure was established in the event that the aircraft becomes uncontrollable. This emergency procedure prevented the possibility of a careening aircraft that could fly uncontrolled for a number of miles. If the Piccolo lost communication with the aircraft for longer than the communications time-out limit (2.0 seconds for communications timeout, 0.2 seconds for Pilot timeout) the Piccolo would automatically engage and command the aircraft to go to the lost communications waypoint. This waypoint was a fixed orbit in the middle of the flight test area with a radius of 500 ft. Reacquisition of the communication link

would be attempted while the aircraft is orbiting. The pilot would continue to attempt control reacquisition until the aircraft is terminated or control could be reestablished and an emergency landing attempted with zero power. If communication could not be reestablished the engine would be killed using the 72 MHz emergency engine kill switch and the aircraft should descend and crash. In the event that the aircraft could not maintain the lost communications orbit and appeared to be careening out of the flight test area the pilot would call "KILL KILL KILL" and the safety officer would hit the engine kill switch on the 72 MHz Futaba transmitter, killing the engine.

6.4 Flight Test Area

Yak-54 flight tests were conducted principally at the Foley Airfield (Figure 31) south of Lawrence, KS (38°49'37.85"N 95°16'2.28"W).

Figure 31: Foley Airfield and Flight Test Area

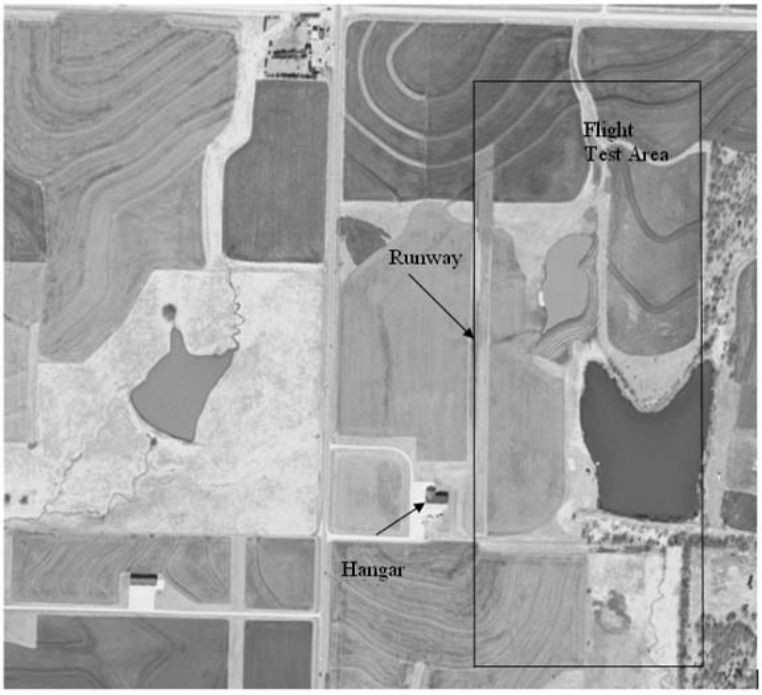

7 Manual Control Flight Test

The objective of the manual control test was to determine the controllability of the aircraft with the Piccolo system installed and operating in the RC mode. The Piccolo in ground testing had exhibited some discrete time lag between pilot inputs and control surface movement. Additionally there were discrete motions in the actuator movement that were caused by 10 Hz sampling of the Futaba pilot console. These discrete actuator movements were not present when a standard RC controller and receiver were used. The Hitec HS-5985MG servos were high performance hobby grade digital servos, with an operating speed of 0.13 sec/60º, and thus it was anticipated that the aircraft dynamics would damp out any discrete servo operation because the servos operated so quickly. Discussions with Cloud Cap Technology about the discrete servo operation caused by the 10 Hz pilot console sampling revealed that the pilot console sampling rate could not be increased and because no improvements could be made on the user-end with the resources available it was decided to accept these limitations for the Yak-54/Piccolo test program and proceed. The discrete time-lag of the Piccolo system under manual control remained the biggest concern to the flight test team and the effects on handling qualities needed to be determined.

The standard test maneuver was a "race track" (Figure 32) as well as full stop takeoffs and landings. The pilot will then give an analysis of the handling qualities of the aircraft in general and as compared with those of the same aircraft under standard RC control. If adjustments could be made with the pilot analysis they would be

performed, otherwise the flight test program would proceed to the next phase. The reader is referenced to Appendix L for the handling qualities flight test dance card.

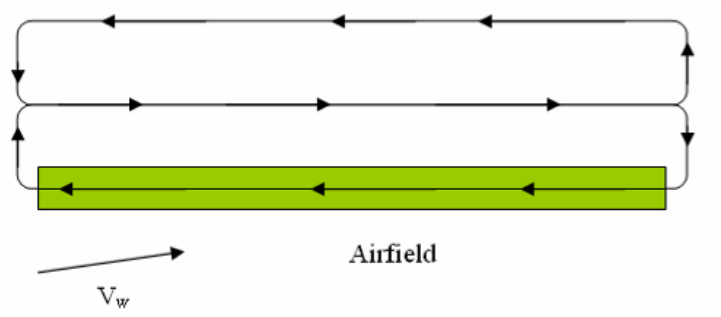

Figure 32: Race Track Pattern

7.1 Manual Control Tests Results

During the in pattern flights of the Yak-54 the pilot did not report deficient manual control. However, during the approach to landing phase of the flight test the pilot had significant difficulty landing the aircraft. It was originally supposed that poor short period damping due to low static margin was the cause of this pitch instability. The C.G. was placed at the manufacturers recommended location, 3.5 inches to the rear of the leading edge of the wingtip, but it was theorized that perhaps the increase in weight of 5 lbs due to the Piccolo system had decreased short period damping with the C.G. at this location. The true cause of the poor pitch stability was determined later to be not only the 10 Hz sampling of the pilot console, which adds as much as a 0.1 second lag in pilot control, but additional discrete time lag due to uplink data dropouts (Figure 33).

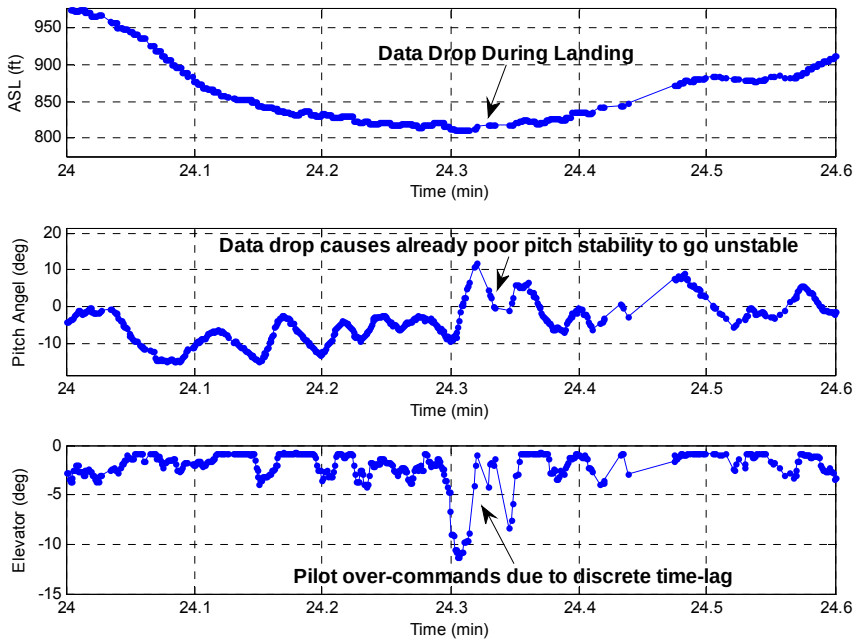

Figure 33: Pilot-in-loop Pitch Instability

Figure 33 shows poor pitch damping during approach to landing that goes unstable when there are indications of data dropouts. It should be noted that uplink data drops (e.g. pilot commands) are NOT shown in the stored telemetry data. Thus there could be additional loss of pilot commands not shown in the telemetry.

The data uplink issues were not known at this point of the flight test but several measures were taken to increase pitch stability. First the C.G. was moved forward 0.5 inches. It was shown in the parameter identification flight tests that this resulted in a short period mode damping of $\zeta_{sp} = 1.0$. The pilot also made a conscious effort to "lead" the aircraft, thus counteracting some of the discrete time lags associated with the 10 Hz sampling. Figure 34 shows improved pitch stability, although the pilot still reported poor handling qualities as compared with a standard RC controlled Yak-54.

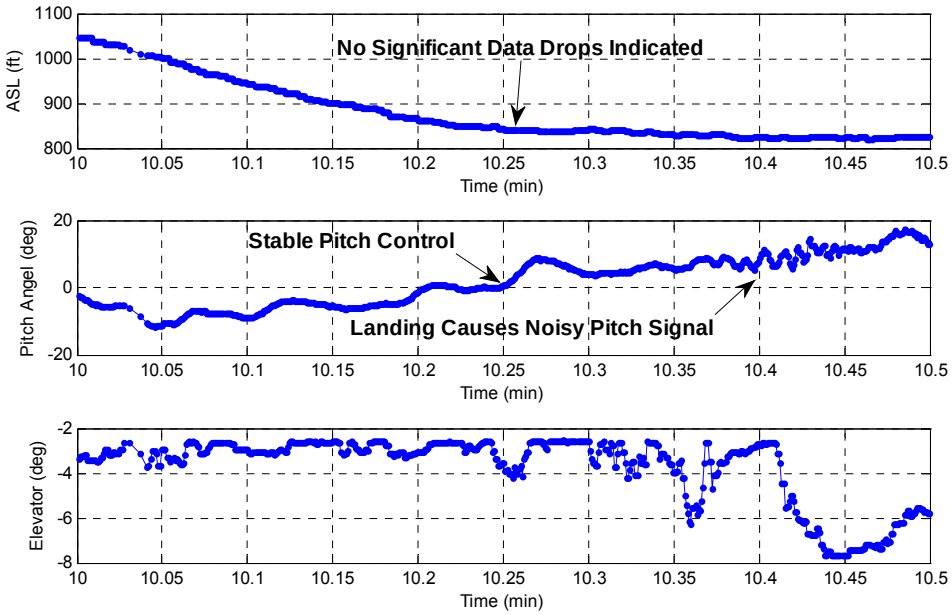

Figure 34: Stabilized Pilot-in-Loop Pitch Control

It should be noted that in this telemetry there was no indication of downlink data loss.

At this point, as the data uplink issue had not been discovered, it was decided that the handling qualities, although poor, were good enough to continue on to the open-loop Yak-54 flight testing program.

8 Parameter Identification Flight Testing

As stated in Chapter 5, there existed some significant discrepancies between the various simulation model dynamics. In order to determine the "real" dynamics flight tests had to be performed. Three open-loop flight tests were performed and analyzed: Dutch roll, short period and Phugoid mode flight tests. A fourth flight test that excited the roll mode was performed but the roll mode dynamics were difficult to compare with simulation without direct flight test data input into the simulator as the pilot commands are not constant and the roll mode is so fast (0.05 seconds). This section will describe in detail the tests, data reduction and results. Finally a comparison with the simulator dynamics will be presented. Appendix M can be referenced for the open loop flight testing dance card.

8.1 Dutch Roll Mode Flight Test

The Dutch roll mode flight test was designed similarly to the Dutch roll mode test performed on the AVL-Piccolo HIL simulator (Section 5.3.5). The first task in any flight test is to trim the aircraft properly. Reference [14] states that the general rule of thumb for trim in a manned aircraft is ± 0.5 KIAS and ± 20 ft altitude for 10 seconds. These values were doubled for our remotely piloted aircraft, so that trim was taken as ± 1.0 KIAS and ± 20 ft altitude for 5 seconds.

After trimming the aircraft properly the pilot excited the Dutch roll mode using a rudder doublet or singlet. The response could then be analyzed using the modified transient peak ratio method.

8.1.1 Dutch Roll Mode Flight Test Results

One Dutch roll excitation with a rudder singlet and two Dutch roll excitations with a rudder doublet were performed on the Yak-54. The three Dutch roll responses are presented in Figure 35, Figure 36 and Figure 37.

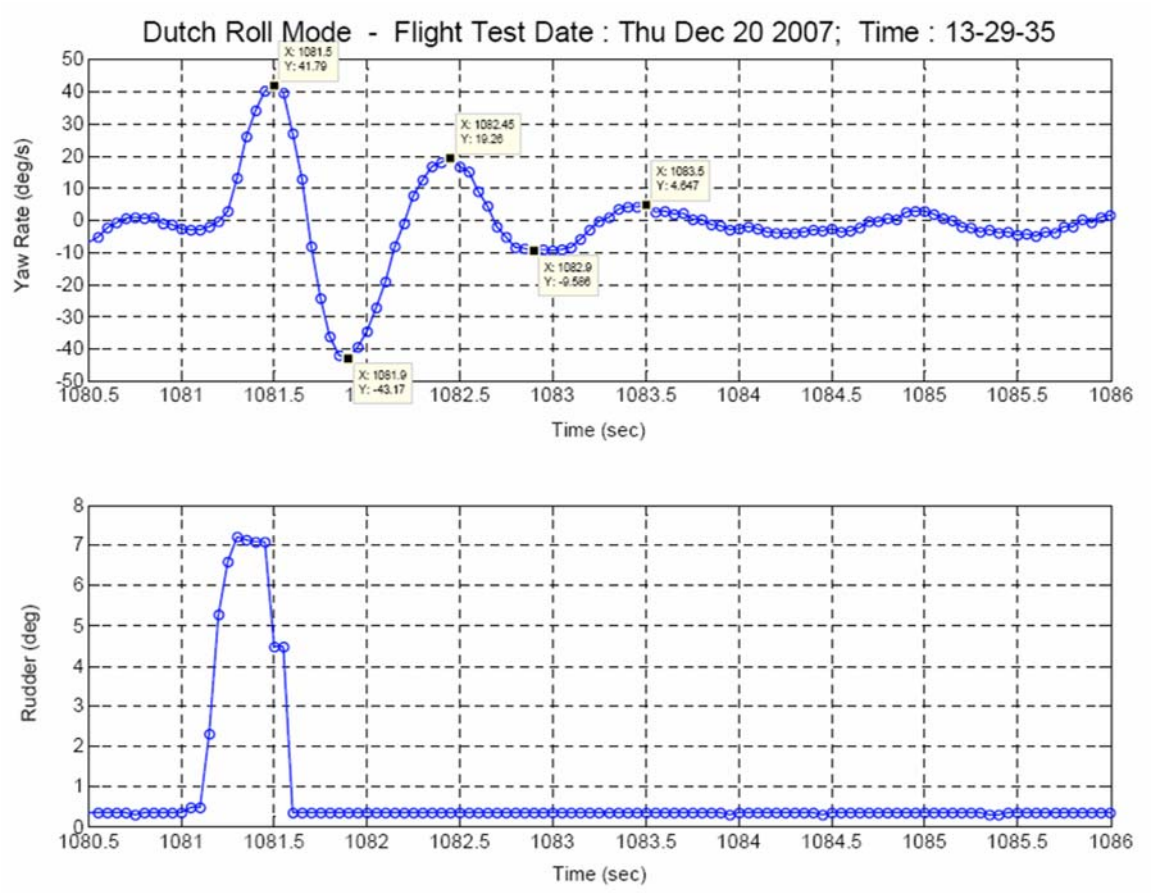

Figure 35: Flight Test Dutch Roll Excitation #1 [33]

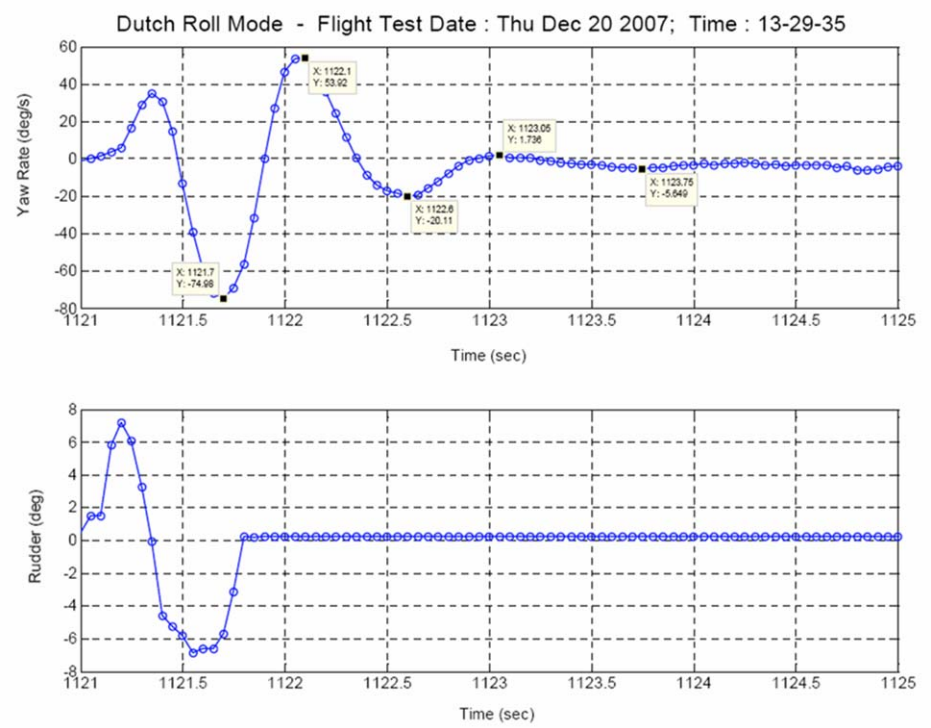

Figure 36: Flight Test Dutch Roll Excitation #2 [33]

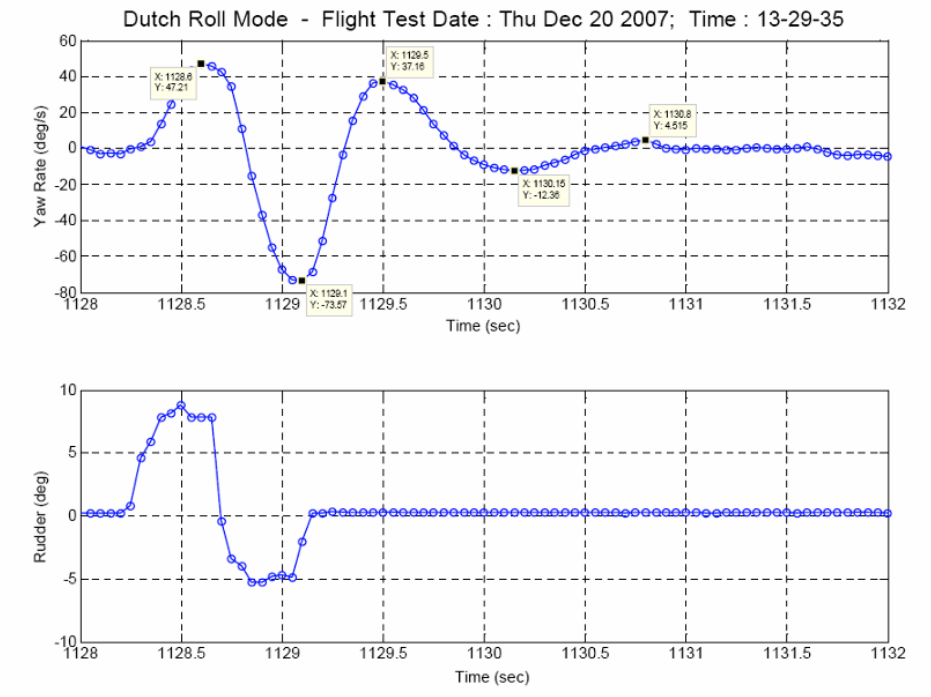

Figure 37: Flight Test Dutch Roll Excitation #3 [33]

Using the MTPR method the frequency and damping ratio can be extracted from the flight test data. The data analysis tables can be found in Appendix N and the results of this analysis are presented in Table 18.

Table 18: Dutch Roll Flight Test Results

	Test I	***Test II***	***Test III***	***Average***
Damping Ratio, ζ_{dr}	0.23	0.22	0.26	0.24
Natural Frequency, $\omega_{n\,dr}$ (rad/sec)	6.05	5.68	5.92	5.88

An analysis of these results versus the simulation models is presented at the end of this chapter.

8.2 Short Period Mode Flight Test

As with the AVL-Piccolo HIL simulation test (Section 5.3.4) the short period mode was excited using an elevator doublet.

8.2.1 Short Period Mode Flight Test Results

Three short period data sets were used for dynamic analysis and are presented in Figure 38, Figure 39, and Figure 40.

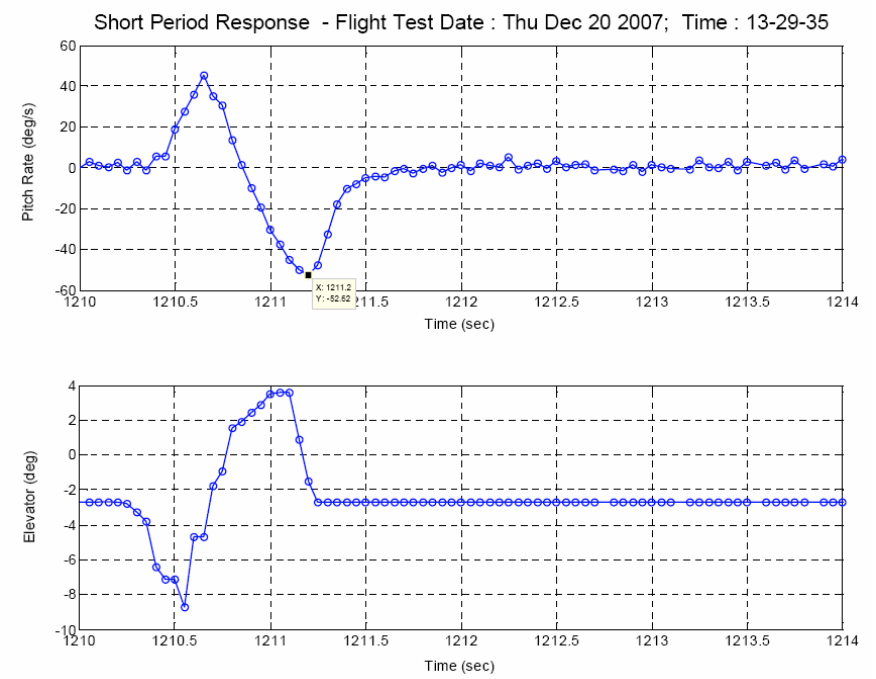

Figure 38: Flight Test Short Period Excitation #1 [33]

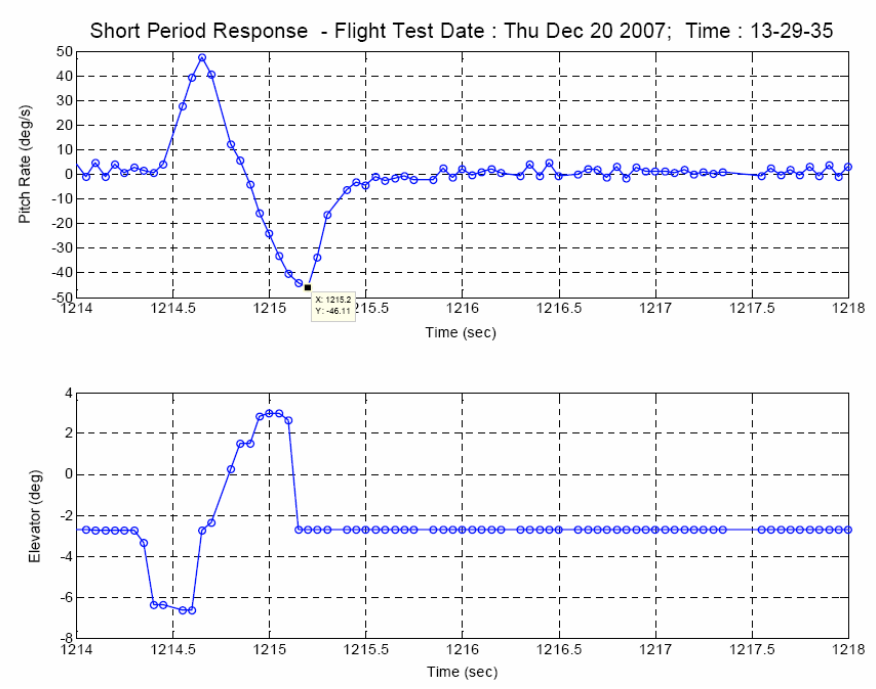

Figure 39: Flight Test Short Period Excitation #2 [33]

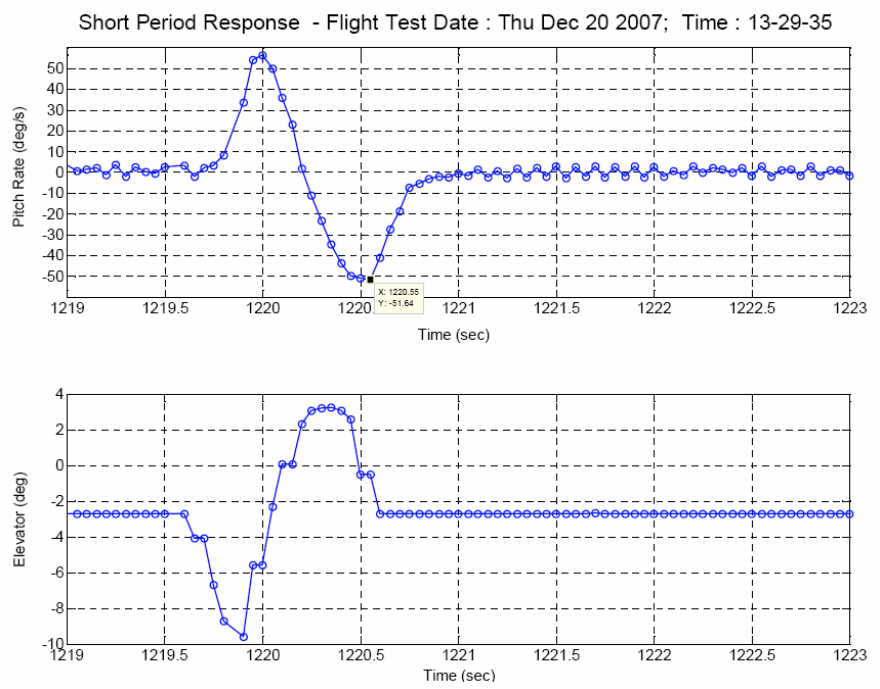

Figure 40: Flight Test Short Period Excitation #3 [33]

8.2.2 Short Period Data Processing Using the Time-Ratio Method

Reference [33] used the time-ratio (TR) method to analyze the short period data presented above. This method, as described in Reference [14], is useful when the damping ratio is near $\zeta = 1.0$. The TR utilizes three specific values with respect to the steady state value along the response curve. The time along the response curve for 0.736Δx, 0.406Δx and 0.199Δx, as shown in Figure 41, was taken.

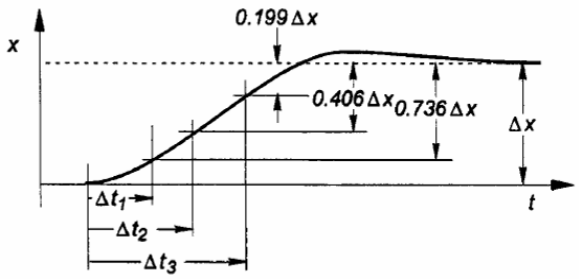

Figure 41: Time-Ratio Method [14]

From these values the ratios $\Delta t_2/\Delta t_1$, $\Delta t_3/\Delta t_1$, and $(\Delta t_3 - \Delta t_2)/(\Delta t_2 - \Delta t_1)$ were used in Figure 42 to obtain three estimates of ζ. These three estimates are then averaged together to obtain the final value of ζ.

The results of this analysis technique are presented in Table 19.

Table 19: Short Period Mode Flight Test Results

	Test I	***Test II***	***Test III***	***Average***
Damping Ratio, ζ_{sp}	0.97	1.0	1.03	1.0
Natural Frequency, $\omega_{n\,sp}$ (rad/sec)	13.47	19.96	16.44	16.62

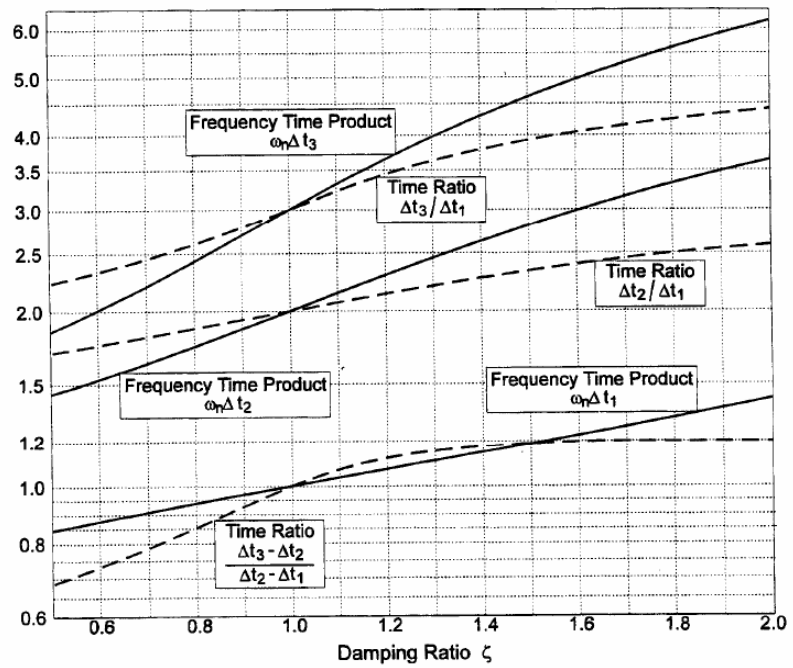

Figure 42: Time-Ratio Method Data Reduction Plot [14]

From the plots it was easy to see the short period response is more or less first order. This was easy to anticipate, as the forward movement of the C.G. would result in a highly damped short period mode. This highly damped short period mode helps

maintain pitch stability during loss of pilot data packets during manual operations. A comparison with the simulation models will be presented at the end of this chapter.

8.3 Phugoid Mode Flight Test

The Phugoid mode was the most difficult of the three oscillatory modes to analyze in flight test, as it was so slow that one period of motion, and sometimes even a half-period, cannot be achieved before the pilot has to reestablish control before the aircraft leaves safe visual range. The Phugoid mode in flight test was excited using an elevator step input. The elevator was held until the airspeed drops about 10 knots from trim (≈ 70 knots). Once the airspeed drop has occurred the pilot releases the elevator and the aircraft is allowed to oscillate freely. Figure 43 and Figure 44 show the results of the open-loop Phugoid mode flight tests.

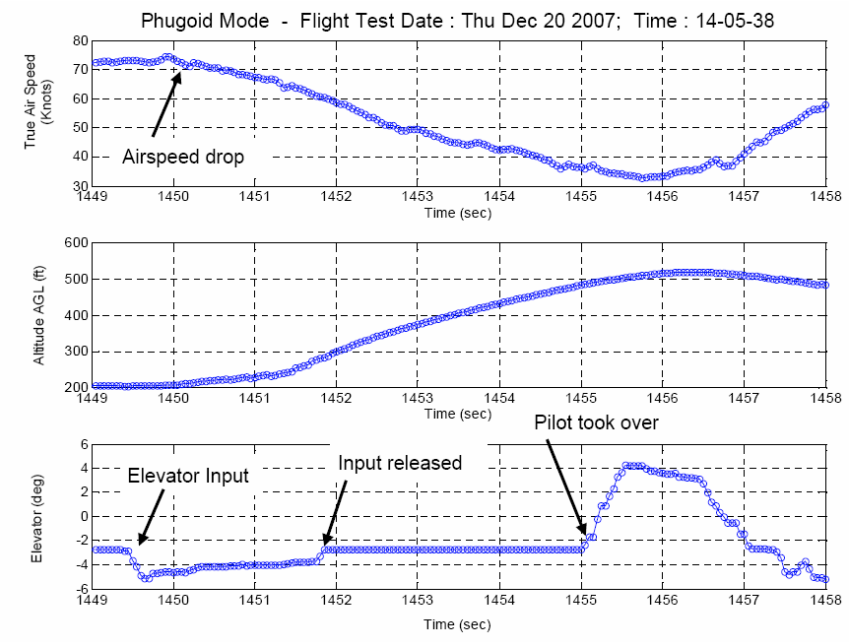

Figure 43: Flight Test Excitation of the Phugoid Mode #1 [33]

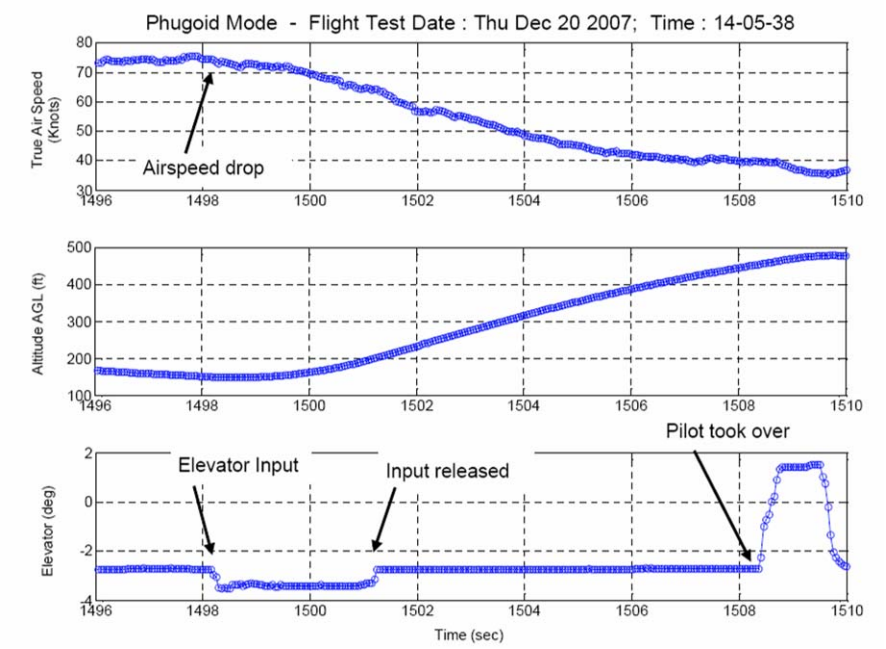

Figure 44: Flight Test Excitation of the Phugoid Mode #2 [33]

As can be seen by the figures, the Phugoid mode was extremely slow, coming close to reaching the half-period peak at about 10 seconds into the test in the second plot. The airspeed also drops significantly, all the way to around 40 knots IAS. Classical data reduction techniques, like the MTPR method, cannot be used to analyze the dynamics presented in these data. However, it can be useful to make a graphical comparison with the various modeling and simulation packages analyzed before. This will be done in the following section.

8.4 Flight Test vs. Simulation Model Dynamics

It is now appropriate to compare the simulation model dynamics with the flight test data. Table 20 presents all the open-loop dynamic results presented in this document.

Table 20: Flight Test vs. Simulation Model Dynamics

	Dutch Roll		*Short Period*		*Phugoid*	
Source	ω_n ***(rad/sec)***	ζ	ω_n ***(rad/sec)***	ζ	ω_n ***(rad/sec)***	ζ
AAA	6.64	0.18	9.65	0.90	0.27	0.49
SCCS	9.08	0.15	12.67	0.67	0.36	0.16
AVL	7.13	0.16	7.50	0.65	0.37	0.15
AVL-HIL	7.06	0.15	12.89	0.85	0.30	0.17
Flight Test	6.05	0.24	16.62	1.0	~	~

Table 20 shows the Dutch roll mode shows higher damping and lower frequency than all the simulation models predict. The AAA model is the closest to the real dynamics. As with the Dutch roll mode, the short period mode has higher damping than the any of the simulation models predict. The short period mode also had much higher frequency than any of the simulation models predict. The AVL-HIL simulation shows the closest short period frequency while the AAA shows the closes damping ratio. None of the modeling methods show major differences in either short period or Dutch roll. It should be noted that the time ratio method and the maximum slope method of data reduction can be highly inaccurate in their estimation of natural frequency. This was most likely the cause of the discrepancy between the AAA and AVL short period natural frequencies and the SCCS, AVL-HIL and flight test short period natural frequencies. Damping ratio is generally much more accurately calculated with the flight test data reduction techniques.

There were, however, large differences between the models in Phugoid mode damping. The frequency predicted by the AAA model and the AVL-HIL simulator was very close but the damping ratio of the AAA model Phugoid mode is a full 0.32

higher. Because of the incomplete flight data, direct comparison with the Phugoid mode could not be made. However, plots of the various modal predictions were a useful tool in evaluating the Phugoid dynamics.

Simulink was used to simulate the state space model presented in Section 5.1.2. Using similar elevator inputs to those shown in Figure 44 a 10 second time period plot was made and is shown in Figure 45.

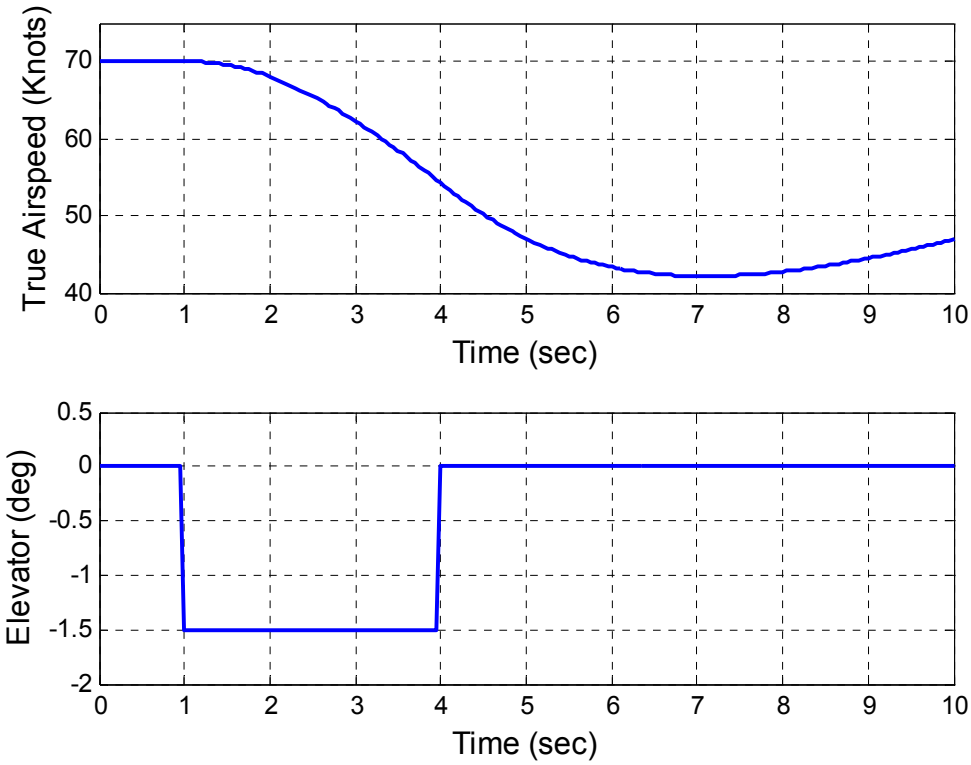

Figure 45: AAA Yak-54 Phugoid Simulation

The damped airspeed response in Figure 45 was slightly faster than the results of the flight test, with a half period peak occurring about 6 seconds into the response. It should also be noted that with these large airspeed changes the validity of the

model tends to degrade. The AVL-HIL simulation shows a faster initial response (Figure 46).

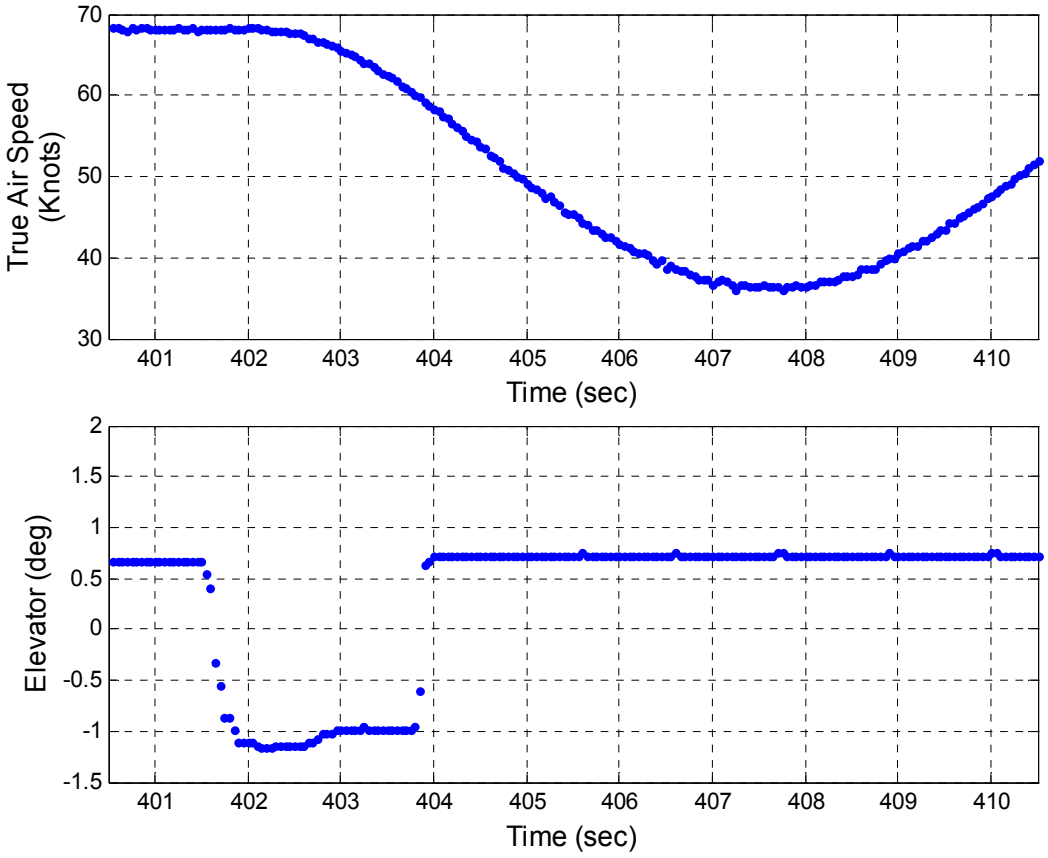

Figure 46: AVL-HIL Yak-54 Phugoid Simulation

The response in Figure 46 was less damped, with the aircraft both decelerating more and pitching up faster once the elevator is released. A noticeable time-delay was also present in Figure 46 which was most likely due to the sampling of the inherent lag in the Piccolo system. In any event, the Phugoid response in flight test appeared to be slower than either simulator. This indicates that the actual dynamics fit closer to the higher damped Phugoid predicted by AAA model.

8.5 Open-Loop Flight Test Conclusions and Recommendations

From the comparison of the flight test results with various simulation and modeling platforms it was seen that the more traditional AAA parametric model does the best job of modeling the aircraft dynamics but further refinement is clearly necessary. The AVL-HIL modeling and simulation environment does a moderately good job at modeling all of the dynamics except Phugoid. This will have a significant effect on optimizing the systems altitude and airspeed loops as Phugoid dominates these loops. The AVL-HIL model cannot be improved upon as the simulation is a "black-box" where the user is unable to input data from secondary sources. Improvements can be made to the AAA model however. System identification, wind tunnel testing, CFD, engine modeling, etc. can be performed to enhance the dynamic model further and are easily implemented in MATLAB/Simulink's modular simulation environment.

The major problem with the AAA model and Simulink simulator is that it is totally open-loop. Further engineering work is required to allow the AAA simulator, functioning in MATLAB/Simulink, to operate hardware-in-loop with the Piccolo II avionics. Thus it is recommended that if the Piccolo II UAV autopilot system is to be used on the Meridian a real-time nonlinear 6 DoF hardware-in-loop simulation platform using MATLAB/Simulink or auto generated C code using real-time workshop and the AAA model as the base dynamics model should be developed. It is highly recommended that higher fidelity modeling tools (wind tunnel, CFD) be used prior to first flight of the Meridian in order to ensure the closed-loop response is the

closest possible to the predicted response. Once first flight has taken place system identification will greatly improve the closed loop performance, as system identification will allow for the enhancement of high fidelity models even further and allow for gain tuning to continue in a laboratory environment where the vehicle is not at risk. It is also recommended that autonomous Phugoid mode flight tests be performed to fully evaluate dynamic models.

9 Closed-Loop Piccolo II Flight Control System Tuning Using Simulation

In Chapter 8 it was seen that the AAA model showed the best open loop response matching with the Yak-54 flight test data. It was further determined that significant engineering work still exists in order for the AAA model in a MATLAB/Simulink simulation environment to function hardware-in-loop with the Piccolo II autopilot. In the mean time, further test and evaluation of the Piccolo II avionics was performed on the Yak-54. The Piccolo II was tested for closed-loop performance (i.e. steady state error, response times, overshoot, response to disturbances, etc.), communication system robustness, user-friendliness (i.e. how difficult is it for the command and control engineer to manage the system in a flight environment) and finally the system's overall effectiveness was evaluated. In this chapter the closed-loop gain tuning for the Yak-54 under simulation is shown.

9.1 Closed-Loop Gain Tuning Using AVL Hardware-in-Loop Simulation

While the AAA model was the best for open-loop simulation it is not an option at this stage for closed-loop gain tuning. The AVL-Piccolo HIL simulation model provided the next best model of the Yak-54 dynamics and it was decided it would be used for closed-loop simulations and gain tuning. The first step in closed loop gain tuning was setting the Piccolo's gain scaling terms.. The gain scaling terms were set using the AAA generated stability derivatives and the 3W 80cc engine

information as provided by the manufacturer and are presented in Table 21.

Table 21: Yak-54/Piccolo Gain Scaling Terms

Geometry		
Wing Area (S_w)	10.90	ft^2
Wing Span (b_w)	7.90	ft
Vertical Tail Arm ($x_{ac_{vt}} - x_{cg}$)	3.71	ft
Mass		
Gross Mass	0.874	slugs
Empty Mass	0.845	slugs
I_{XX}	1.0886	slug ft^2
I_{YY}	2.1068	slug ft^2
I_{ZZ}	3.0382	slug ft^2
Longitudinal Aerodynamics		
Elevator Power ($C_{m_{\delta_e}}$)	-0.8778	rad^{-1}
C_{L_0}	0	~
Elevator Effectiveness ($\frac{dC_L}{d\delta_e}$)	-9.76	rad^{-1}
Lateral Aerodynamics		
Aileron Effectiveness ($\frac{\partial \overline{p}}{\partial \delta_a}$)	-0.9139	rad^{-1}
Rudder Power ($C_{n_{\delta_r}}$)	-0.0996	rad^{-1}
Rudder Effectiveness ($\frac{\partial \beta}{\partial \delta_r}$)	-1.0429	rad/rad
Sideslip Effect (C_{y_β})	-0.3462	rad^{-1}
Engine		
Power	11.5	Hp

The Piccolo II was designed to have stable response with these gain scaling terms and the default gain settings. Further tuning of the gains resulted in enhanced performance. The default gain settings for the Piccolo II autopilot are given in Table 22 and Table 23.

Table 22: Piccolo Default Lateral-Directional Gains

Gain Parameter	Default Gain
Roll Command Inner Loop	
Roll Error to Roll Rate	1.00
Roll Rate Error to Aileron	0.00
Roll Rate Error Integral to Aileron	1.00
Yaw Inner Loop	
Yaw Rate Error to Rudder	1.00
Side Force Error Integral to Rudder	0.00
Heading Control Outer Loop	
Heading Error to Turn Rate	0.40
Heading Error Derivative to Turn Rate	0.10
Waypoint Navigation	
Tracker Convergence	0.35

Table 23: Piccolo Default Longitudinal Gains

Gain Parameter	Default Gain
Elevator Inner Loop	
Elevator Prediction Trust	0.00
Z Acceleration Error Integral to Elevator	1.50
Pitch Damper	
Pitch Error to Elevator	0.00
Pitch Rate Error to Elevator	0.00
Airspeed Control Outer Loop	
TAS Error to TAS Rate	0.15
TAS Rate Error to Z Acceleration	1.00
Throttle Prediction Trust	0.00
Energy Rate Error Integral to Throttle	1.00
Altitude Control Outer Loop	
Altitude Error to Altitude Rate Command	0.20
Altitude Error to Z Acceleration Command	0.50

9.2 Lateral-Directional Response with Default Gains

Prior to tuning the initial gains it was important to analyze the time response to these default gains. Insight can be gained from these time responses and the gains were tuned in a more deliberate manner. There were three main control loops for the lateral-directional dynamics; the roll command inner loop, heading command outer loop and the yaw damper. The turn coordinator was also in the lateral directional

control loops but the gain was set solely based on the gain scaling term $\frac{\partial \beta}{\partial \delta_r}$.

Performance parameters were computed in the following manner:

All Responses:

1. Rise Time (t_r): The time it takes for the system to go from the initial value to 100% of the commanded value.
2. Steady State Error (e_{ss}): The difference between the commanded value and the steady state value.

Underdamped Responses:

3. Maximum Overshoot (M_p): The maximum response from the steady state value defined as a percentage. Maximum overshoot is defined as:

$$M_p = \frac{y(t_p) - y_{ss}}{y_{ss}} \tag{9.1}$$

4. Settling Time: The time that is required for the response to reach and maintain a value within 2% of the difference between the initial value and the command value.

The closed loop bank angle response was the first item analyzed. Figure 47 presents the closed loop response to a ten degree bank angle command. Table 24 shows the performance parameters of the system.

The bank angle control loop with the default gains showed an overdamped response. The steady state error was low and would be acceptable for a final system. Gain tuning focused on improving the rise time of the system (i.e. decreasing

damping).

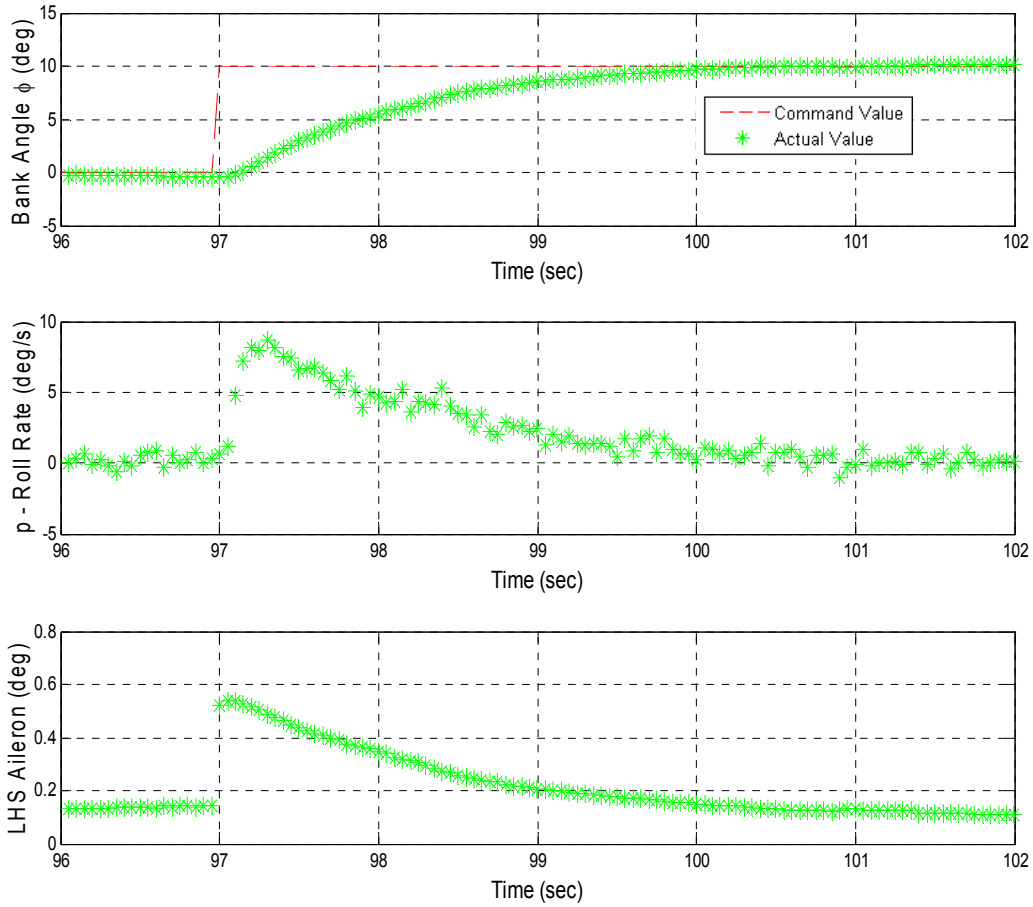

Figure 47: AVL-HIL Bank Angle Response with Default Gains

Table 24: Bank Angle Control Loop Performance with Default Gains

Rise Time (t_r)	3.65	sec
Steady State Error (e_{ss})	0.2	deg

The heading command outer-loop response to a 10 degree heading change is shown in Figure 48 and the performance parameters are presented in Table 25.

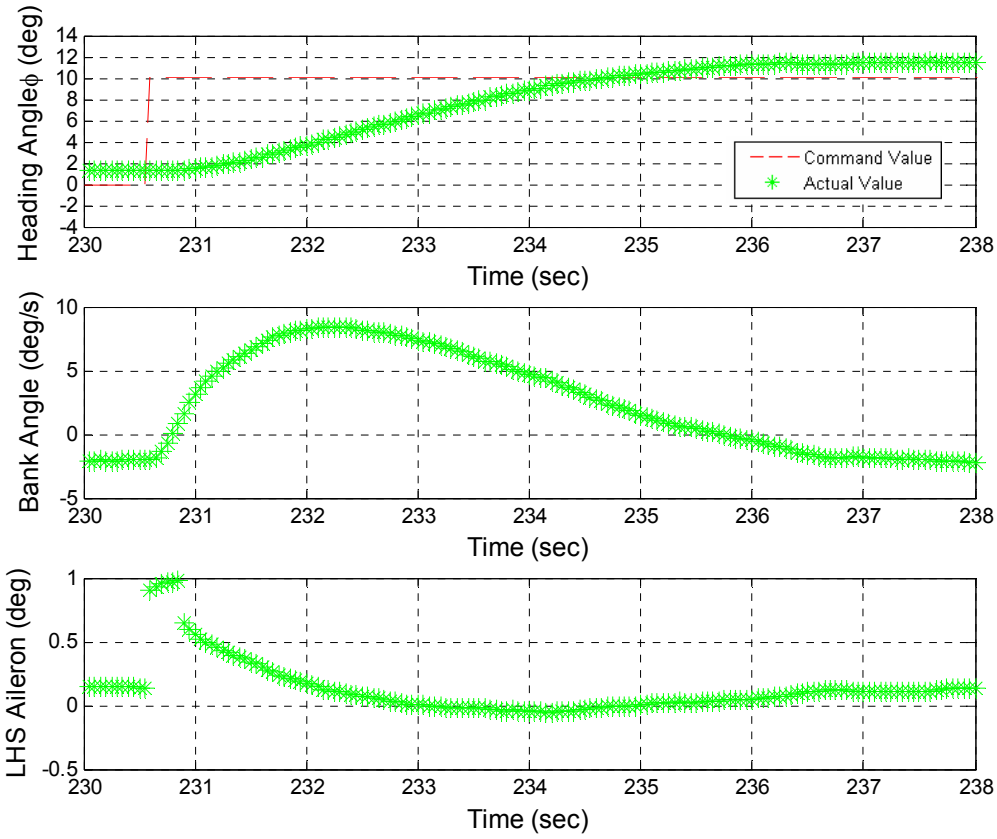

Figure 48: AVL-HIL Heading Angle Response with Default Gains:

Table 25: Heading Angle Control Loop Performance with Default Gains

Rise Time (t_r)	4.1	sec
Steady State Error (e_{ss})	1.5	deg

The closed loop heading command response showed a slow, overdamped response with only a small amount of bank used of the 30 degree bang angle limit. There was also a significant steady state error of 1.5 degrees. Gain tuning focused on increasing rise time and reducing steady state error.

9.3 Longitudinal Command Performance with Default Gains

The airspeed command loop performance to a 5 knot airspeed change command with default gains is presented in Figure 49 and the performance parameters are given in Table 26.

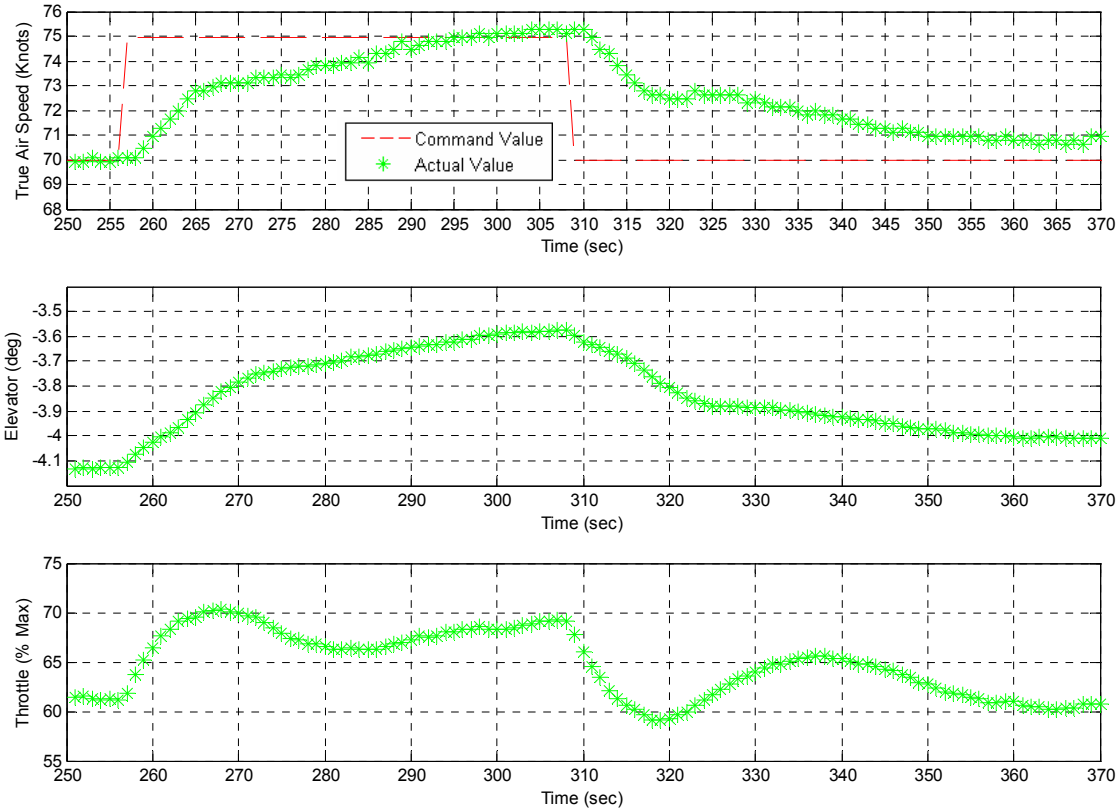

Figure 49: AVL-HIL Airspeed Response with Default Gains

Table 26: Airspeed Control Loop Performance with Default Gains

Rise Time (t_r)	43.0	sec
Steady State Error (e_{ss})	0.25	knots

The closed loop response showed very good steady state tracking but exhibits a highly over damped response. The elevator response is very slow, winding up type response, and there is little throttle change. Gain tuning will focus on increasing the

rise time of the default response.

The altitude command loop performance to a 50 foot altitude change with default gains is presented in Figure 50 and the performance parameters are given in Table 27.

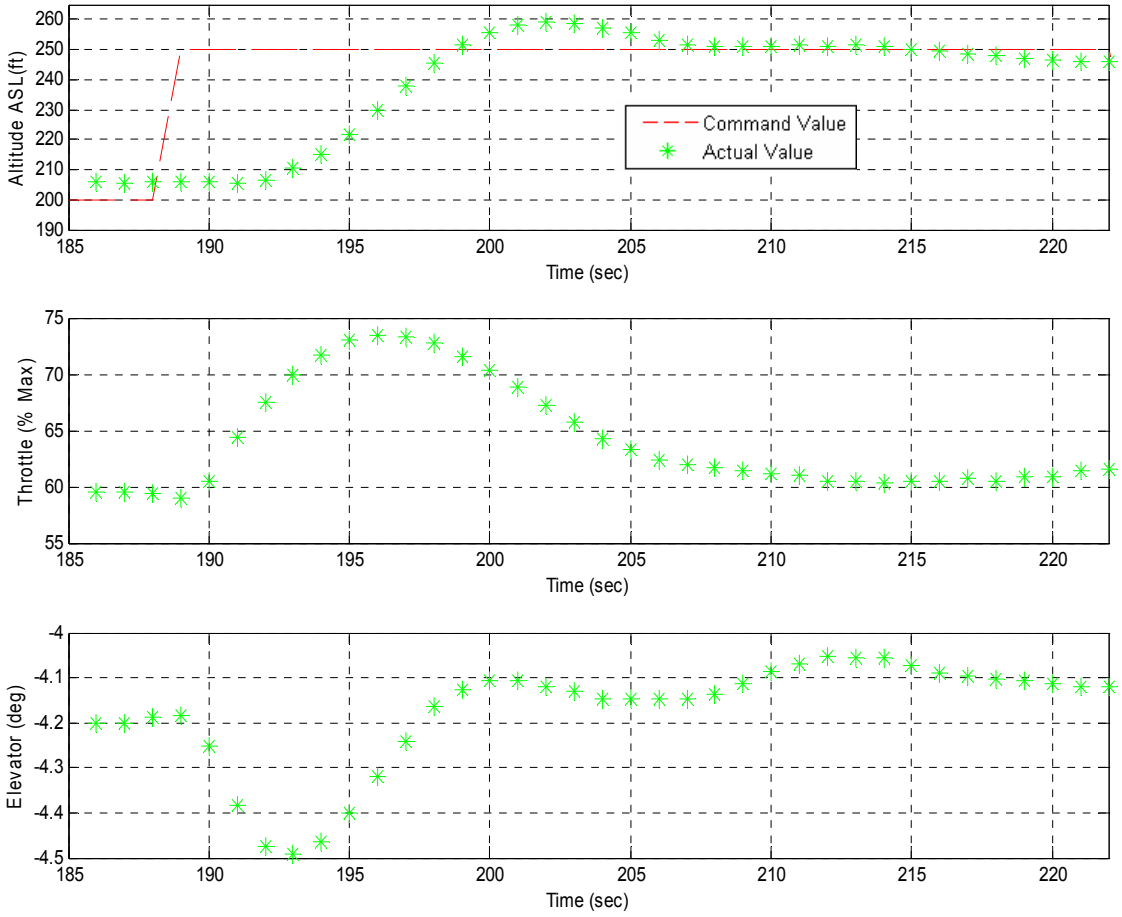

Figure 50: AVL-HIL Altitude Response with Default Gains

Table 27: Altitude Control Loop Performance with Default Gains

Rise Time (t_r)	11.0	sec
Settling Time (t_s)	32.0	sec
Maximum Overshoot (M_p)	5.37	%
Steady State Error (e_{ss})	-4.1	ft

The altitude response closed loop had underdamped behavior. The altitude response should be an overdamped response, as overshoot of altitude commands is to be avoided. Closed loop gain tuning focused on increasing damping and reducing steady state error, while trying to maintain good rise time performance.

9.4 Lateral Gain Tuning Using AVL-Piccolo HIL Simulation

The lateral gains were tuned using the AVL-Piccolo HIL simulation. Tuning the Piccolo gains can be difficult and laborious, as there are 20 total gains. The lateral gains are the straightest forward as there are not as many gains as in the longitudinal controller. An iterative process was used because other techniques, as discussed in Chapter 2, require detailed knowledge of the control system block diagrams. Without these block diagrams a solid engineering approach to gain tuning could not be used, which is a serious deficiency in the Piccolo II autopilot system. The final lateral-directional gains were set to the values shown in Table 28.

The largest increase in the gains was the roll error to roll rate gain. This should greatly increase the rise time of the response. The roll rate error integral to aileron was decreased by half as a larger gain was not needed. There was also sufficient yaw damping that the yaw damper gain was reduced by 50 %. The closed loop bank angle response to these gains is shown in Figure 51 and the new performance values are shown in Table 29.

Table 28: AVL-HIL Tuned Lateral-Directional Gains

Gain Parameter	Default Gain	Simulator Tuned Gain
Roll Command Inner Loop		
Roll Error to Roll Rate	1.00	5.00
Roll Rate Error to Aileron	0.00	0.00
Roll Rate Error Integral to Aileron	1.00	0.50
Yaw Inner Loop		
Yaw Rate Error to Rudder	1.00	0.50
Side Force Error Integral to Rudder	0.00	0.00
Heading Control Outer Loop		
Heading Error to Turn Rate	0.40	0.50
Heading Error Derivative to Turn Rate	0.10	0.00
Waypoint Navigation		
Tracker Convergence	0.35	0.25

Table 29: AVL-HIL Bank Angle Control Loop Performance with Simulator Tuned Gains

Rise Time (t_r)	0.9	sec
Settling Time (t_s)	2.4	sec
Maximum Overshoot (M_p)	5.90	%
Steady State Error (e_{ss})	0.1	deg

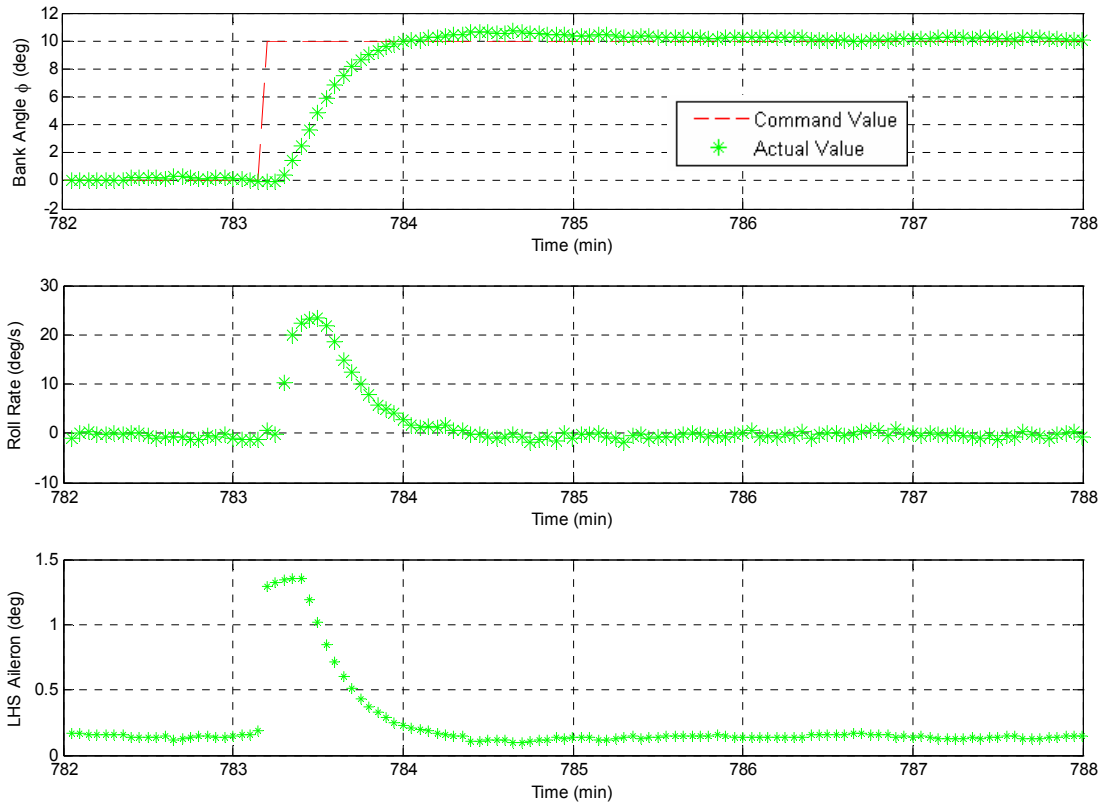

Figure 51: AVL-HIL Bank Angle Control Response with Simulator Tuned Gains

The new closed loop bank angle response was much improved from the bank angle performance with default gains. The steady state error was reduced by half and the rise time was decreased significantly. This type of bank angle response should allow for rapid response to atmospheric turbulence and faster heading changes.

The heading response with the new lateral gains is shown in Figure 52 and the new performance statistics are shown in Table 30.

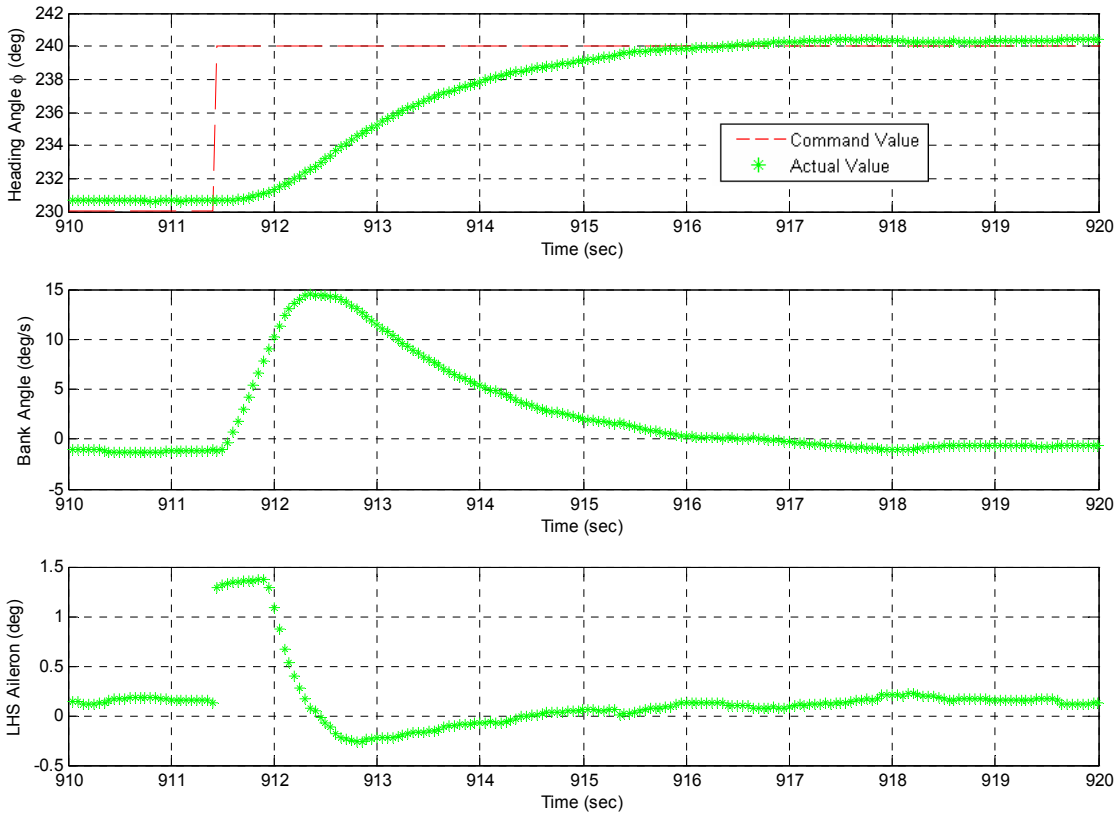

Figure 52: AVL-HIL Heading Angle Control Loop Performance with Simulator Tuned Gains

Table 30: Heading Angle Control Loop Performance with AVL-HIL Tuned Gains

Rise Time (t_r)	4.8	sec
Steady State Error (e_{ss})	0.4	deg

The heading controller was difficult to tune, as increasing the heading error to turn rate gain too much caused large steady state error and decreasing it too much resulted in high rise times. Strange bank angle auto command generation (large, step like bank angle commands) was also observed when this gain was too high. The Piccolo suffers some performance here because of the lack of a heading tracker integral. These problems are somewhat corrected when the outer waypoint tracking

loops are turned on, as the steady state error is driven to zero.

9.5 Longitudinal Gain Tuning Using AVL-Piccolo HIL Simulation

The lateral gains were tuned using the AVL-Piccolo HIL simulation. The longitudinal gains are the most difficult to tune, as the Piccolo uses the throttle and elevator to simultaneously control altitude and airspeed. Trade-offs in performance must be taken into account when tuning the gains. The final closed loop longitudinal gains were set to the values shown in Table 31 using an iterative approach.

Table 31: AVL-HIL Tuned Longitudinal Gains

Gain Parameter	Default Gain	Simulator Tuned Gain
Elevator Inner Loop		
Elevator Prediction Trust	0.00	0.50
Z Acceleration Error Integral to Elevator	1.50	1.50
Pitch Damper		
Pitch Error to Elevator	0.00	0.10
Pitch Rate Error to Elevator	0.00	0.10
Airspeed Control Outer Loop		
TAS Error to TAS Rate	0.15	0.60
TAS Rate Error to Z Acceleration	1.00	1.00
Throttle Inner Loop		
Throttle Prediction Trust	0.00	0.50
Energy Rate Error Integral to Throttle	1.00	1.80
Altitude Control Outer Loop		
Altitude Error to Altitude Rate Command	0.20	0.40
Altitude Error to Z Acceleration Command	0.50	1.20

The elevator prediction trust was increased to 0.5 from 0. The elevator prediction trust is the innermost gain that is placed on the scaled feedforward elevator controller. This gain had a significant impact on the amount and aggressiveness of elevator responses to outer-loop commands.

$$\delta_{e_{pred}} = K_p \frac{C_{L_{cmd}} - C_{L_0}}{dC_L / d\delta_e} \tag{9.2}$$

Without the elevator prediction trust all of the elevator inner-loop commands came from the Z acceleration integral to aileron gain.

Pitch damping (both rate and angle) was added, although with very low gains. These may (and most likely will not) be needed in flight test as both the short period and Phugoid modes are more well damped than the AVL-Piccolo HIL simulations predict.

The throttle prediction trust was also been raised from a zero value. This increased the amount of throttle commanded from outer loop inputs. Finally the altitude error to Z-acceleration command gain has been increased so that there is more elevator input (elevator changes were issued from acceleration commands) for precisions regulation of altitude.

The final closed loop airspeed simulation response is given in Figure 53 and the performance characteristics are given in Table 32. The airspeed command rise time increased dramatically. There is slightly more steady state error, but it is still less than a knot which is acceptable.

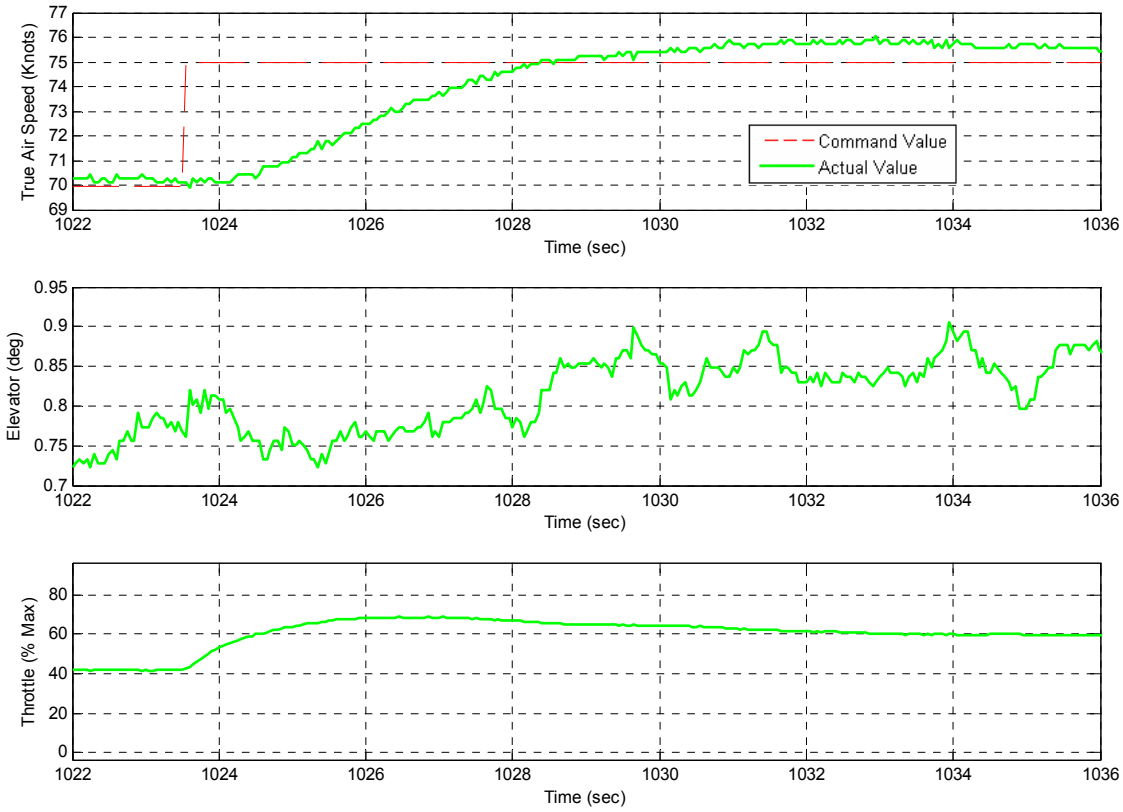

Figure 53: AVL-HIL Airspeed Control Response with Simulator Tuned Gains

Table 32: AVL-HIL Airspeed Control Performance with Simulator Tuned Gains

Rise Time (t_r)	5	sec
Settling Time (t_s)	11.2	sec
Maximum Overshoot (M_p)	0.62	%
Steady State Error (e_{ss})	0.58	knots

The altitude command response to the new gains is shown in Figure 54 and the performance characteristics are shown in Table 33.

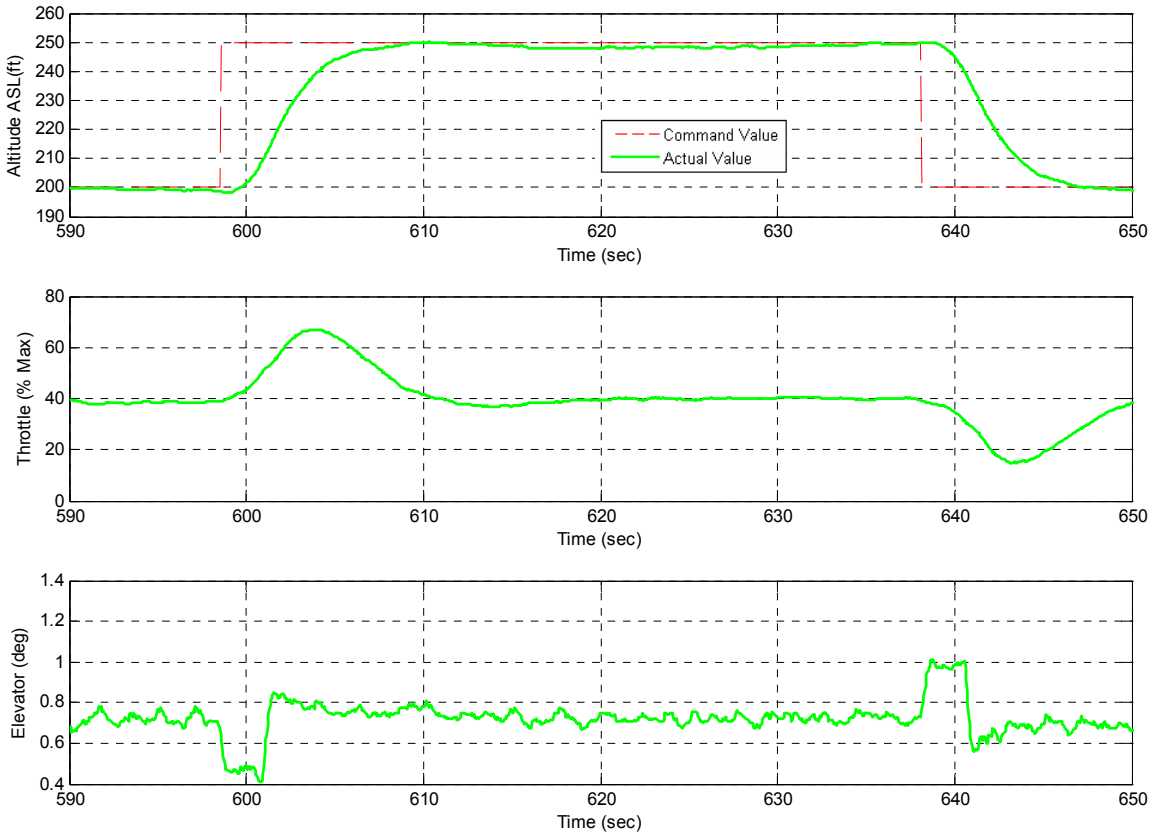

Figure 54: AVL-HIL Altitude Control Response with Simulator Tuned Gains

Table 33: AVL-HIL Altitude Control Performance with Simulator Tuned Gains

Rise Time (t_r)	11.7	sec
Settling Time (t_s)	15.6	sec
Maximum Overshoot (M_p)	0.68	%
Steady State Error (e_{ss})	-1.6	ft

As can be seen in Table 33 the rise time performance of the closed loop altitude controller was slightly slower than the default gains, however the settling time was greatly reduced. The maximum overshoot and steady state error, which can be dangerous in altitude controllers, was also reduced significantly.

9.6 Closed Loop Gain Margins

The closed loop response of the system was improved from the default configuration. The performance could not be said to be the best possible, as maximizing gain performance is extremely difficult to perform unless the block diagram structure is known. The system at this point was ready for flight testing, but first a gain margin analysis was performed so that the flight engineer had a better understanding of which gains are the most critical with regards to stability. To determine the gain margins of the lateral and directional systems each gain was increased from the tuned value until it drove the system unstable or it reached the maximum value possible. System stability was also checked when the gains were set to zero (i.e. control loop off). Table 34 and Table 35 present the gain margins for the longitudinal and lateral controllers.

In nearly every case the there was substantial gain margin in the system. The lowest margin is in the roll rate error to aileron gain. Unpublished documentation was available to the team that showed that this gain mixed Euler and body axis roll angles. Driving the error between the Euler and body axis angles to zero can cause the system to go unstable as the angles should not be equal during maneuver, and thus it was decided that this term would be kept at zero. The instability of the system at a roll rate error to aileron gain of 1.25 reinforced this decision.

The typical flight test increase or decrease in gain value is ± 20%. This would make the possibility of driving the system unstable low. It is also gives the flight test engineer some level of confidence that the system can be tested without undue risk to

the system or ground crew due to closed loop instability.

Table 34: Piccolo II AVL-HIL Lateral-Directional Gain Margins

Gain Parameter	Initial Gain	Destabilizing Gain	Destabilizes with Zero Gain
Roll Command Inner Loop			
Roll Error to Roll Rate	4.00	N/A	Yes
Roll Rate Error to Aileron	0.00	1.75	No
Roll Rate Error Integral to Aileron	0.50	15.00	No
Yaw Inner Loop			
Yaw Rate Error to Rudder	0.50	16.00	No
Side Force Error Integral to Rudder	0.00	Any Gain	No
Heading Control Outer Loop			
Heading Error to Turn Rate	0.50	N/A	No
Heading Error Derivative to Turn Rate	0.00	N/A	No
Waypoint Navigation			
Tracker Convergence	0.25	600	No

9.7 Closed Loop Phase Margins

A significant disadvantage to the Piccolo system was that there was no straight forward way to do phase margin calculations. The simulator did not allow for closed loop phase delays to be added to the system and frequency sweeps to produce Bode diagrams cannot be performed on the system closed loop. A possible way to approximate technique to determine phase margin would be to add a discrete time delay to targeted states in the CAN bus (pitch angle for example). This technique would require significant engineering effort, as the CAN signal would have

had to have been hacked, and thus it was not performed. Thus no closed loop phase margins were determined prior to flight test.

Table 35: Piccolo II AVL-HIL Longitudinal Gain Margins

Gain Parameter	Initial Gain	Destabilizing Gain	Destabilizes with Zero Gain
Elevator Inner Loop			
Elevator Prediction Trust	0.50	N/A	No
Z Acceleration Error Integral to Elevator	2.50	50.00	Yes
Pitch Damper			
Pitch Error to Elevator	0.10	N/A	No
Pitch Rate Error to Elevator	0.10	60.00	No
Airspeed Control Outer Loop			
TAS Error to TAS Rate	0.60	N/A	No
TAS Rate Error to Z Acceleration	1.40	N/A	No
Throttle Inner Loop			
Throttle Prediction Trust	0.50	N/A	No
Energy Rate Error Integral to Throttle	1.80	N/A	Yes
Altitude Control Outer Loop			
Altitude Error to Altitude Rate Command	0.40	9999999	No
Altitude Error to Z Acceleration Command	1.20	N/A	No

10 Closed Loop Piccolo II Gain Tuning in Flight Test

This chapter will present the results of closed loop flight testing of the Piccolo II avionics on the one-third scale Yak-54 using the initial gains set in Chapter 8. Three control loops were successfully tuned: the bank angle command loop, the heading angle command loop, and the airspeed command loop. Flight test planning and preparation were made according to the system described in Chapter 6.

10.1 Bank Angle Control Flight Test

The first flight test performed was the bank angle command loop flight test. It was decided that tuning the lateral-directional terms first would be the best route to take in closed loop flight testing. There are several reasons for this. First the bank angle controller was the simplest controller, with only two gains to tune. Also once the bank angle controller was tuned tuning the heading controller was straight forward, as there was also only one gain in the controller. Additionally, this will allowed the flight test team to become more accustomed to in-flight gain tuning without undue stress or confusion associated with the more complex longitudinal control system. Finally, once the lateral control system was tuned it could be turned on during longitudinal flight testing, preventing the aircraft from banking out of control due to the unstable spiral mode.

Tuning of the bank angle controller was straight forward. First the pilot climbed to approximately 200 ft AGL and trimmed the aircraft based on the criterion stated in Chapter 7. The flight test engineer received a “trimmed” call from the pilot

when the aircraft was trimmed and then noted the trim control surfaces. These control surface positions were then be sent to the Piccolo II avionics unit. When the autopilot was activated all of the control surfaces that were not being commanded by the controller (i.e. elevator and throttle) were be set to the trim position. This allowed the aircraft to more or less maintain altitude and airspeed during the lateral-directional flight tests.

Once the aircraft was trimmed and the Piccolo had received the trim control surface positions the flight test engineer, after confirming good telemetry, set the bank angle command to zero, with all other control loops off. This in effect regulated bank angle. Appendix O can be referenced for the bank angle control dance card. The initial response to this test is given in Figure 55.

Figure 55 shows that getting the aircraft to an initial bank angle of zero can be difficult, thus the response was actually a 10 degree bank angle command. The initial transient was good, but the tracking was fairly poor, with steady state errors as high as 2 degrees. Before any gain tuning was performed however, a larger bank angle command was attempted. The results of this test are presented in Figure 56 and Table 36.

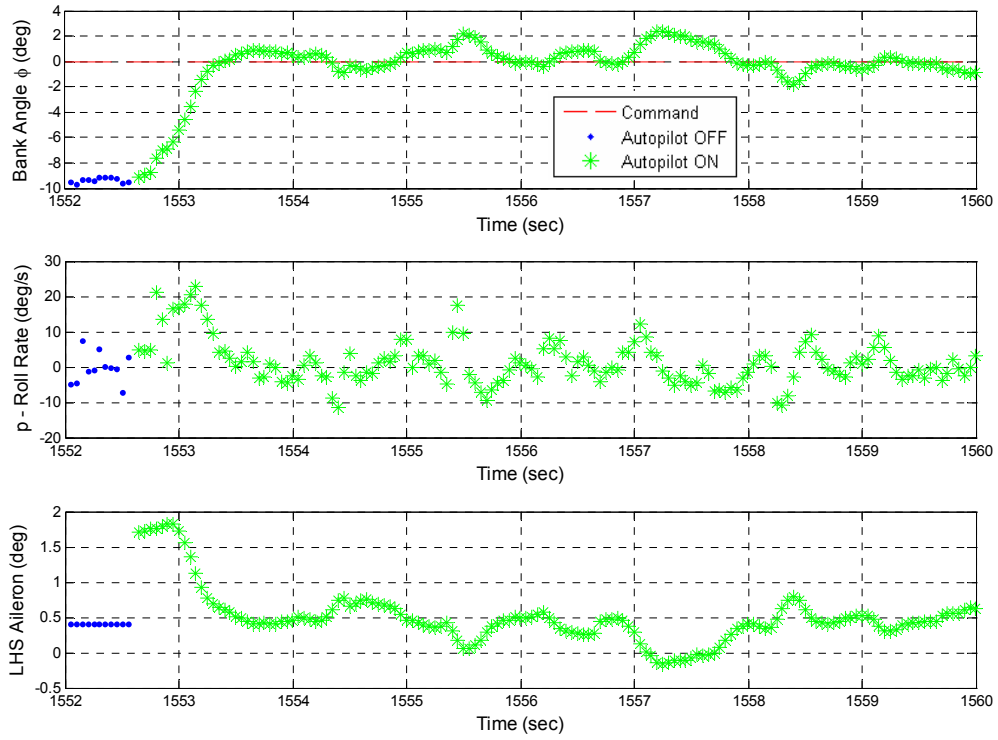

Figure 55: Initial Bank Angle Control Flight Test with AVL-HIL Tuned Gains

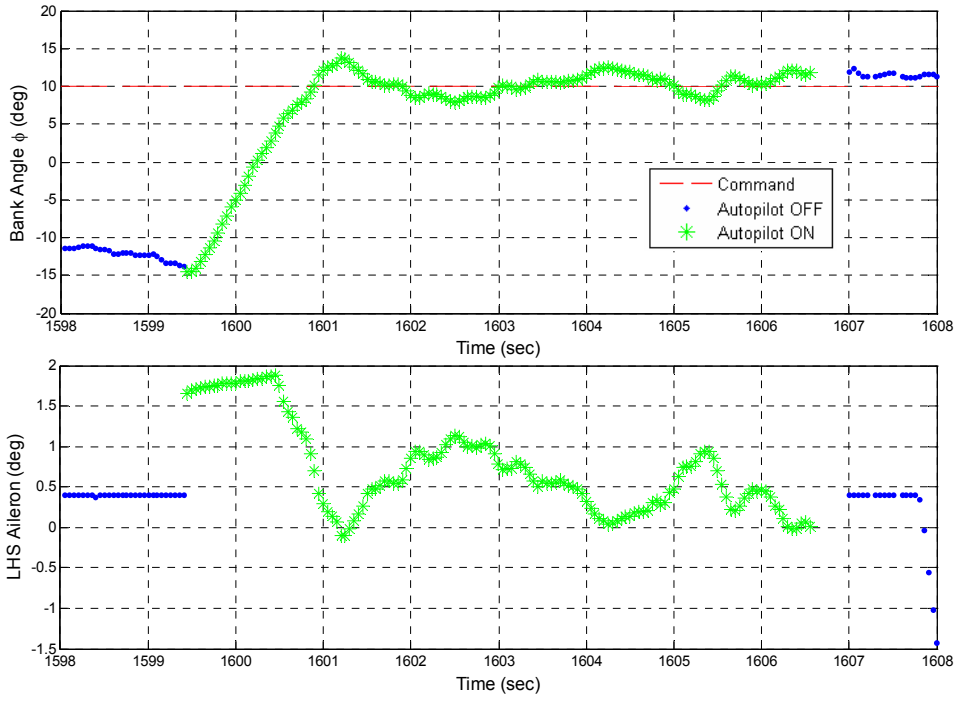

Figure 56: 20 Degree Bank Angle Command Flight Test with Simulator Tuned Gains

Table 36: Roll Control Loop Performance with Simulator Tuned Gains

Rise Time (t_r)	1.7	sec
Settling Time (t_s)	> 7	sec
Maximum Overshoot (M_p)	37.5	%
Steady State Error (e_{ss})	~	ft

The closed loop response shows a large amount of overshoot and poor regulation, with the response never settling. It was decided to decrease the roll error to roll rate gain by 20% to 4.0. This resulted in the response shown in Figure 57 and the performance parameters presented in Table 37.

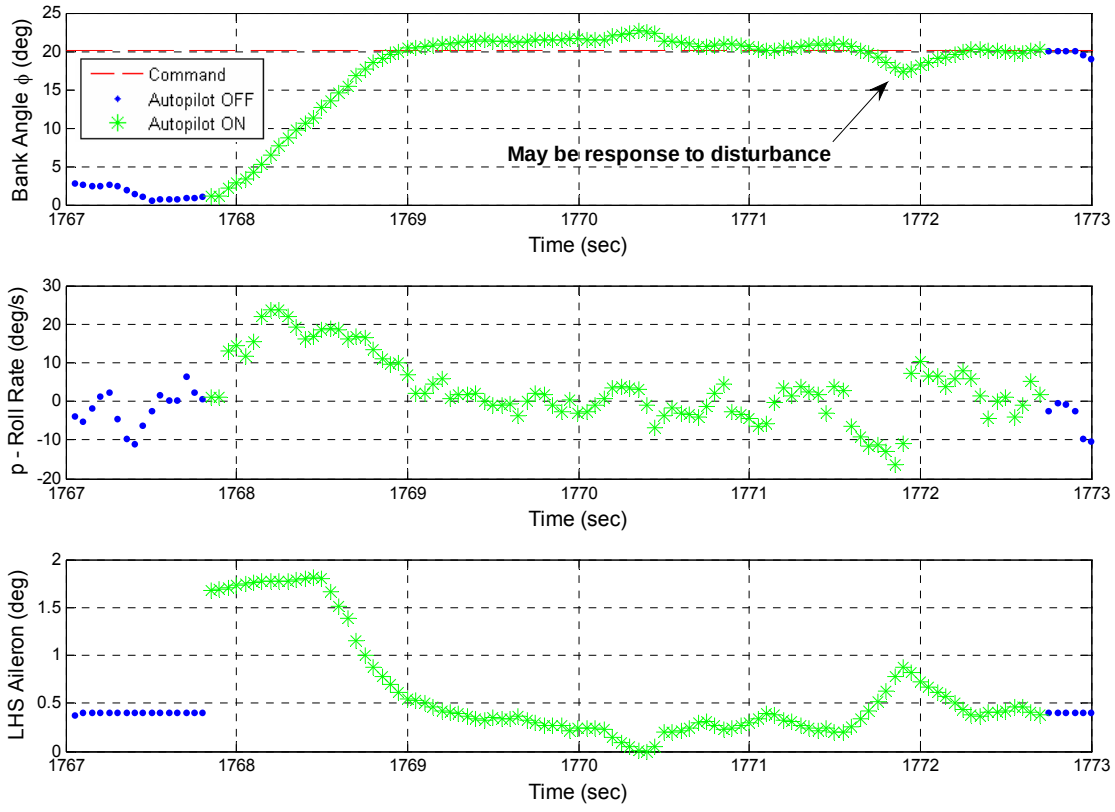

Figure 57: Final Roll Control Flight Test with Tuned Gains

Table 37: Final Roll Control Performance

Rise Time (t_r)	1.1	sec
Settling Time (t_s)	1.3	sec
Maximum Overshoot (M_p)	0.52	%
Steady State Error (e_{ss})	$\approx$ 1.3	deg

As can be seen by the performance parameters, the closed loop bank angle response was much improved. The rise time was slightly worse than simulation, but the settling time was much better than the first flight test and the overshoot was much lower. It is difficult to determine what the actual steady state error was as the low test times made it difficult to observe periodic behavior that would indicate poor controller behavior as opposed to random disturbances. At this point the performance was acceptable and the flight team decided to move on to heading angle control testing.

10.2 Heading Angle Control Flight Test

The heading angle control flight test was setup similar to the bank angle control flight test. The aircraft was setup for a trim altitude of 200 ft AGL and this time the flight engineer took note of the upwind trim heading. The flight test engineer used this trim heading as the initial heading command. The trim heading functioned as the base heading for follow up heading changes (Appendix P) of 10 degrees, 20 degrees and 30 degrees. The initial heading response is shown in Figure 58.

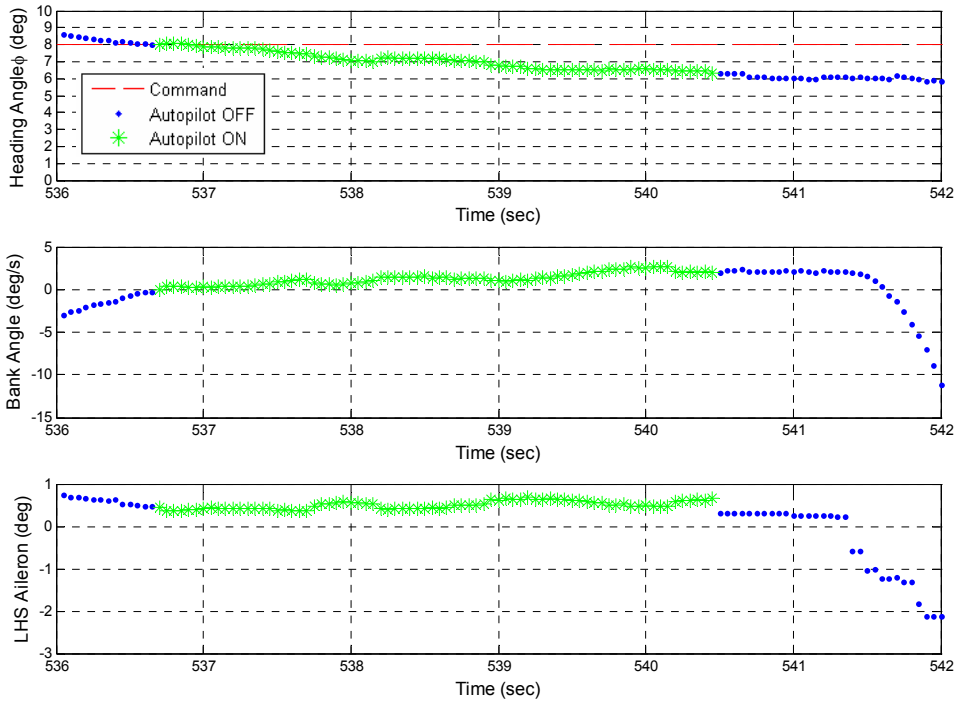

Figure 58: Initial Heading Command Flight Test with Simulator Tuned Gains

$$e_{ss} = -1.5 \text{ deg}$$

There is an identical steady state error to the heading command response seen in simulation (Table 25). A larger heading command (10 degrees) is shown in Figure 59.

The larger heading command resulted in a very similar steady state error. As mentioned in Chapter 8, the heading controller steady state tracking suffers from the lack of an integrator term. This may or may not be a problem in the final system, as waypoint tracking may correct these errors. Testing will be required to determine the acceptability of this steady state error in the heading command loop. As the heading command response was very similar to the final simulation values no further gain tuning was performed.

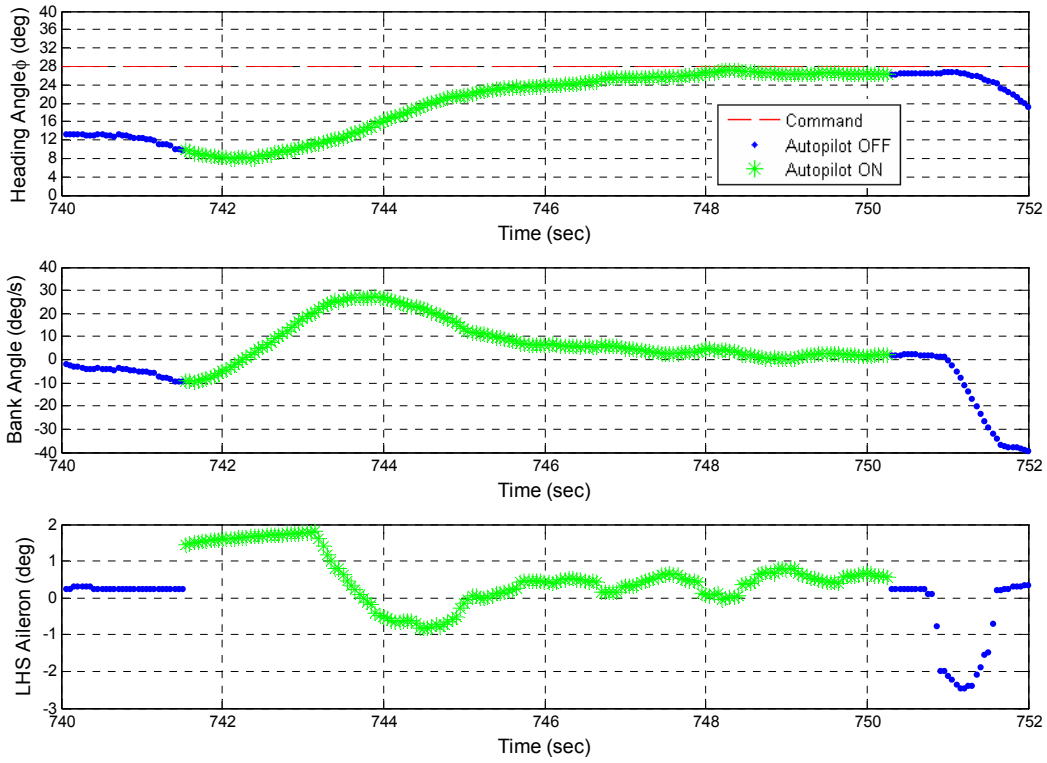

Figure 59: Final Heading Angle Command Flight Test with Tuned Gains

Table 38: Final Heading Angle Control Performance with Tuned Gains

Rise Time (t_r)	5.7	sec
Steady State Error (e_{ss})	-1.6	deg

10.3 Tuned Gains for the Lateral-Directional Control System

Table 39 is a table of the final gains for the lateral-directional control system and shows there was little need for substantial gain tuning.

Table 39: Final Lateral-Directional Gains

Gain Parameter	Default Gain	Simulator Tuned Gain	Flight Test Tuned Gain
Roll Command Inner Loop			
Roll Error to Roll Rate	1.00	5.00	4.00
Roll Rate Error to Aileron	0.00	0.00	0.00
Roll Rate Error Integral to Aileron	1.00	0.50	0.50
Yaw Inner Loop			
Yaw Rate Error to Rudder	1.00	0.50	0.50
Side Force Error Integral to Rudder	0.00	0.00	0.00
Heading Control Outer Loop			
Heading Error to Turn Rate	0.40	0.50	0.50
Heading Error Derivative to Turn Rate	0.10	0.00	0.00
Waypoint Navigation			
Tracker Convergence	0.35	0.25	TBD

10.4 Airspeed Control Flight Test

The airspeed control flight test was the first of the more difficult longitudinal closed loop flight tests. The biggest difficulty was that the airspeed controller cannot be tested without the altitude controller being enabled. The IAS threshold term can be set to -1 knots, thus giving the maximum possible weight to the airspeed controller, but this would not totally disable altitude control. If the altitude controller

was set to OFF simulation has shown that the system would be driven unstable. The airspeed controller thus had to be iterated with the altitude controller to find the ideal configuration, giving more weight to altitude than airspeed as exact altitude tracking is more crucial to successful mission performance.

Airspeed control testing was performed with the heading controller set to ON and a command value of 8 degrees. This prevented the aircraft from spiraling out of control during the test. The initial trim airspeed, and also the first command airspeed, was 70 knots at an altitude of 200 ft AGL (1300 ft ASL). Appendix Q can be referenced for the airspeed control flight test dance card.

The results of the first airspeed flight test are given in Figure 60.

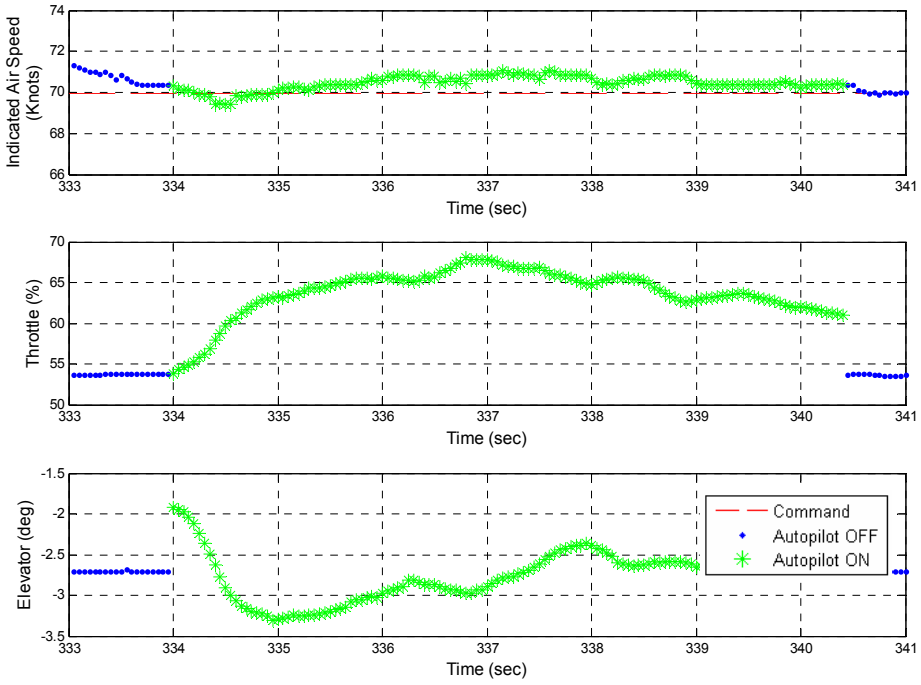

Figure 60: Initial Airspeed Regulator Flight Test with Simulator Tuned Gains

$$e_{ss} \approx 0.3 \text{ knots} \qquad 10.2$$

The airspeed regulator response was very good, with the error never getting above one knot and the steady state error settling out to about 0.3 knots. The next test was to command an airspeed change of 5 knots. The response to this command is given in Figure 61 and Table 40.

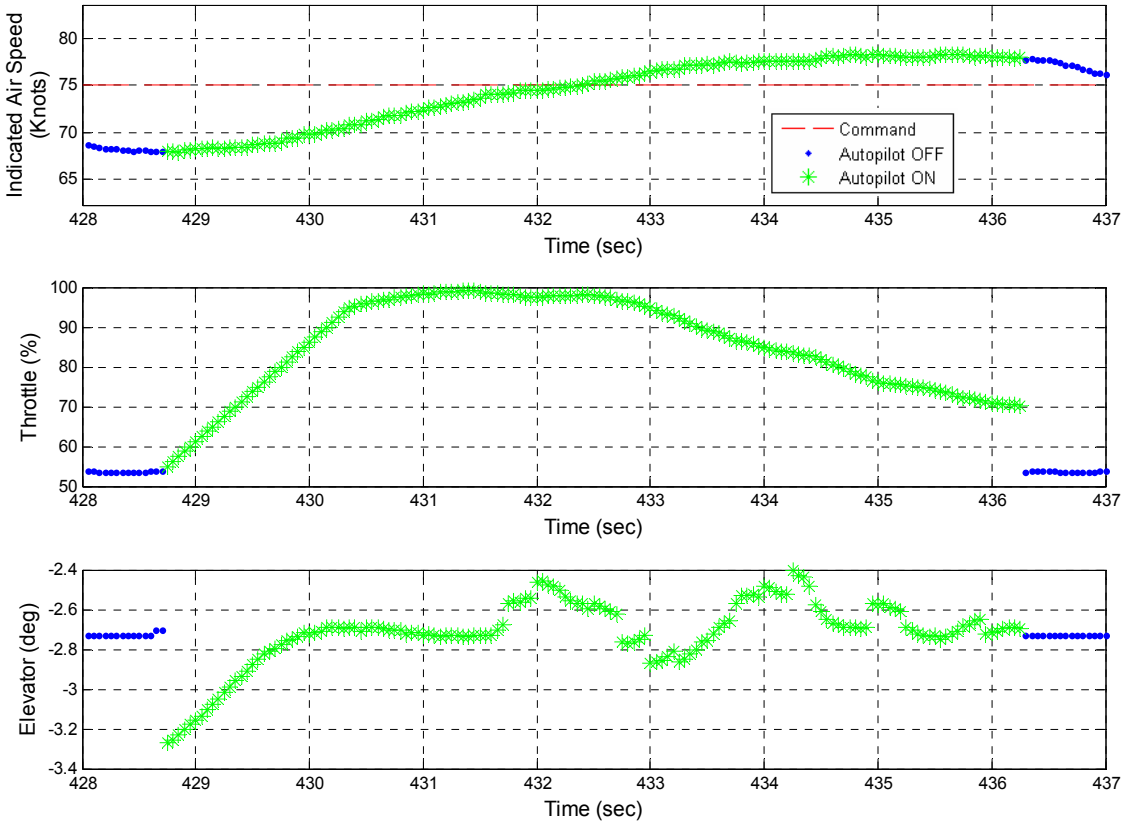

Figure 61: Second Airspeed Command Flight Test Response with Simulator Tuned Gains

Table 40: Second Airspeed Command Flight Test Performance with Simulator Tuned Gains

Rise Time (t_r)	6.2	sec
Steady State Error (e_{ss})	3.2	knots

The response to an approximately 5 knot airspeed change is slow and first order, with a fairly large steady state error. Gain tuning in flight focused on improving the steady state response. Twenty-six iterations were performed with

different gain sets to get the final gains. Appendix R shows the gain change log sheet with the different gain value used. The final response to the gain values set in flight is given in Figure 62 with the performance parameters shown in Table 41.

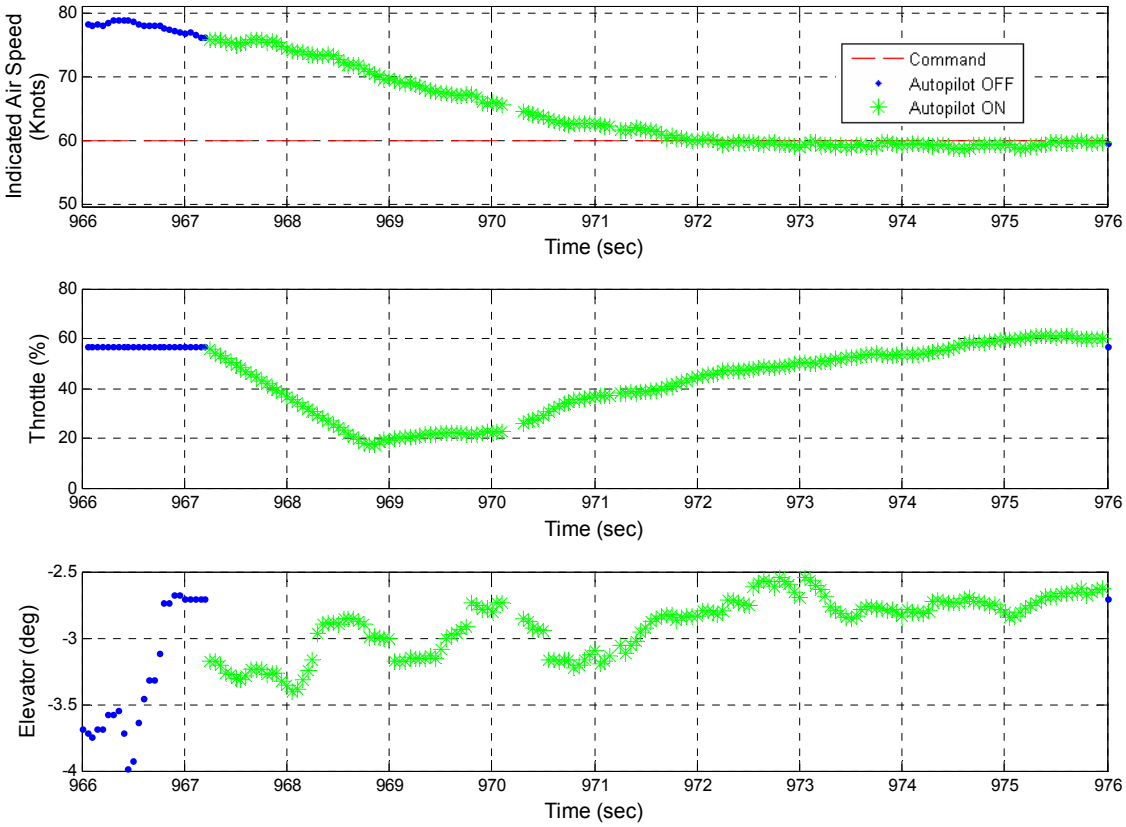

Figure 62: Final Airspeed Command Flight Test Response with Tuned Gains

Table 41: Final Airspeed Command Response Performance with Tuned Gains

Rise Time (t_r)	5.4	sec
Steady State Error (e_{ss})	-1.2	knots

Figure 62 shows, the closed loop response has increased rise time and reduced steady state error over the response to the initial gains. The response is actually quite similar to the response seen in simulation (Figure 53). The airspeed controller is now working in an acceptable manner and the altitude controller can be tuned.

Table 42 shows the new gains after the airspeed controller tuning.

Table 42: Final Longitudinal Gains

Gain Parameter	Default Gain	Simulator Tuned Gain	Flight Test Tuned Gain
Elevator Inner Loop			
Elevator Prediction Trust	0.00	0.50	0.30
Z Acceleration Error Integral to Elevator	1.50	1.50	1.65
Pitch Damper			
Pitch Error to Elevator	0.00	0.10	0.10
Pitch Rate Error to Elevator	0.00	0.10	0.10
Airspeed Control Outer Loop			
TAS Error to TAS Rate	0.15	0.60	0.70
TAS Rate Error to Z Acceleration	1.00	1.00	1.00
Throttle Inner Loop			
Throttle Prediction Trust	0.00	0.50	0.50
Energy Rate Error Integral to Throttle	1.00	1.80	1.80
Altitude Control Outer Loop			
Altitude Error to Altitude Rate Command	0.20	0.40	TBD
Altitude Error to Z Acceleration Command	0.50	1.20	TBD

10.5 Piccolo II Closed Loop Flight Test Conclusions

The closed loop response of the Piccolo Yak-54 system was promising. All of the closed loop responses were stable and not so underdamped as to be worrisome to the flight test team. Significant gain tuning was needed, however, to get the system working in proper order, especially with the airspeed controller. A total of 26 flight

test runs were made to get the gains to the final values shown in Table 42. This would be very difficult to perform on the Meridian UAS, given the difficulty in maintaining manual control. Flight test is an expensive, time-consuming and inefficient arena for gain tuning as the airspeed test shows. This would reinforce the conclusion of Chapter 8 that a hardware-in-loop simulation model be developed that will produce high fidelity closed loop simulations, thus minimizing any in-flight gain tuning.

11 Yak-54 Flight Incident and Investigation

On March 13th, 2008 the CReSIS flight test team conducted a flight test of the Piccolo II autopilot system. The flight test was to tune the gains of the heading controller, the airspeed controller and the altitude controller. Three separate flights were conducted, with a crash of the Yak-54 occurring during final approach on the last flight.

11.1 First Flight

During the closing minutes of the first flight test the flight test pilot reported a temporary loss of control of the aircraft. The flight test was ended at that time and the pilot proceeded to land the aircraft. After the landing the RSSI signal was checked by the flight test engineers. Figure 63 shows a plot of the RSSI during the time the pilot reported a loss of control and Figure 64 shows the RSSI during the entire flight.

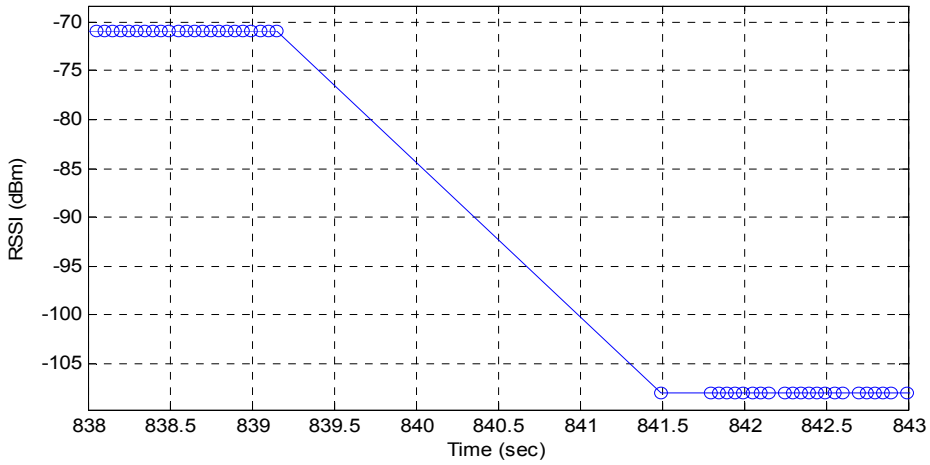

Figure 63: RSSI Levels during First Flight Pilot Control Loss

The drop out lasted approximately 2.5 seconds, with the RSSI changing from -71 dB to -108 dB. Because the RSSI drop was temporary (the RSSI at most other

times appeared to be satisfactory) and the pilot was able to successfully regain manual control it was decided that the flight test would continue.

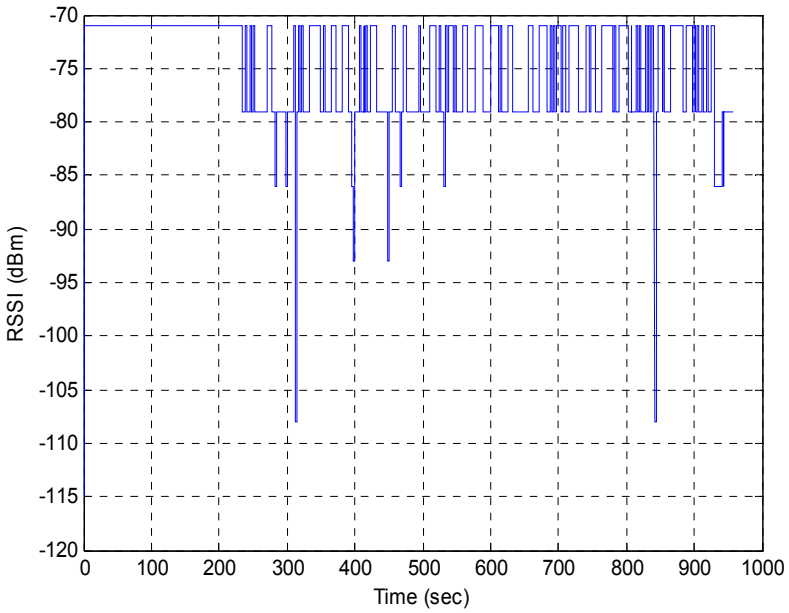

Figure 64: RSSI during First Flight Test

11.2 Second Flight

During the second flight the pilot also reported a temporary loss of control. The pilot regained control after a few seconds and the flight test continued. Figure 65 shows the RSSI at the time of control loss and Figure 66 shows the RSSI over the entire second flight.

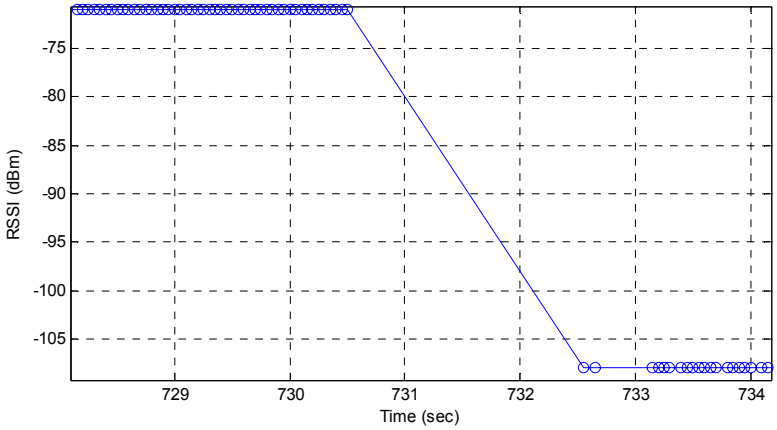

Figure 65: RSSI during Second Flight Test Pilot Control Loss

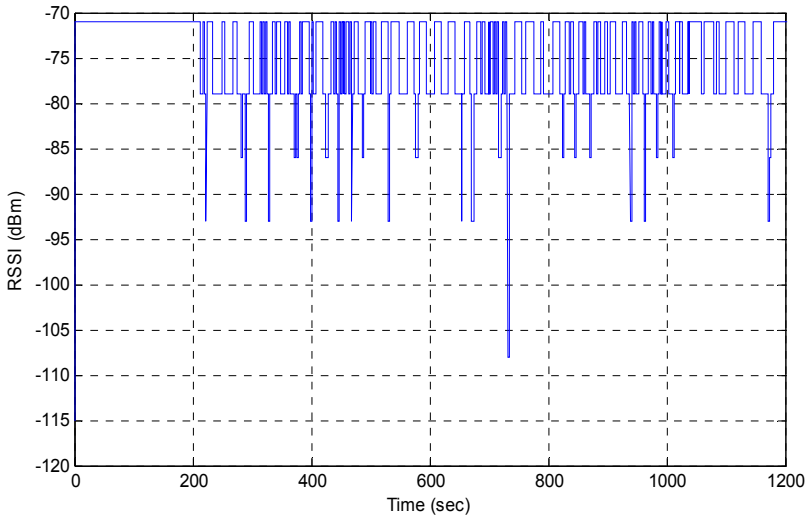

Figure 66: RSSI during Second Flight Test

The RSSI data on the second flight was similar to that of the first flight, with one large drop to -108 dB with more than 2 seconds of missing data in-between.

11.3 Third Flight

During the third and final flight the pilot reported one loss of control during flight. The behavior was similar to the first flight as shown in Figure 67.

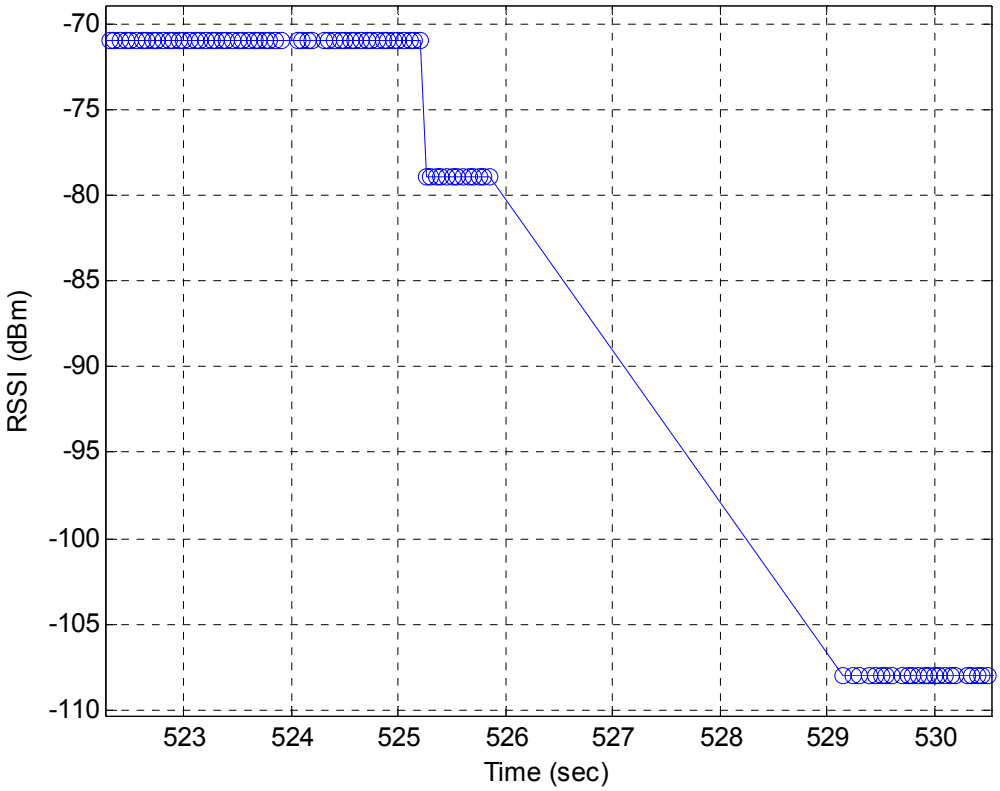

Figure 67: RSSI during Third Flight Pilot Control Loss

As in the second flight the flight test proceeded as planned despite the RSSI drops causing brief losses of pilot control. During final approach communication was lost again with the Yak-54. After communication with the ground station timed out the Piccolo activated the autopilot. As the aircraft was immediately commanded by the autopilot to accelerate to 70 knots the engine went to full power and the elevator deflected positively. This caused the aircraft to impact the runway. Figure 68 shows the RSSI drop during final approach that caused the autopilot activation and Figure 69 shows the engine RPM and throttle position at crash. The RPM is zero when communication is reacquired after the crash.

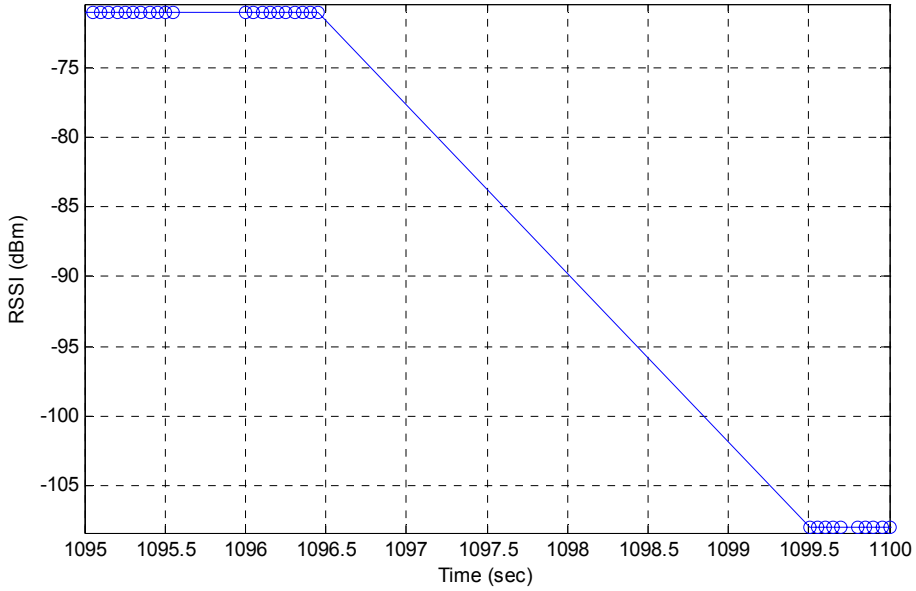

Figure 68: RSSI during Crash

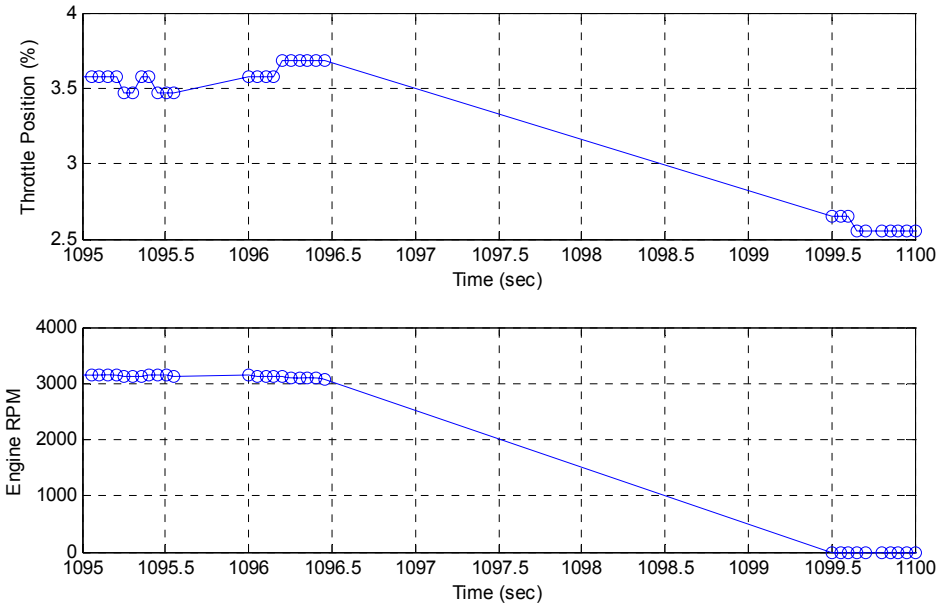

Figure 69: Engine Data during Crash

Figure 69 shows that at no point was the increase in RPM that was heard by the ground crew recorded by the ground station.

11.4 Accident Investigation

Post flight inspection of the communications equipment showed no damage to the aerial or ground antenna and cables. To help determine the cause of the crash a new RSSI analysis method was developed to analyze the communication system. The previous method of analyzing RSSI was to simply look at RSSI levels (i.e. did they drop below a certain threshold). The problem with this analysis was it only shows RSSI values that are received in the telemetry packet. Even when the RSSI was satisfactory there could be data drops. By analyzing the time between packets, however, a clearer picture of the communication system was developed. This analysis method, developed by Edmond Leong, computes the time between the current data packet and the last data packet and this value was displayed graphically. Figure 70 shows a plot of RSSI using this method.

The top plot on Figure 70 shows the previous method of analyzing RSSI. This was the RSSI plot for the taxi test before the March 13th flight test. This plot to the flight test team indicated excellent signal integrity, with the signal only dropping below the maximum level of -71 dB for a few moments during taxi, and then only to -86 dB. The bottom plot however showed a different story, with data drop outs higher than 1.5 seconds, even when RSSI is at maximum. It was seen in the bottom plot of Figure 70 that there appears to be a random autopilot ON instance at about 500 seconds into ground testing. Figure 71 shows a zoomed in view of this point.

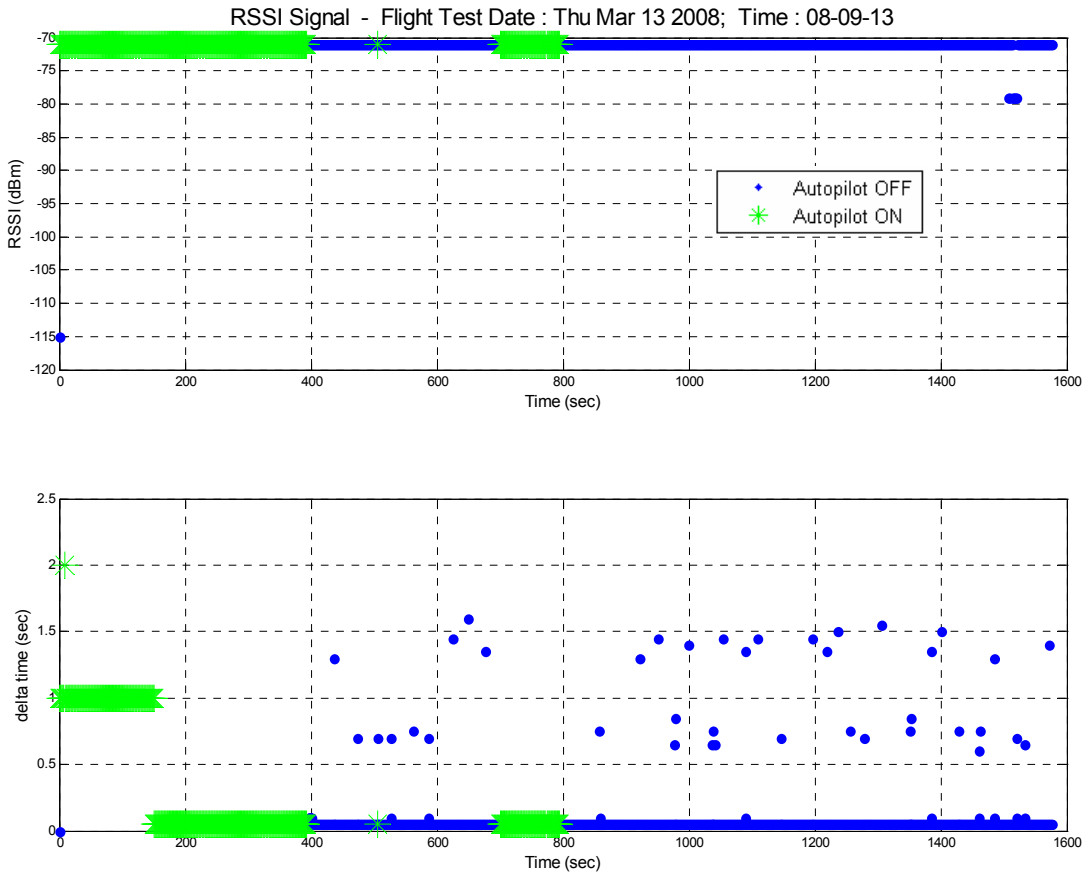

Figure 70: RSSI and Time between Packets during Ground Testing

Figure 71 shows that the autopilot has activated for about 0.5 seconds. This autopilot ON action was not done manually, but automatically. The only way it could happen automatically is if the pilot timeout limit was reach. The pilot timeout is defined as when uplink data (i.e. pilot commands) are no longer being received by the avionics. The timeout limit was set to 0.2 seconds. Thus the loss of pilot control was at least 0.9 seconds, as the autopilot ON telemetry was received for 0.7 seconds. There was an additional 0.7 seconds of lost telemetry where the autopilot may or may not have been activated.

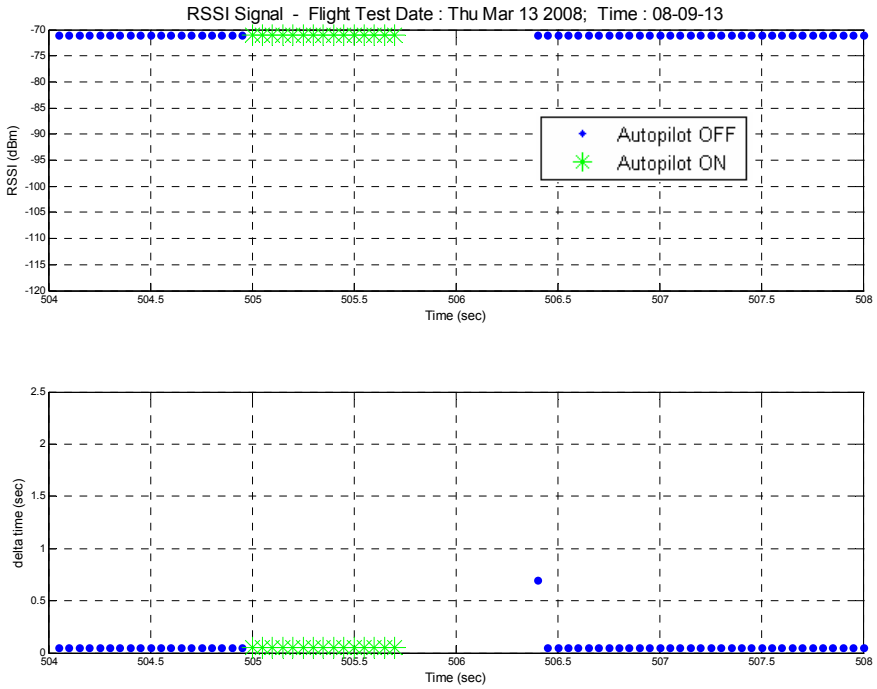

Figure 71: RSSI during Uncommanded Autopilot Activation

After these revelations of pilot timeout were made, a statistical analysis of the flight test was made.

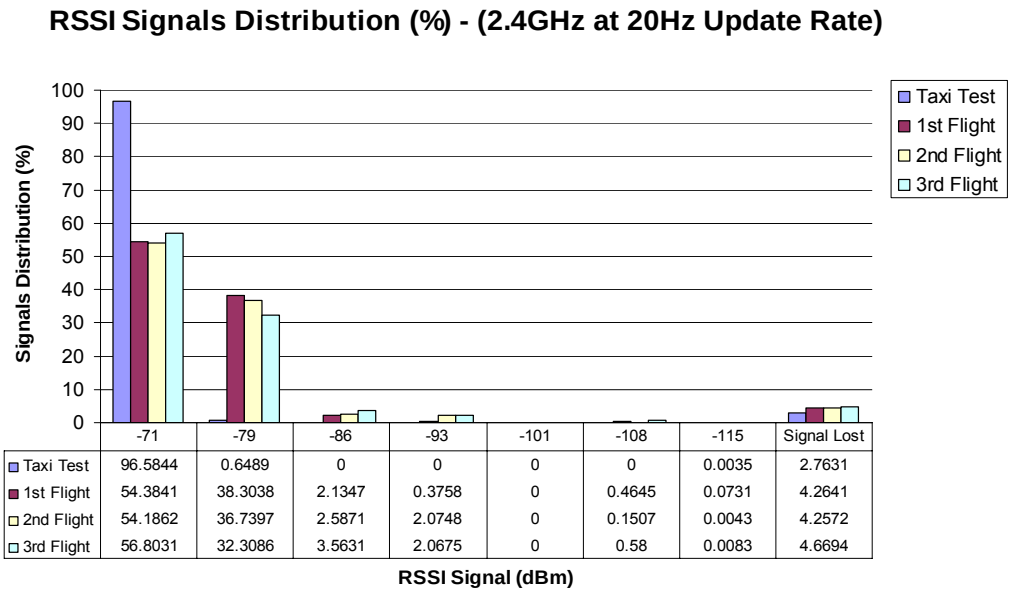

	-71	-79	-86	-93	-101	-108	-115	Signal Lost
Taxi Test	96.5844	0.6489	0	0	0	0	0.0035	2.7631
1st Flight	54.3841	38.3038	2.1347	0.3758	0	0.4645	0.0731	4.2641
2nd Flight	54.1862	36.7397	2.5871	2.0748	0	0.1507	0.0043	4.2572
3rd Flight	56.8031	32.3086	3.5631	2.0675	0	0.58	0.0083	4.6694

Figure 72: RSSI Signal Strength Levels and Percentage of Data Lost

Figure 72 shows there was a significant percentage of a data drop during the flight test, during flight averaging about 4.5%. Figure 73 shows the drop out time distribution for the flight test.

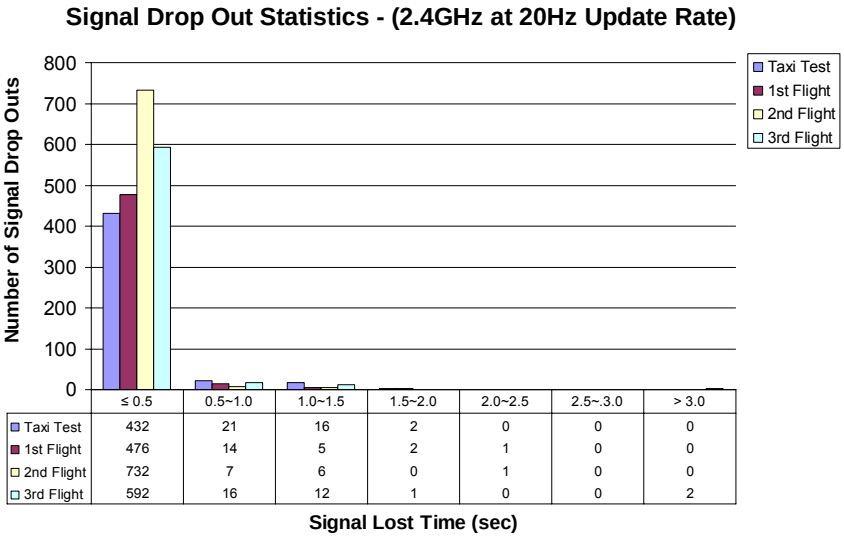

	≤ 0.5	0.5~1.0	1.0~1.5	1.5~2.0	2.0~2.5	2.5~3.0	> 3.0
Taxi Test	432	21	16	2	0	0	0
1st Flight	476	14	5	2	1	0	0
2nd Flight	732	7	6	0	1	0	0
3rd Flight	592	16	12	1	0	0	2

Figure 73: Data Loss Magnitudes

As can be seen in Figure 73 the communication dropouts last for significant amounts of time, some as long as 3.0 seconds. An analysis of the previous flight tests was also performed to examine if this phenomena was limited to the March 13th, 2008 flight test. Figure 74 shows the average dropout time per minute for all the previous Yak-54 Piccolo flight tests.

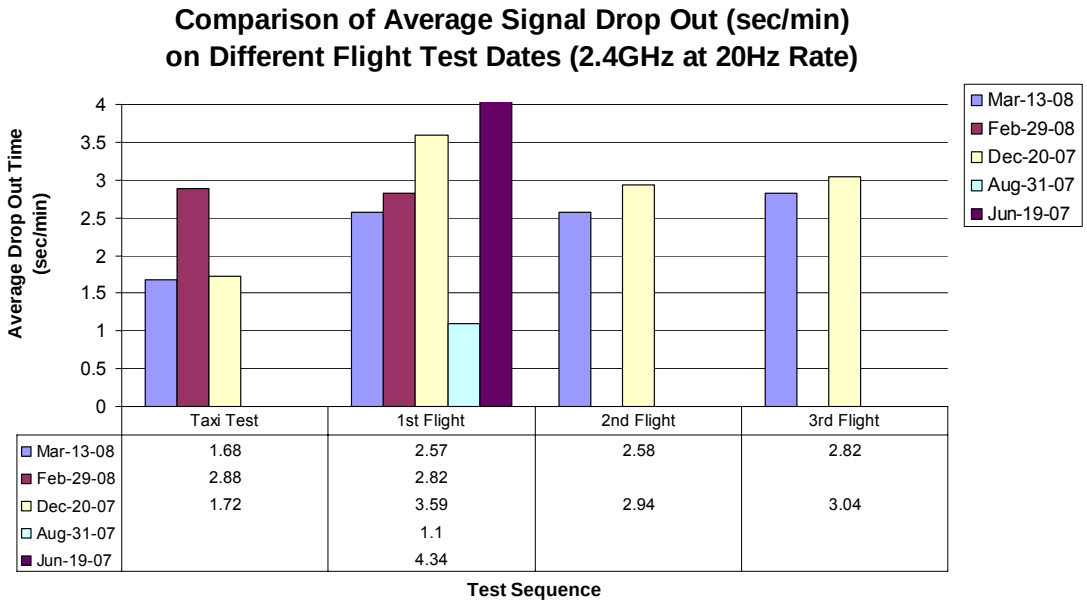

Figure 74: Data Dropout Rates during All Flight Tests

Figure 74 reveals that the average dropout per minute was actually lower for the March 13th, 2008 flight test than all other flight tests save the August 31st, 2007 flight test.

11.5 Communication System Laboratory Test

To help isolate the cause of the telemetry drops a series of lab tests were conducted. These tests analyzed:

1. Update Rate: 1 Hz vs. 20 Hz
2. Autopilot Mode: Manual vs. autopilot ON
3. Piccolo Unit: 1024 vs. 1027
4. Radio Module: Radio modules were switched between 1024 and 1027
5. Piccolo Power: Battery vs. Bench Power

6. Ground Station Networking: ON vs. OFF
7. Ground Station Power: Battery Powered vs. Wall Power
8. Transmission Frequency: 2.4 GHz vs. 900 MHz

The first lab test, 20 Hz vs. 1 Hz yielded some interesting results. Figure 75 shows the signal loss percentages for the test.

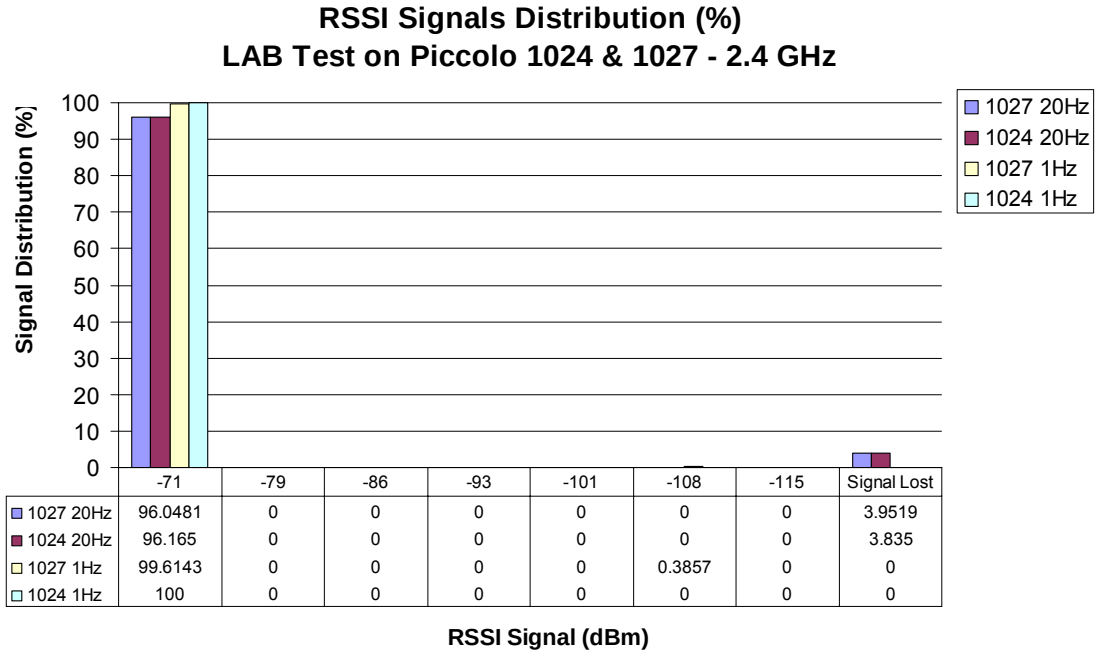

	-71	-79	-86	-93	-101	-108	-115	Signal Lost
1027 20Hz	96.0481	0	0	0	0	0	0	3.9519
1024 20Hz	96.165	0	0	0	0	0	0	3.835
1027 1Hz	99.6143	0	0	0	0	0.3857	0	0
1024 1Hz	100	0	0	0	0	0	0	0

Figure 75: RSSI Signal Strength and Percentage of Data Loss during Laboratory Test

The lab test shows that there was only a small difference in the performance of Piccolo 1024 and 1027 at both 20 Hz and 1 Hz. The lab test showed that there were no dropouts during the 1 Hz test for either Piccolo unit. There was however a small percentage of the time where the signal strength dropped to -108 dB on Piccolo 1027. A closer look at the data revealed some interesting data, which is presented in Figure 76.

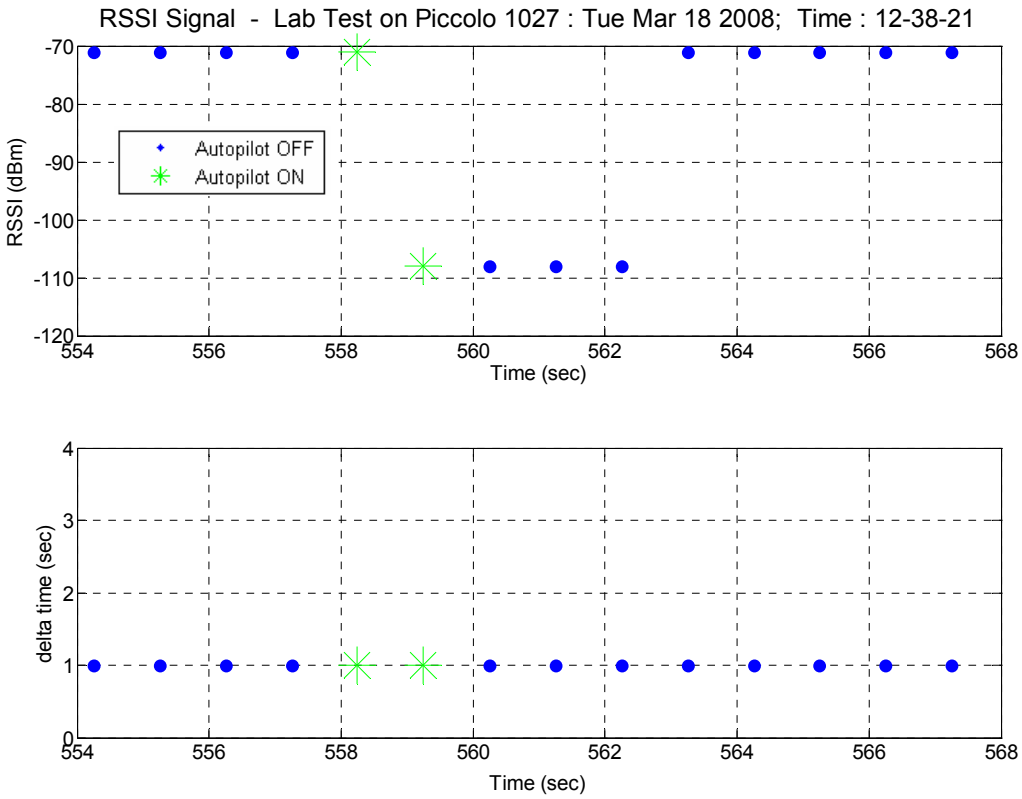

Figure 76: RSSI and Packet Time at Autopilot Activation during Lab Test

Figure 76 clearly shows that the autopilot was activated for at least 1 second. This could only have occurred due to the pilot timeout limit having been reached and thus that the autopilot can activate even in situations where no downlink data is missing.

The second laboratory test also revealed some very interesting information. The second test tested the system autopilot ON and OFF at 1 Hz and 20 Hz. The results are presented in Figure 77.

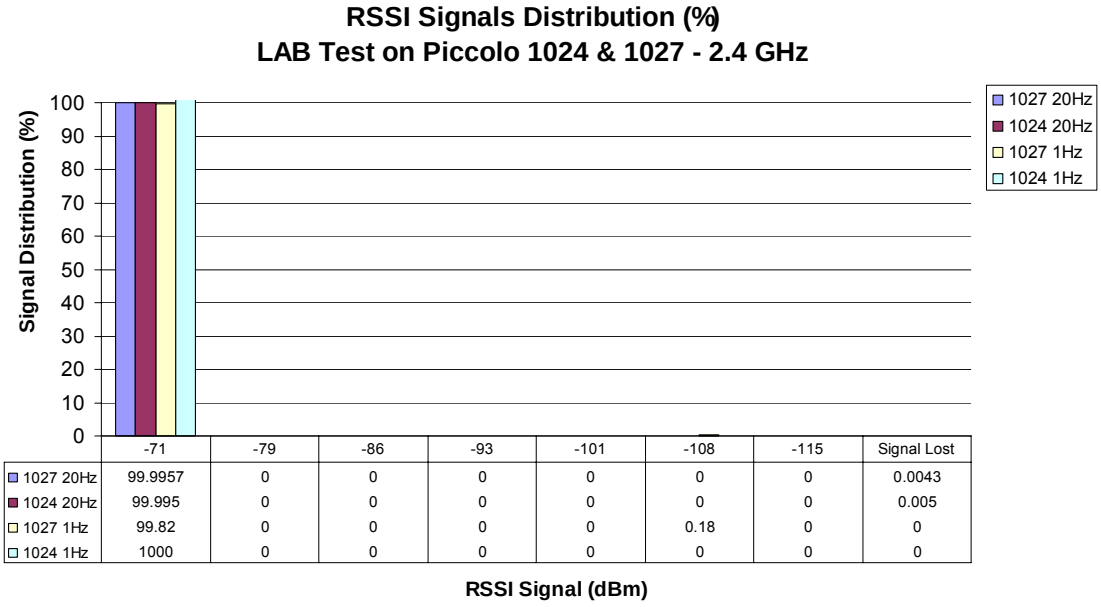

	-71	-79	-86	-93	-101	-108	-115	Signal Lost
1027 20Hz	99.9957	0	0	0	0	0	0	0.0043
1024 20Hz	99.995	0	0	0	0	0	0	0.005
1027 1Hz	99.82	0	0	0	0	0.18	0	0
1024 1Hz	1000	0	0	0	0	0	0	0

Figure 77: RSSI Signal Strength and Percentage of Data Loss during Autopilot ON Lab Test

Figure 77 shows that on autopilot mode ON there are virtually no dropouts. It should be noted that when the autopilot is on the only uplink data being sent to the Piccolo is the command to the Piccolo to send telemetry information to the ground station.

The other tests showed little statistical difference between the flight test data or the original laboratory manual tests at 20 Hz. Figure 78 shows the results of the other tests. Figure 78 does show another instance of -108 dB RSSI during the Piccolo 1027 bench power test. A closer look at the data once again reveals autopilot activation.

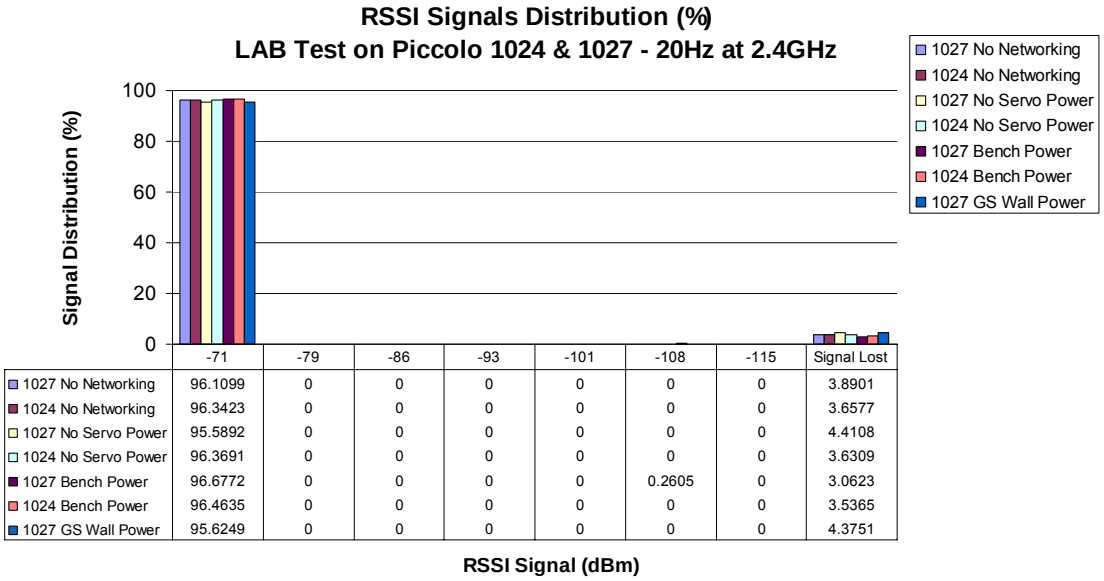

	-71	-79	-86	-93	-101	-108	-115	Signal Lost
1027 No Networking	96.1099	0	0	0	0	0	0	3.8901
1024 No Networking	96.3423	0	0	0	0	0	0	3.6577
1027 No Servo Power	95.5892	0	0	0	0	0	0	4.4108
1024 No Servo Power	96.3691	0	0	0	0	0	0	3.6309
1027 Bench Power	96.6772	0	0	0	0	0.2605	0	3.0623
1024 Bench Power	96.4635	0	0	0	0	0	0	3.5365
1027 GS Wall Power	95.6249	0	0	0	0	0	0	4.3751

Figure 78: RSSI Levels and Data Dropouts during Various Lab Tests

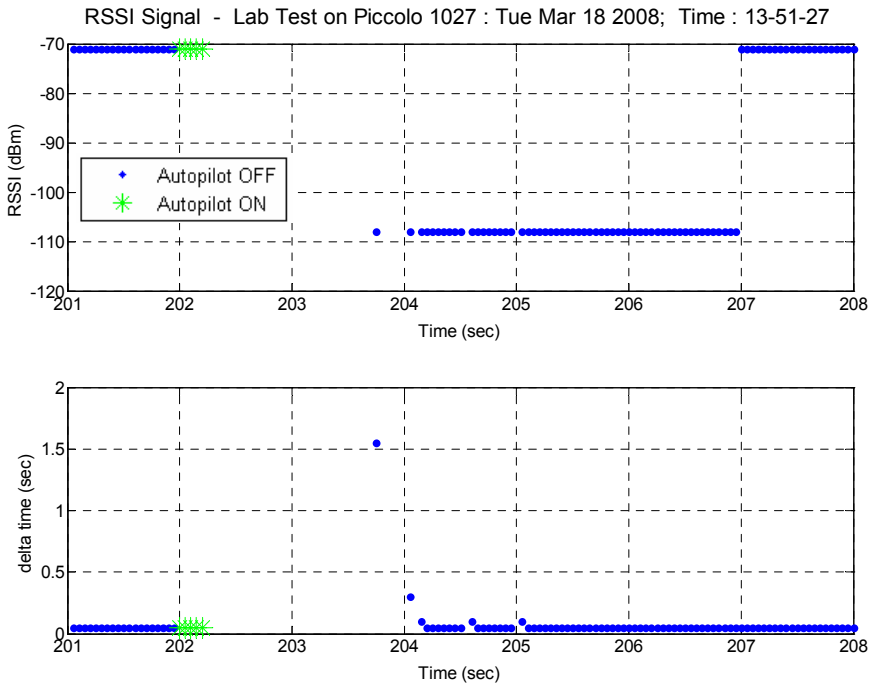

Figure 79: Autopilot Activation during Laboratory Test

Figure 80 shows that there is almost no difference in the different test scenarios except autopilot ON.

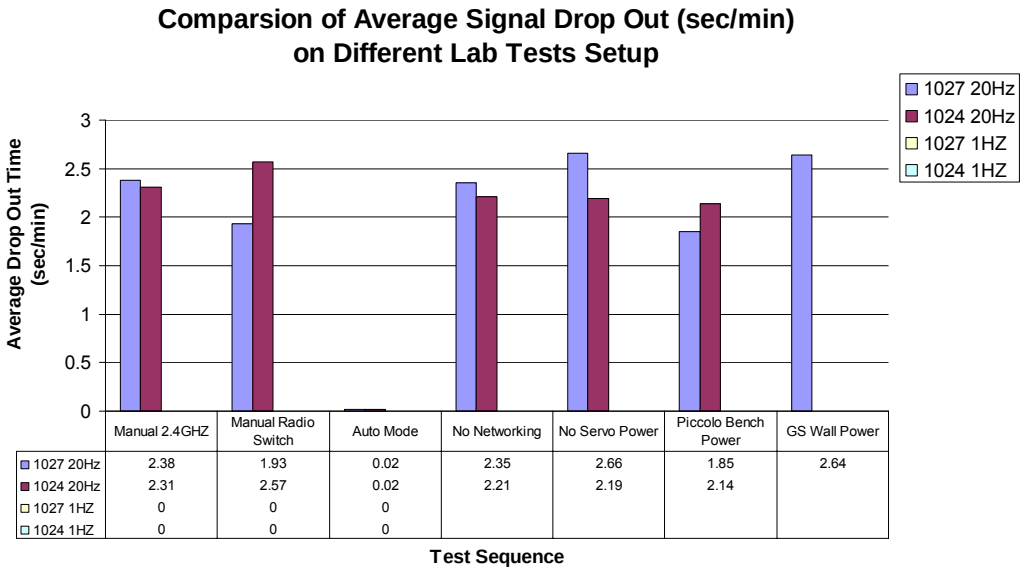

Figure 80: Dropout Rates for Laboratory Tests

The pilot timeout that occurred during the bench power test prompted an investigation of how many times during all testing (lab and flight) the autopilot activated. Figure 81 shows the number of times the autopilot activated due to the pilot communications timeout.

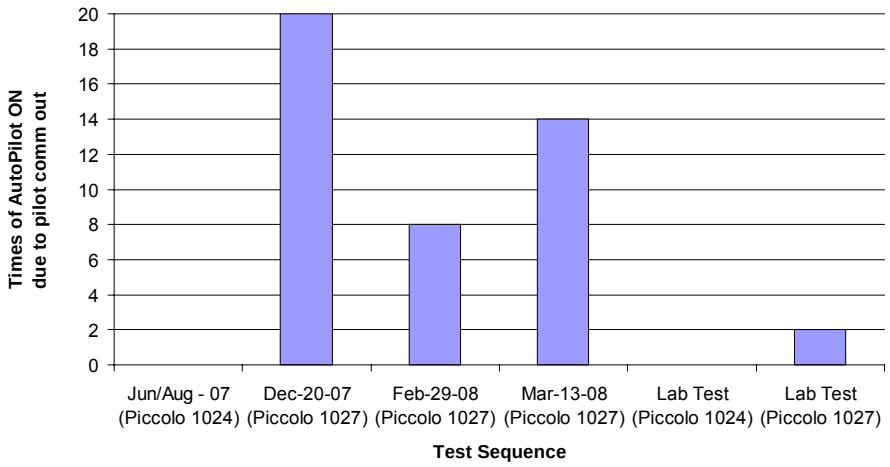

Figure 81: Autopilot Activation during Flight and Lab Test Activities

Figure 81 clearly shows that a significant number of times during flight test the autopilot activated on its own. It should be noted that during the Jun/Aug 2007 flight tests the pilot comm. timeout was set to 2.0 seconds. It should also be noted that these numbers only show the times when the autopilot activation was detected in telemetry. All of the pilot reported activations occurred did not show up in the telemetry and are thus not included in the number of activations shown in the figure.

The final test to be performed was to switch from 2.4 GHz to 900 MHz data transfer frequency. Figure 82 shows once again that the same random data drop occurs at this frequency.

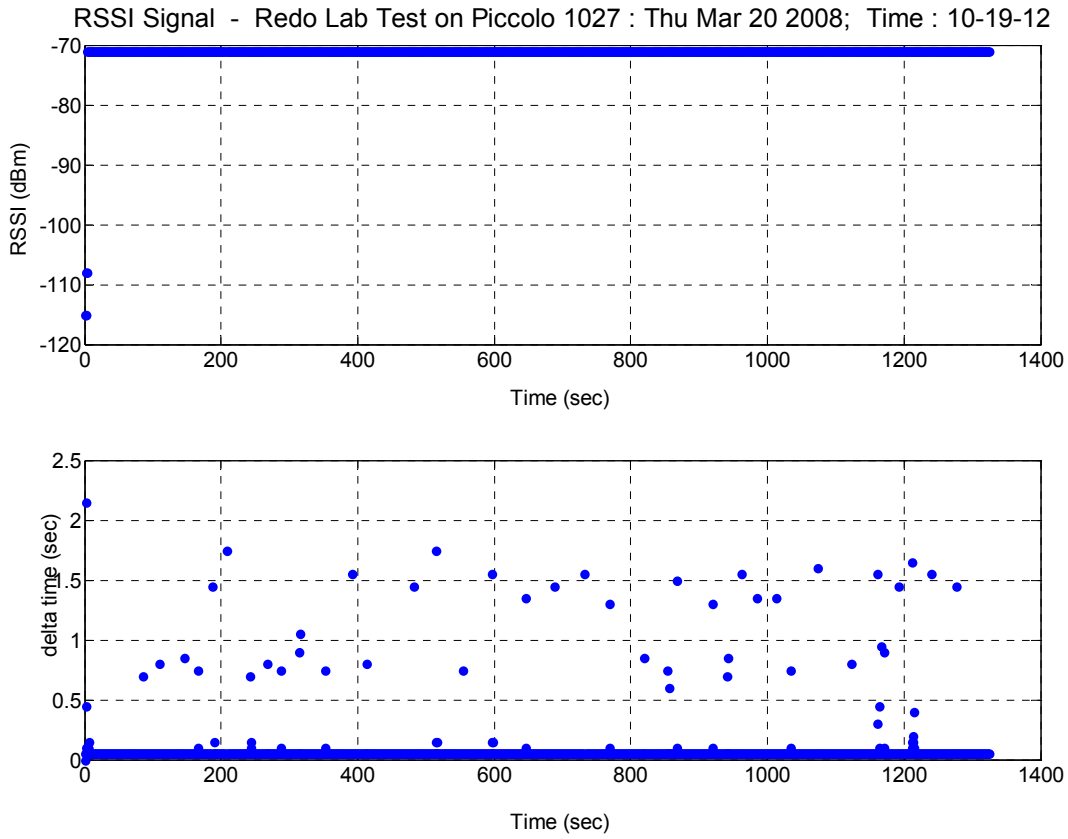

Figure 82: RSSI and Data Dropout Times during 900 MHz Lab Tests

11.6 Effect of Discrete Drop of Pilot Commands on Handling Qualities

After that laboratory investigation a new analysis of some of the final approaches was performed, as was described in Section 7.1. Figure 83 shows again the final approach where both time lag and data drops appear to have caused pitch instability and the pilot was forced to abort the landing.

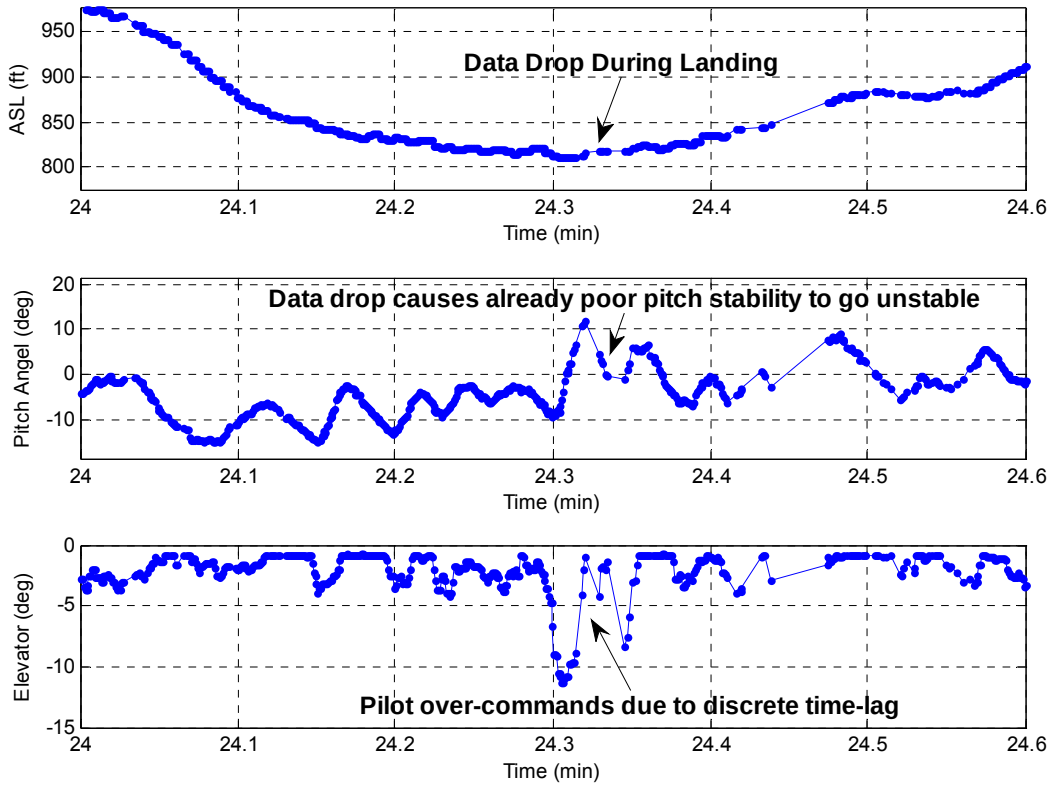

Figure 83: Poor Pilot-in-loop Pitch Stability Due to Time-Lag and Data Drop

Fortunately the thrust to weight ratio of the Yak-54 ($\frac{T_{max}}{W_g} = 1.38$) was such that extreme maneuvering and flight path angles were possible during aborted landings, thus preventing a crash. Using Roskam (Reference [36]) the effect that

these discrete data drops had on the system was analyzed. Roskam used the pilot transfer function approximation of:

$$Y_p(s) = \frac{K_p e^{-\tau s}(T_{lead}s + 1)}{(T_{lag}s + 1)(T_n s + 1)} \qquad 11.1$$

The $e^{-\tau s}$ term represents the pilot reaction time delay. A pilot is not an instantaneous controller and will have come delay while his senses perceive what is going on. Roskam stated that the typical pilot time delay is 0.12 to 0.2 seconds. Given that a remote pilot cannot perceive things as quickly as a manned pilot, as he only has his sense of vision to rely on, it was reasonable to say that the pilot time delay may be double to 0.24 to 0.4 seconds. As mentioned previously the pilot console was sampled by the ground station at 10 Hz, thus there can be up to a 0.1 second additional delay in the system. Thus the new pilot time lag was between 0.34 to 0.5 seconds. It has also been shown in lab tests that there are clear documented cases of between 0.2 seconds and 3 second data drops. This means that the new pilot lag time was between 0.34 seconds best case and 3.5 seconds worst case. Roskam states that a drunken pilot has a time delay of 0.6 seconds.

The analysis shows that the pilot in fact will drift in and out of the stability threshold of the system. The pilot does have the ability to lead known faults in the system, like the 0.1 second time delay. He does not, however, have the ability to lead unexpected lags in the system. The stability of the Yak-54 was improved by the addition of faster servos and improved damping of the short period mode, but clearly the aircraft was still operating in a near unstable or unstable flight regime.

11.7 Incident Investigation Conclusions

The incident investigation has shown that during nearly all of the laboratory tests and flight tests that the Piccolo had frequent and unexpected data drops. The data dropouts could not be correlated with RSSI or any other direct measure and hence cannot be predicted in a fluid flight test environment. The data dropouts were shown to not be correlated to the configuration of the system (i.e. power setup, Piccolo unit, etc.). The one variable that effected data dropout was the amount data transmitted both uplink and downlink. When the telemetry rate was reduced to 1 Hz, it is observed that downlink dropouts are negligible, although one instance of autopilot activation was observed. When the autopilot was ON there was no uplink data sent to the Piccolo, save the command for the autopilot to send telemetry to the ground station and in laboratory tests it was shown that when there was no uplink data there was no loss of downlink data. Thus it was reasonable to deduce that the communication system was not robust enough to handle high bandwidth communications. The drop of pilot packets was an inevitable phenomenon within the Piccolo system that cannot be predicted or avoided and caused the system to go unstable for short periods of time varying from 0.2 to 3 seconds.

12 Conclusions, Recommendations and Future Work

12.1 Piccolo II Flight Control System Test and Evaluation Conclusions

A thorough test and evaluation of the Piccolo II autopilot system has been performed and the following conclusions can be made:

- A thorough and deliberate test and evaluation process for modeling, simulation and flight control systems has been developed
- The AAA dynamic model predicts a response that is closer to flight test than the SCCS and AVL-HIL models
- A good simulation model allows the flight control engineer to tune the system much more efficiently than in flight test
- The Piccolo II flight control systems autonomous performance (from a stability and control standpoint) up to the flight incident was promising and could only be said to be positive
- Gain tuning during flight test is difficult, time consuming and expensive and would be very difficult to perform during flight test of the Meridian
- An efficient and safe flight test program was set up for flight testing the Piccolo II flight control system that could easily be adapted to Meridian flight testing, regardless of the flight control system used.
- Pilot induced oscillations occur due to the normal 0.1 second time lag in the system. The oscillations can be overcome somewhat through pilot training.
- Poor communication due to system overload was the cause of the crash.

- Discrete drops of pilot data cause the Piccolo II flight control system to go pilot-in-loop unstable at random points during flight causing extreme hazards to the safety of flight.

12.2 Piccolo II Flight Control System Test and Evaluation Recommendations

The following recommendations can be made from the test and evaluation performed on the Piccolo II flight control system:

- The Piccolo II flight control system should not be used on the Meridian.
- Real time data plotting would greatly enhance the ability of flight test engineers to tune the flight control system and monitor the health of the system and should be implemented on any flight test program.
- The flight test program developed should be duplicated for any other flight control system test program performed by CReSIS.
- Wind tunnel testing, system identification, CFD or other methods of enhancing dynamic models should be performed on the Meridian to maximize closed loop performance and thus optimize the Meridian's ability to perform the science mission.
- Evaluation of the communication system and its impact on safety of flight should be given higher priority in future flight control system evaluations so that problems might be identified sooner.

12.3 Future Work

The following recommendations can be made from the test and evaluation performed on the Piccolo II flight control system:

- A 6 DoF, nonlinear, hardware-in-loop simulator should be developed.
- System identification flight tests should be developed and flown on the Yak-54 to increase the dynamic model fidelity.
- The validity of AAA models of small scale aircraft should be investigated, ideally using system identification.
- The nonlinear effects of large flight regimes and the subsequent effect on controller tuning should be investigated
- A better engine thrust and power model should be developed.
- A secondary manual control system should be developed for further Piccolo II controller flight testing.
- Develop a good way to estimate phase margins with the Piccolo II
- An automatic take-off and landing system should be developed.

13 References

1. L. Berstien, P Bosch, et. al., "Climate Change 2007: Synthesis Report. Summary for Policy Makers," Intergovernmental Panel on Climate Change [online publication] URL: http://www.ipcc.ch/pdf/assessment-report/ar4/syr/ar4_syr_spm.pdf [cited 12 April 2008].

2. R. Hale, W. Donovan, M. Ewing, et. al., "The Meridian UAS: Detailed Design Review," Technical Report 124, Center for Remote Sensing of Ice Sheets, University of Kansas, Lawrence, KS, 25 June 2007.

3. K. Siegle, "Avionics System for the Center for Remote Sensing of Ice Sheets' Meridian UAV," Master's Project Paper, University of Kansas, Lawrence, KS, 1 December 2007.

4. D. Borys and R. Colgren, "Advances in Intelligent Autopilot Systems for Unmanned Aerial Vehicles," AIAA Guidance, Navigation and Control Conference, San Francisco, CA, 15-18 August 2005.

5. D. Jung and P. Tsiotras, "Modeling and Hardware-in-the-Loop Simulation for a Small Unmanned Aerial Vehicle," AIAA Infotech Aerospace Conference, Rohnert Park, CA, 7-10 May 2007.

6. M. Sadraey and R. Colgren, "UAV Flight Simulation: Credibility of Linear Decoupled vs. Nonlinear Coupled Equations of Motion," AIAA Modeling and Simulations Technology Conference, San Francisco, CA, 15-18 August 2005.

7. N. Jodeh, P. Blue and A. Waldron, "Development of Small Unmanned Aerial Vehicle Research Platform: Modeling and Simulation with Flight Test Validation," AIAA Modeling and Simulation Technologies Conference, Keystone, CO, 21-24 August 2006.

8. U. Ly and S. Higashino, "Development of a UAV Flight-Test Vehicle at the University of Washington," 2nd AIAA "Unmanned Unlimited" Systems, Technologies and Operations Aerospace Conference, San Diego, CA 15-18 September 2003.

9. J. Roskam, *Airplane Flight Dynamics and Automatic Flight Controls: Part I*, Fourth Printing, DARcorporation, Lawrence, KS, 2003.

10. B. Etkin and L. Ried, *Dynamics of Flight: Stability and Control*, Third Addition, John Wiley & Sons, Hoboken, NJ, 1996.

11. B. Pamadi, *Performance, Stability, Dynamics and Control of Airplanes*, AIAA, Reston, VA, 1998.

12. B. Stevens and F. Lewis, *Aircraft Control and Simulation*, Second Addition, John Wiley & Sons, Hoboken, NJ, 2003.

13. W. Phillips, *Mechanics of Flight*, John Wiley & Sons, Hoboken, NJ, 2004.

14. D. Ward and T. Strganac, *Introduction to Flight Test Engineering*, Second Edition, Second Printing, Kendall/Hunt Publishing, U.S.A., 2001.

15. R. Kimberlin, *Flight Testing of Fixed-Wing Aircraft*, AIAA, Reston, VA, 2003.

16. R. Jategaonkar, *Flight Vehicle System Identification: A Time Domain Methodology*, AIAA, Reston, VA 2006.

17. P. Hamel and R. Jategaonkar, "Evolution of Flight Vehicle System Identification," AIAA Journal of Aircraft, Vol. 33, No. 1, January-February 1996.

18. Y. Lee, S. Kim, J. Suk, H. Koo and J. Kim, "System Identification of an Unmanned Aerial Vehicle from Automated Flight Tests," AIAA's 1st Technical Conference and Workshop on Unmanned Aerial Vehicles, Portsmouth, VA, 20-23 May 2002.

19. M. Tischler and R. Remple, *Aircraft and Rotorcraft System Identification: Engineering Methods with Flight Test Examples*, AIAA, Reston, VA, 2006.

20. S. Bahndari and R. Colgren, "6-DoF Dynamic Model for a Raptor 50 UAV Helicopter Including Stabilizer Bar Dynamics," AIAA Modeling and Simulation Technologies Conference, Keystone, CA, 21-24 August 2006.

21. C. Theodore, M. Tischler and J. Colbourne, "Rapid Frequency-Domain Modeling Methods for Unmanned Aerial Vehicle Flight Control Applications," AIAA Journal of Aircraft, Vol. 41, No. 4, July-August 2004.

22. K. Ogata, *Modern Control Engineering,* Fourth Edition, Prentice Hall, Upper Saddle River, NJ, 2002.

23. M. Tischler, J. Lee and J. Colbourne, "Comparison of Flight Control System Design Using the CONDUIT Design Tool," AIAA Journal of Guidance, Control and Dynamics, Vol. 25, No. 3, May-June 2002.

24. Y. Miyazawa and T. Motoda, "Stochastic Gain Tuning Method Applied to Unmanned Space Vehicle Flight Control Design," AIAA Guidance, Navigation and Control Conference, Portland, OR, 9-11 August 1999.

25. V. Askue, *Flight Testing Homebuilt Aircarft*, Iowa State University Press, Ames Iowa, 1992.

26. B. Vaglienti, R. Hoag and M. Niculescu, "Piccolo System User's Guide," Version 2.0.5, Cloud Cap Technology, Hood River, OR, 25 June 2007.

27. Raymar Information Solutions Web Page, URL: http://www.raymarinc.com/images2/go%20book%203%20open.jpg, [cited 30 March 30th 2008].

28. B. Vaglienti, "Setup and Tuning of Piccolo Control Laws 2.0.x," Cloud Cap Technology, Hood River, OR, 20 June 2007.

29. B. Vaglienti, M. Niculescu and J. Becker "HIL/SIL Simulator for the Piccolo Avionics," Cloud Cap Technology, Hood River OR, 5 April 2007.

30. J. Becker, "Creating Vortex Lattice Models for the Piccolo Simulator with AVL," Cloud Cap Technology, Hood River, OR, 18 April 2007.

31. Aeroworks Web Page, URL: http://www.aero-works.net/store/images/upload/plane_large/75cc_yak03.jpg, [cited 16 March 2008].

32. S. Keshmiri, E. Leong, R. Jager and R. Hale, "Modeling and Simulation of the Yak-54 Scaled Unmanned Aerial Vehicle Using Parameter and System Identification,", accepted to the proceedings of the AIAA Atmospheric Flight Mechanics Conference and Exhibit, 18 – 21 Aug 2008, Honolulu, Hawaii.

33. E. Leong, R. Jager, S. Keshmiri and R. Colgren, "Complete Open Loop Dynamics Evaluation of a Small Unmanned Aerial Vehicle Using Different Modeling and Simulation Platforms with Flight Test Validation", accepted to the proceedings of the AIAA Atmospheric Flight Mechanics Conference and Exhibit, 18-21 Aug 2008, Honolulu, Hawaii.

34. 3W Modelmotoren Web Page, URL: http://www.3w-modellmotoren.com/english/www_3W_Modellmotoren_com.html, [cited 21 March 2008].

35. Electrodynamics Web Page, URL: http://electrodynam.com/rc/EDR-107/images/107s.jpg, [cited 25 March, 2008].

36. J. Roskam, *Airplane Flight Dynamics and Automatic Flight Controls: Part II*, Third Printing, DARcorporation, Lawrence, KS, 2003.

Appendix A: SCCS Yak-54 Model (ASCII Format)

```
// Yak-54 with 3W 75US engine and 24x10 prop

//------------------Aerodynamics: Wing------------//

//Reference Area, in m^2
Wing_Area=1.0645

//Wing Span in m
Wing_Span=2.3876

//Taper Ratio
Wing_Taper=0.46

//Wing Aerodynamics Look Up Table
Wing_LUT=Yak_wing.lut

//Incidence angle wrt fuselage center line, in deg
Wing_Incidence=0

// Dihedral angle, in deg
Wing_Dihedral=0

//Quarter Chord Sweep Angle
Wing_Sweep=-2

//Oswald's Efficiency Factor
Wing_Span_Efficiency=0.9

// Position of wing ac wrt to cg, in m
Wing_X=-0.037338
Wing_Z=0


//-----------Wing Control Surfaces--------------//

//Left Aileron

// Spanwise location of inboard station, in m
Left_Aileron_Inboard=-0.1778

// Spanwise location of outboard station, in m
```

```
Left_Aileron_Outboard=-1.1862

// Average aileron chord, in m
Left_Aileron_Chord=0.1247

// Channel number
Left_Aileron_Channel=0

//Right aileron

// Spanwise location of inboard station, in m
Right_Aileron_Inboard=0.1778

// Spanwise location of outboard station, in m
Right_Aileron_Outboard=1.1862

// Average aileron chord, in m
Right_Aileron_Chord=0.1247

// Channel number
Right_Aileron_Channel=5

//--------------------  AERODYNAMICS: HORIZONTAL TAIL  ----------------------//

// Reference area, in m^2
Tail_Area=0.21368

// Span, in m
Tail_Span=0.9144

// Taper ratio
Tail_Taper=0.81

//Tail Aerodynamics
Tail_LUT=Yak_tail.lut

// Location of tail ac wrt to aircraft cg, in m
Tail_X=-1.0762
Tail_Z=-0.0127

// Oswald efficiency factor
Tail_Span_Efficiency=1.0

// Incidence angle wrt to fuselage center line, in deg
```

```
Tail_Incidence=0

// Dihedral angle, in deg
Tail_Dihedral=0

// Sweep angle of the quarter chord line, in deg
Tail_Sweep=12.6

// HORIZONTAL TAIL CONTROL SURFACES

// (Elevators move in unison, controlled by the same servo channel)

// Left elevator

// Spanwise location of the inboard station, in m
Left_Elevator_Inboard=0

// Spanwise location of the outboard station, in m
Left_Elevator_Outboard=-0.4572

// Average chord, in m
Left_Elevator_Chord=0.10668

// Channel number
Left_Elevator_Channel=1

// Sense of rotation
Left_Elevator_Sign=1

// Right elevator

// Spanwise location of the inboard station, in m
Right_Elevator_Inboard=0

// Spanwise location of the outboard station, in m
Right_Elevator_Outboard=0.4572

// Average chord, in m
Right_Elevator_Chord=0.10668

// Channel number
Right_Elevator_Channel=1

// Sense of rotation
```

```
Right_Elevator_Sign=1


//--------------------  AERODYNAMICS: VERTICAL TAIL  --------------------//

// Reference area, in m^2
Left_Fin_Area=0.1486
// Span, in m
Left_Fin_Span=0.4318
// Taper ratio
Left_Fin_Taper=0.35

//Fin Aerodynamics
Left_Fin_LUT = Yak_fin.lut

// Oswald efficiency factor
Left_Fin_Span_Efficiency=1.0

// Location of vertical tail ac wrt to aircraft cg, in m
Left_Fin_X=-1.12649
Left_Fin_Z=-0.231902
Left_Fin_Y=0.0

// VERTICAL TAIL CONTROL SURFACES

// Rudder

// Position of bottom section wrt to aircraft cg, in m
Left_Rudder_Bottom=0.016

// Position of top section, wrt to aircraft cg, in m
Left_Rudder_Top=-0.4478

// Average chord, in m
Left_Rudder_Chord=0.2159

// Channel number
Left_Rudder_Channel=3

// Sense of rotation
Left_Rudder_Sign=1


//--------------------  AERODYNAMICS: FUSELAGE  --------------------//
```

```
// Reference area, in m^2
Fuse_Area=0.05587

// Total length, in m
Fuse_Length=2.0574

// Parasitic drag
Fuse_Parasitic_Drag=0.013

// Slope of lift coefficient
Fuse_Lift_Slope=0.0

// Slope of side force coefficient
Fuse_SideForce_Slope=0.0

// Slope of pitch moment coefficient
Fuse_Pitching_Moment_Slope=0

// Slope of yaw moment coefficient
Fuse_Yawing_Moment_Slope=0

// Position of fuselage ac wrt to aircraft cg, in m
Fuse_X=0.0
Fuse_Y=0.0



//--------------------  PROPULSION  ---------------------//

// Engine is 3W 75cc, 7.5 hp

//Engine Type is Piston
Left_Engine_Type=0

// Channel number
Left_Engine_Channel=2

// Engine parameters look-up table
Left_Engine_LUT=Fuji86ccEngine.lut

// Propeller is APC 24x10

// Prop diameter, in m
```

```
Left_Prop_Diameter=0.60696

// Position of propeller hub wrt to aircraft cg, in m
Left_Prop_X=0.5715

//Propellor Pan Angle
Left_Prop_Pan=3

// Moment of inertia in kg/m^2
Left_Prop_Inertia=0.0025

// Propeller coefficients look-up table
Left_Prop_LUT=apc24x10.prd

//-----------------Inertia Model--------------//

//Gross Mass in Kg
Gross_Mass=12.755

//Empty Mass in Kg
Empty_Mass=12.33

//Moments of Inertia
Roll_Inertia=1.30592385
Pitch_Inertia=3.92075434
Yaw_Inertia=5.15970078
Roll_Yaw_Coulpled_Inertia = 0
```

Appendix B: SCCS Wing File (ASCII Format)

```
//Yak-54 Wing Properties
// alpha  CL             CD       CM

-15     -1.072068493 0.086106841  0
-14     -1.00059726  0.076323293  0
-13     -0.929126027 0.067214472  0
-12     -0.857654794 0.058780379  0
-11     -0.786183562 0.051021013  0
-10     -0.714712329 0.043936374  0
-9      -0.643241096 0.037526463  0
-8      -0.571769863 0.031791279  0
-7      -0.50029863  0.026730823  0
-6      -0.428827397 0.022345095  0
-5      -0.357356164 0.018634093  0
-4      -0.285884931 0.01559782   0
-3      -0.214413699 0.013236274  0
-2      -0.142942466 0.011549455  0
-1      -0.071471233 0.010537364  0
0       0.0000000000 0.010200000  0
1       0.071471233  0.010537364  0
2       0.142942466  0.011549455  0
3       0.214413699  0.013236274  0
4       0.285884931  0.01559782   0
5       0.357356164  0.018634093  0
6       0.428827397  0.022345095  0
7       0.50029863   0.026730823  0
8       0.571769863  0.031791279  0
9       0.643241096  0.037526463  0
10      0.714712329  0.043936374  0
11      0.786183562  0.051021013  0
12      0.857654794  0.058780379  0
13      0.929126027  0.067214472  0
14      1.00059726   0.076323293  0
15      1.072068493  0.086106841  0
```

Appendix C: SCCS Horizontal Tail File (ASCII Format)

```
//Yak-54 H-Tail
// alpha  CL              CD      CM

Alpha  CL      CD      CM
-15    -0.952949772 0.076371255  0
-14    -0.889419787 0.066850071  0
-13    -0.825889802 0.05798552   0
-12    -0.762359817 0.049777603  0
-11    -0.698829832 0.042226319  0
-10    -0.635299848 0.035331669  0
-9     -0.571769863 0.029093652  0
-8     -0.508239878 0.023512268  0
-7     -0.444709893 0.018587518  0
-6     -0.381179909 0.014319401  0
-5     -0.317649924 0.010707917  0
-4     -0.254119939 0.007753067  0
-3     -0.190589954 0.00545485   0
-2     -0.12705997  0.003813267  0
-1     -0.063529985 0.002828317  0
0      0.0000000000 0.002500000  0
1      0.063529985  0.002828317  0
2      0.12705997   0.003813267  0
3      0.190589954  0.00545485   0
4      0.254119939  0.007753067  0
5      0.317649924  0.010707917  0
6      0.381179909  0.014319401  0
7      0.444709893  0.018587518  0
8      0.508239878  0.023512268  0
9      0.571769863  0.029093652  0
10     0.635299848  0.035331669  0
11     0.698829832  0.042226319  0
12     0.762359817  0.049777603  0
13     0.825889802  0.05798552   0
14     0.889419787  0.066850071  0
15     0.952949772  0.076371255  0
```

Appendix D: SCCS Vertical Tail File (ASCII Format)

```
//Yak-54 V-Tail
//Beta  CY       CD      CM

-15     -0.952949772 0.075571255  0
-14     -0.889419787 0.066050071  0
-13     -0.825889802 0.05718552   0
-12     -0.762359817 0.048977603  0
-11     -0.698829832 0.041426319  0
-10     -0.635299848 0.034531669  0
-9      -0.571769863 0.028293652  0
-8      -0.508239878 0.022712268  0
-7      -0.444709893 0.017787518  0
-6      -0.381179909 0.013519401  0
-5      -0.317649924 0.009907917  0
-4      -0.254119939 0.006953067  0
-3      -0.190589954 0.00465485   0
-2      -0.12705997  0.003013267  0
-1      -0.063529985 0.002028317  0
0       0.0000000000 0.001700000  0
1       0.063529985  0.002028317  0
2       0.12705997   0.003013267  0
3       0.190589954  0.00465485   0
4       0.254119939  0.006953067  0
5       0.317649924  0.009907917  0
6       0.381179909  0.013519401  0
7       0.444709893  0.017787518  0
8       0.508239878  0.022712268  0
9       0.571769863  0.028293652  0
10      0.635299848  0.034531669  0
11      0.698829832  0.041426319  0
12      0.762359817  0.048977603  0
13      0.825889802  0.05718552   0
14      0.889419787  0.066050071  0
15      0.952949772  0.075571255  0
```

Appendix E: SCCS Engine File (ASCII Format)

```
# 3W 80cc
# Look-up Table
# Wide open throttle
# RPM Power[W]
   0    0.00
1100  100.00
2000  725.75
3000 1421.00
4000 2116.30
5000 2811.60
6000 3506.90
7000 4202.20
8000 4897.50
9000 5592.75
```

Appendix F: SCCS Propeller File (ASCII Format)

```
//Bolly 26 x 10 Propeller
  J       Cp      Ct
-1.00  -0.0188  0.0699
-0.95  -0.0153  0.0698
-0.90  -0.0118  0.0696
-0.85  -0.0083  0.0695
-0.80  -0.0049  0.0693
-0.75  -0.0014  0.0692
-0.70   0.0021  0.0691
-0.65   0.0056  0.0689
-0.60   0.0091  0.0688
-0.55   0.0126  0.0687
-0.50   0.0160  0.0685
-0.45   0.0195  0.0684
-0.40   0.0230  0.0682
-0.35   0.0265  0.0681
-0.30   0.0300  0.0680
-0.25   0.0335  0.0678
-0.20   0.0370  0.0677
-0.15   0.0404  0.0675
-0.10   0.0439  0.0674
-0.05   0.0474  0.0673
 0.00   0.0509  0.0661
 0.05   0.0544  0.0641
 0.10   0.0569  0.0686
 0.15   0.0557  0.0683
 0.20   0.0551  0.0675
 0.25   0.0548  0.0670
 0.30   0.0547  0.0665
 0.35   0.0530  0.0661
 0.40   0.0492  0.0664
 0.45   0.0494  0.0660
 0.50   0.0493  0.0654
 0.55   0.0495  0.0643
 0.60   0.0496  0.0628
 0.65   0.0496  0.0604
 0.70   0.0490  0.0569
 0.75   0.0470  0.0518
 0.80   0.0439  0.0460
 0.85   0.0404  0.0400
 0.90   0.0362  0.0339
```

0.91	0.0353	0.0327
0.92	0.0344	0.0314
0.93	0.0335	0.0302
0.94	0.0325	0.0290
0.95	0.0316	0.0277
0.96	0.0306	0.0265
0.97	0.0296	0.0253
0.98	0.0285	0.0240
0.99	0.0274	0.0228
1.00	0.0264	0.0215
1.01	0.0252	0.0203
1.02	0.0241	0.0190
1.03	0.0229	0.0177
1.04	0.0218	0.0165
1.05	0.0206	0.0152
1.06	0.0193	0.0139
1.07	0.0181	0.0127
1.08	0.0168	0.0114
1.09	0.0155	0.0101
1.10	0.0142	0.0088
1.11	0.0128	0.0076
1.12	0.0115	0.0063
1.13	0.0101	0.0050
1.14	0.0086	0.0037
1.15	0.0072	0.0024
1.16	0.0057	0.0010
1.17	0.0046	-0.0002
1.18	0.0032	-0.0015
1.19	0.0019	-0.0028
1.20	0.0005	-0.0041
1.21	-0.0008	-0.0053
1.22	-0.0022	-0.0066
1.23	-0.0035	-0.0079
1.24	-0.0049	-0.0092
1.25	-0.0062	-0.0105
1.26	-0.0076	-0.0118
1.27	-0.0089	-0.0131
1.28	-0.0103	-0.0144
1.29	-0.0116	-0.0156
1.30	-0.0130	-0.0169
1.31	-0.0143	-0.0182
1.32	-0.0157	-0.0195
1.33	-0.0170	-0.0208
1.34	-0.0184	-0.0221

1.35 -0.0197 -0.0234
1.36 -0.0211 -0.0247
1.37 -0.0224 -0.0259
1.38 -0.0238 -0.0272
1.39 -0.0252 -0.0285
1.40 -0.0265 -0.0298
1.41 -0.0279 -0.0311
1.42 -0.0292 -0.0324
1.43 -0.0306 -0.0337
1.44 -0.0319 -0.0350
1.45 -0.0333 -0.0362
1.46 -0.0346 -0.0375
1.47 -0.0360 -0.0388
1.48 -0.0373 -0.0401
1.49 -0.0387 -0.0414
1.50 -0.0400 -0.0427
1.51 -0.0414 -0.0440
1.52 -0.0427 -0.0453
1.53 -0.0441 -0.0465
1.54 -0.0454 -0.0478
1.55 -0.0468 -0.0491
1.56 -0.0481 -0.0504
1.57 -0.0495 -0.0517
1.58 -0.0508 -0.0530
1.59 -0.0522 -0.0543
1.60 -0.0535 -0.0556
1.61 -0.0549 -0.0568
1.62 -0.0562 -0.0581
1.63 -0.0576 -0.0594
1.64 -0.0589 -0.0607
1.65 -0.0603 -0.0620
1.66 -0.0616 -0.0633
1.67 -0.0630 -0.0646
1.68 -0.0643 -0.0659
1.69 -0.0657 -0.0671
1.70 -0.0670 -0.0684
1.71 -0.0684 -0.0697
1.72 -0.0697 -0.0710
1.73 -0.0711 -0.0723
1.74 -0.0725 -0.0736
1.75 -0.0738 -0.0749
1.76 -0.0752 -0.0762
1.77 -0.0765 -0.0774
1.78 -0.0779 -0.0787

1.79	-0.0792	-0.0800
1.80	-0.0806	-0.0813
1.81	-0.0819	-0.0826
1.82	-0.0833	-0.0839
1.83	-0.0846	-0.0852
1.84	-0.0860	-0.0865
1.85	-0.0873	-0.0877
1.86	-0.0887	-0.0890
1.87	-0.0900	-0.0903
1.88	-0.0914	-0.0916
1.89	-0.0927	-0.0929
1.90	-0.0941	-0.0942
1.91	-0.0954	-0.0955
1.92	-0.0968	-0.0968
1.93	-0.0981	-0.0980
1.94	-0.0995	-0.0993
1.95	-0.1008	-0.1006
1.96	-0.1022	-0.1019
1.97	-0.1035	-0.1032
1.98	-0.1049	-0.1045
1.99	-0.1062	-0.1058
2.00	-0.1076	-0.1071

Appendix G: AVL Input Geometry File (ASCII Format)

```
#************************************
#AVL dataset for Yak-54 wing/tail
#************************************
AEROSONDE
#Mach
0.1
#IYsym   IZsym   Zsym
0       0       0.0
#Sref    Cref    Bref
1.06   0.465  2.288
#
#AVL Axes:
#  +X   downstream
#  +Y   out the right wing
#  +Z   up
#Xref, Yref, Zref is the CG
#Xref    Yref    Zref
0.00     0.0       0.0
#
#**********************************
SURFACE
RWing
#Nchordwise  Ccpace  Nspanwise  Sspace
8            1.0     14         -2.0
#root chord wing 0.242 (old wing keep at 0.254)
#
#=================Center section
SECTION
#Xle        Yle   Zle   Chord AngleOfIncidence
-0.224 0.0 0.0 0.61 0.0 14 -2.0
#
NACA
0016
#Set  dcl/da  =  2 pi CLaf, i.e. CLaf = CLalpha/(2*pi)
CLAF
0.6517
#Set parabolic drag polar
#CL1 CD1  CL2 CD2  CL3 CD3    |  CD(CL) function parameters
CDCL
0.2142 0.00737 0.4235 0.00741 1.3075 0.01381
#
#=================Define section where aileron starts
SECTION
#Xle    Yle    Zle     Chord   AngleOfIncidence
-0.218 0.197 0.0 0.559 0.0 14 -2.0
CONTROL
#control angle is in degrees (for radians set gain=180/pi=57.29578
#label   gain xfrac  vx vy vz sgn
Raileron  1.0  0.75  0. 0. 0.  -1.
NACA
```

```
0016
#Set  dcl/da  =  2 pi CLaf, i.e. CLaf = CLalpha/(2*pi)
CLAF
0.6517
#Set parabolic drag polar
#CL1 CD1  CL2 CD2  CL3 CD3    |  CD(CL) function parameters
CDCL
0.2142 0.00737 0.4235 0.00741 1.3075 0.01381

#=================Define wingtip section
SECTION
#Xle    Yle    Zle     Chord   AngleOfIncidence
-0.1849 1.3811 0. 0.2794 0. 14 -2.0
CONTROL
#label   gain xfrac  vx vy vz sgn
Raileron  1.0  0.705  0. 0. 0.  -1.
NACA
0017
#Set  dcl/da  =  2 pi CLaf, i.e. CLaf = CLalpha/(2*pi)
CLAF
0.6517
#Set parabolic drag polar
#CL1 CD1  CL2 CD2  CL3 CD3    |  CD(CL) function parameters
CDCL
0.2142 0.00737 0.4235 0.00741 1.3075 0.01381
#**********************************
SURFACE
LWing
#Nchordwise  Ccpace  Nspanwise  Sspace
8            1.0     14         2.0
#=================Define wingtip section
SECTION
#Xle    Yle    Zle     Chord   AngleOfIncidence
-0.1849 -1.3811 0.0 0.2794 0. 14 -2.0
CONTROL
#label   gain xfrac  vx vy vz sgn
Laileron  1.0  0.705  0. 0. 0.  -1.
NACA
0017
#Set  dcl/da  =  2 pi CLaf, i.e. CLaf = CLalpha/(2*pi)
CLAF
0.6517
#Set parabolic drag polar
#CL1 CD1  CL2 CD2  CL3 CD3    |  CD(CL) function parameters
CDCL
0.2135 0.00651 0.4310 0.00702 1.0646 0.01161
#=================Define section where aileron starts
SECTION
#Xle    Yle    Zle     Chord   AngleOfIncidence
-0.218 -0.197 0. 0.559 0. 14 -2.0
CONTROL
#control angle is in degrees (for radians set gain=180/pi=57.29578
#label   gain xfrac  vx vy vz sgn
Laileron  1.0  0.75  0. 0. 0.  -1.
```

```
NACA
0016
#Set  dcl/da  =  2 pi CLaf, i.e. CLaf = CLalpha/(2*pi)
CLAF
0.6517
#Set parabolic drag polar
#CL1 CD1  CL2 CD2  CL3 CD3    |  CD(CL) function parameters
CDCL
0.2142 0.00737 0.4235 0.00741 1.3075 0.01381
#=================Center section
SECTION
#Xle    Yle    Zle     Chord   AngleOfIncidence
-0.224 0. 0. 0.61 0. 14 -2.0
NACA
0016
#Set  dcl/da  =  2 pi CLaf, i.e. CLaf = CLalpha/(2*pi)
CLAF
0.6517
#Set parabolic drag polar
#CL1 CD1  CL2 CD2  CL3 CD3    |  CD(CL) function parameters
CDCL
0.2142 0.00737 0.4235 0.00741 1.3075 0.01381
#
#**********************************
SURFACE
RHTail
#Nchordwise  Cspace   Nspanwise   Sspace
8            1.0       8          1.0
#
#================R H Tail Center section
#Tail 4.15 m from Datum to LE h tail
SECTION
#Xle    Yle    Zle     Chord   AngleOfIncidence
0.798 0. 0.01 0.164 0. 8 1.0
NACA
0015
CONTROL
#label   gain xfrac  vx vy vz sgn
Relevator  1  1.00  0. 0. 0.   1.
#=================R H Tail Elevator Starts
SECTION
#Xle    Yle    Zle     Chord   AngleOfIncidence
0.808 0.0254 0.01 0.184 0. 8 1.0
NACA
0015
CONTROL
#label   gain xfrac  vx vy vz sgn
Relevator  1  0.862  0. 0. 0.   1.
#=================R H Tail Elevator Shifts Forward
SECTION
#Xle    Yle    Zle     Chord   AngleOfIncidence
0.831 0.138 0.01 0.3 0. 8 1.0
NACA
0012
```

```
CONTROL
#label   gain xfrac  vx vy vz sgn
Relevator  1  0.46  0. 0. 0.   1.
#=================R H Tail Elevator Goes Big
SECTION
#Xle    Yle    Zle     Chord   AngleOfIncidence
0.887 0.354 0.01 0.2261 0. 8 1.0
NACA
0010
CONTROL
#label   gain xfrac  vx vy vz sgn
Relevator  1  0.32  0. 0. 0.   1.
#=================R H Tail Tip
SECTION
#Xle    Yle    Zle     Chord   AngleOfIncidence
0.902 0.419 0.01 0.2096 0. 8 1.0
NACA
0009
CONTROL
#label   gain xfrac  vx vy vz sgn
Relevator  1  0.0  0. 0. 0.   1.
#**********************************
SURFACE
LHTail
#Nchordwise  Cspace   Nspanwise   Sspace
8            1.0       8          1.0
#=================L H Tail Tip
SECTION
#Xle    Yle    Zle     Chord   AngleOfIncidence
0.887 -0.419 0.01 0.2096 0. 8 1.0
NACA
0009
CONTROL
#label   gain xfrac  vx vy vz sgn
Lelevator  1  0.0  0. 0. 0.   1.
#=================L H Tail Elevator Goes Big
SECTION
#Xle    Yle    Zle     Chord   AngleOfIncidence
0.887 -0.354 0.01 0.2261 0. 8 1.0
NACA
0010
CONTROL
#label   gain xfrac  vx vy vz sgn
Lelevator  1  0.32  0. 0. 0.   1.
#=================L H Tail Elevator Shifts Forward
SECTION
#Xle    Yle    Zle     Chord   AngleOfIncidence
0.831 -0.138 0.01 0.3 0. 8 1.0
NACA
0012
CONTROL
#label   gain xfrac  vx vy vz sgn
Lelevator  1  0.46  0. 0. 0.   1.
#=================L H Tail Elevator Starts
```

```
SECTION
#Xle    Yle    Zle     Chord   AngleOfIncidence
0.808 -0.0254 0.01 0.184 0. 8 1.0
NACA
0015
CONTROL
#label   gain xfrac  vx vy vz sgn
Lelevator  1  0.862  0. 0. 0.   1.
#=================L H Tail Center section
SECTION
#Xle    Yle    Zle     Chord   AngleOfIncidence
0.798 0. 0.01 0.164 0. 8 1.0
NACA
0015
CONTROL
#label   gain xfrac  vx vy vz sgn
Lelevator  1  1.00  0. 0. 0.   1.
#*********************************
SURFACE
VTail
#Nchordwise  Cspace   Nspanwise   Sspace
8 1.0 8 1.0
#=================V Tail Center section
SECTION
#Xle    Yle    Zle     Chord   AngleOfIncidence
0.7882 0.0 0.05 0.509 0. 8 1.0
NACA
0009
CONTROL
#label   gain xfrac  vx vy vz sgn
Rudder -1 0.415 0. 0. 0. 1.
#=================V Tail Tip section
SECTION
#Xle    Yle    Zle     Chord   AngleOfIncidence
0.9872 0.0 0.481 0.1778 0. 8 1.0
NACA
0010
CONTROL
#label   gain xfrac  vx vy vz sgn
Rudder -1 0.415 0. 0. 0. 1.
#***************************
```

Appendix H: AVL Simulator File (ASCII Format)

```
// AVL Simulator model for the Yak-54

Alpha_sweep_xml_file=alpha.xml
//Beta dynamics are currently disabled.
#Beta_sweep_xml_file=beta.xml

Actuators=Actuator.txt

// Right aileron
Channel_d1=5
// Left aileron
Channel_d2=0
// Left elevator
Channel_d3=1
// Left elevator
Channel_d4=1
//Rudder
Channel_d5=3


//Note that if inertia data is not directly available, it can be calculated from
components (wing,horizontal tail,fins)
// Wing geometry
Wing_Area=1.06
Wing_Span=2.2


//Some parameters to increase parasitic drag
Fuse_Area=0.06596
Fuse_Length=2.0574
Fuse_Parasitic_Drag=0.01


//Inertia if available, in kg*m^2
Roll_Inertia=1.4759
Pitch_Inertia=2.8564
Yaw_Inertia=4.1192
Roll_Yaw_Coulpled_Inertia = 0


//Gross Mass in Kg
```

```
Gross_Mass=12.755

//Empty Mass in Kg
Empty_Mass=12.33


//--------------------  PROPULSION  --------------------//

// Engine is 3W 80cc, 7.5 hp

//Engine Type is Piston
Left_Engine_Type=0

// Channel number
Left_Engine_Channel=2

// Engine parameters look-up table
Left_Engine_LUT=Fuji86ccEngine.lut

// Propeller is APC 24x10

// Prop diameter, in m
Left_Prop_Diameter=0.60696

// Position of propeller hub wrt to aircraft cg, in m
Left_Prop_X=0.5715

//Propellor Pan Angle
Left_Prop_Pan=3

// Moment of inertia in kg/m^2
Left_Prop_Inertia=0.0025

// Propeller coefficients look-up table
Left_Prop_LUT=apc26x10.prd


//------------------  CONTROL SURFACES, OTHER AERODYNAMICS (only needed
if AVL is disabled    ------------------//

//------------------  AVIONICS MOUNTING  ------------------//

// Avionics (IMU sensor) orientation with respect to the aircraft body axes
// Euler angles in deg
```

```
IMU_Sensor_Roll_Angle=0.0
IMU_Sensor_Pitch_Angle=0.0
IMU_Sensor_Yaw_Angle=0.0

// Avionics (IMU sensor) position vector with respect to the aircraft CG, in body axes
// Vector components in m
IMU_Sensor_Position_X=0.0
IMU_Sensor_Position_Y=0.0
IMU_Sensor_Position_Z=0.0
```

Appendix I: AVL Modal Data Reduction

AVL Phugoid Mode (Modified Transient Peak Ratio Method)

t			Va	ΔVa	ΔVa/ΔVa	
383.8			62.61			
394.3	10.5		77.5	14.89	0.519812	
405.2	10.9		69.76	-7.74	0.593023	
415.1	9.9		74.35	4.59	0.647059	
425.2	10.1		71.38	-2.97	0.535354	
436.7	11.5		72.97	1.59		

Tavg/2	Period	ω_d	ΔVa	ζ	ω_n
10.58	21.16	0.296937	0.573812	0.17	0.301323

AVL Short Period Mode (Maximum Slope Method)

q1	q2	q3	Δq1	Δq	Δq1/Δq
-36.74	4.057	-3	7.057	40.797	0.172978

t1	t2	Δt	ζ	$\Delta t\omega_n$	ω_n
224.73	224.92	0.19	0.85	2.45	12.89474

AVL Dutch Roll Mode (Modified Transient Peak Ratio Method)

t			r	Δr	Δr/Δr	
458.9			46.2			
459.4	0.5		-29.33	-75.53	0.600159	
459.8	0.4		16	45.33	0.595632	
460.3	0.5		-11	-27	0.611741	
460.7	0.4		5.517	16.517		

Tavg/2	Period	ω_d	Δxavg	ζ	ω_n
0.45	0.9	6.981317	0.602511	0.15	7.061208

Appendix J: Yak-54/Piccolo Ground Testing Procedures

Test Overview:

The tests described in this appendix will lay out the ground testing phases of the Piccolo II avionics system that will be installed in the Yak-54. The purpose of these tests is to give flight test engineers a high level of confidence in the accuracy and robustness of the avionics package.

Test Objectives:

The following ground tests of the Piccolo II avionics system will be performed

Servo Calibration

The Piccolo produces pulse widths from 1103 to 1929 μs. The Piccolo provides calibration tables for 9 pulse widths. This allows the system to cancel out nonlinearities in the system, to a certain degree. For each surface a pulse width will be inputted into the system and its deflection measured. This deflection will be placed in the calibration table, allowing the avionics system to know what pulse to command for an inputted deflection.

Range Check

Satisfactory Piccolo II avionics signal strength at one field length at the Model Master's R/C aircraft field will be verified prior to flight-testing.

Telemetry Check

Prior to flight-testing the following telemetry will be verified:

1. GPS: A satisfactory 3-D GPS solution will be verified

2. Air Data: Air data will be zeroed and its accuracy in the calculation of airspeed and altitude will be verified using a Pitot-static tube calibration kit. The maximum leakage of the static system is not to exceed 100 ft/min and the Pitot system is not to exceed 2 knots/min.

3. Attitude: The aircraft attitude solution will be calibrated and verified by rotating the aircraft from the steady level trim state, with the telemetry checked to match that of an inclinometer.

4. Rate Gyro: The aircraft attitude rate solution will be verified by rotating the aircraft from the steady level trim state and observing if the subsequent rate telemetry is reasonable

5. Check signal strength: RSSI telemetry should not drop below -79 dB at anytime during range checking and not drop below -71 dB while the aircraft is next to the ground station.

Weight and Balance Check

The weight and balance of the aircraft will be set to between 10.2 and 10.6 inches aft of the firewall

Taxi Testing

The aircraft will be taxied for a minimum of 10 minutes after any vehicle modifications are performed. All structural connections will be checked for security after the minimum of 10 minutes has passed, and that the Piccolo has not vibrated out of position. The controllability of the aircraft with the actuated tail-wheel will also be monitored and adjusted as needed.

Signatures of Completion

_____
Vehicle Engineer

_____
Flight Test Engineer

_____
Pilot in Command

Appendix K: Yak-54/Piccolo Pre-Flight Checklist

DATE:____/____/____ **FLIGHT NO._____**

This checklist is to be completed prior to every flight, without exception. Place initials in the space provided as each item is checked. Where necessary, write flight specific information in the spaces provided. **CHECK LIST MUST BE COMPLETED BY TWO PERSONS USING VERBAL CONFIRMATION OF CHECKS**

- Pre-flight Briefing
  - Check and set predicted trim requirements ____
  - Verify suitable weather ____
  - Discuss appropriate crosswind corrections ____
  - Decide upon flight path ____
  - Check radio and monitor local traffic. ____
- Transmitter ready
  - Correct flight profile selected ____
  - Control sweeps completed (correct direction and magnitude of deflection, no more than ± 2 difference in split aileron at max deflection) ____
    - Left Aileron (±12°) ____
    - Right Aileron (±12°) ____
    - Left Elevator (+12°, -12°) ____
    - Right Elevator (+12°, -12°) ____
    - Rudder (±25°) ____
    - Tail wheel ____
    - Throttle (Full Range) ____
  - Range check ____
- Airframe ready
  - Batteries charged
    - Ignition ____
    - Receiver ____
  - Servo wires connected to correct receiver channel with safety clips in place where appropriate.
    - Tail Wheel ____

- Rudder ____
- Throttle ____
- Left Elevator ____
- Right Elevator ____
- Left Aileron ____
- Right Aileron ____
- Ignition Kill Switch ____

- Servo control connections secured and free.
  - Tail Wheel ____
  - Rudder ____
  - Left Elevator ____
  - Right Elevator ____
  - Throttle ____
  - Left Aileron ____
  - Right Aileron ____
- Landing gear secured.
  - Wheels, spacers and collars present and secure. ____
  - All landing gear mounting bolts secure. ____
- Payload secure. ____
- Ballast secure. ____
- Appropriate fuel on board
  - Fuel lines secure. ____
  - Fuel tank secure. ____
- Hatches installed.
  - Service hatches ____
  - Payload hatch ____
- Structural connections secure.
  - Engine mount ____
  - Wings ____
  - Propeller and spinner ____
  - Pitot and Static Tubes Clear ____
- Weight and Balance Correct. ____

  Specify: C.G._____

- <u>Avionics and Ground Station Ready</u>
  - External Power Source Ready ____
  - Ground Station Computer and Operator Interface Power Supplied ____
  - Deactivate 802.11 Transmitter on Operator Interface PC ____
  - GPS Telemetry Check ____
  - Set Altimeter ____
  - Zero Air Data Sensors ____

- Attitude and Rate Telemetry Check ____
- Map Page Configured ____
- Flight Plans Set ____
- Emergency Flight Plan Set ____
- Verify Correct Gains ____
- Verify Correct Limits ____
- Verify Correct Trims ____
- Verify Mission Limits ____
- RSSI Signal Strength Check (CHECK TIME HISTORY MUST BE -71 or -79 DURING RANGE CHECK AT ALL TIMES) ____
- Set Telemetry to Fast Rate ____

Post-Shutdown Checklist

- Ignition switch off ____
- Receiver switch off ____
- Transmitter off ____
- Post flight walk around ____
  - Check for damage
    Specify:_____

Signatures of Completion

_____
Flight Test Engineer

_____
Vehicle Engineer

Appendix L: Handling Qualities Flight Test Dance Card

Test Card #1: Yak-54 Handling Qualities Test

1. Take-off
2. Climb to approximate altitude of 200 ft AGL
3. Remain in the pattern.
4. Perform one full revolution of a left hand "race track" pattern
5. Perform one full revolution of a right hand "race track" pattern
    i. Verify 3-D GPS solution
    ii. Verify airspeed
    iii. Verify attitude and rate data
    iv. Verify control surface telemetry
    v. Verify altitude
6. Continue with "race track" patterns until pilot is satisfied that he understands the handling characteristics of the aircraft
7. Begin approach to landing
8. Land

Appendix M: Open Loop Dynamics Flight Test Dance Card

Test Card #2: Yak-54 Open Loop Dynamics Test

1. Take-off
2. Climb to approximate altitude of 200 ft AGL
3. Remain in the pattern.
4. Perform one full revolution of a left hand "race track" pattern
5. Perform one full revolution of a right hand "race track" pattern
    i. Verify 3-D GPS solution
    ii. Verify airspeed
    iii. Verify attitude and rate data
    iv. Verify control surface telemetry
    v. Verify altitude
6. Continue with "race track" patterns until pilot is satisfied that he understands the handling characteristics of the aircraft

7. Place aircraft into steady level flight for trim capture, call **"TRIMMED"** on completion
8. Allow the aircraft to fly freely for at least 5 seconds
    i. Check to make sure that the aircraft holds 1 knot and 20 ft for 5 seconds
    ii. Capture control surface trim values

9. Fly the aircraft into a comfortable upwind starting position for the Dutch Roll mode test
10. Apply a rudder singlet
11. Allow the aircraft to fly freely
12. Return to the pattern on the **"KNOCKOFF"** call or when the aircraft is leaving controllable visual range

13. Fly the aircraft into a comfortable upwind starting position for the Dutch Roll mode test
14. Apply a rudder doublet
15. Allow the aircraft to fly freely
16. Return to the pattern on the **"KNOCKOFF"** call or when the aircraft is leaving controllable visual range

17. Fly the aircraft into a comfortable upwind starting position for the Roll mode test
18. Fly the aircraft into an approximately 30 degree banked right turn
    i. Give bank angle feedback to the pilot
19. On **"READY"** bank to a 30 degree bank angle left using constant aileron

20. Hold 30 degree left bank for approximately 2 seconds
21. Return to the pattern

22. Fly the aircraft into a comfortable upwind starting position for the Short Period mode test
23. Apply a pull up singlet
24. Allow the aircraft to fly freely longitudinally and apply corrective lateral inputs
25. Return to the pattern on the **"KNOCKOFF"** call or when the aircraft is leaving controllable visual range

26. Fly the aircraft into a comfortable upwind starting position for the Short Period mode test
27. Apply a push-down to pull-up elevator doublet
28. Allow the aircraft to fly freely longitudinally and apply corrective lateral inputs
29. Return to the pattern on the **"KNOCKOFF"** call or when the aircraft is leaving controllable visual range

30. Return to the pattern and fly the aircraft into a comfortable upwind starting position for the Phugoid mode test
31. Apply up-elevator step and return to trim elevator on **"RELEASE"** call
    i. Call **"RELEASE"** when airspeed has decreased by 5 knots
32. Allow the aircraft to fly freely longitudinally and apply corrective lateral inputs as needed
33. Return to the pattern on the next **"KNOCKOFF"** call or when the aircraft is leaving controllable visual range

34. Continue in the traffic pattern and commence approach to landing.
35. Land
36. Shut-down

Appendix N: Dutch Roll Flight Test Data Reduction

Flight Test #1 Dutch Roll Mode (MTPR Method)

t		r	Δr	Δr/Δr	
1081.5		41.79			
1081.9	0.4	-43.17	-84.96		
1082.45	0.55	19.26	62.43	0.462118	
1082.9	0.45	-9.59	-28.85	0.493588	
1083.5	0.6	4.65	14.24		

Tavg/2	Period	ω_d	Δxavg	ζ	ω_n
0.53333	1.066667	5.890486	0.477853	0.23	6.052757

Flight Test #2 Dutch Roll Mode (MTPR Method)

t		r	Δr	Δr/Δr	
1128.6		47.21			
1129.1	0.5	-73.57	-120.78		
1129.5	0.4	37.16	110.73	0.447214	
1130.15	0.65	-12.36	-49.52	0.340872	
1130.8	0.65	4.52	16.88		

Tavg/2	Period	ω_d	Δxavg	ζ	ω_n
0.56667	1.133333	5.543987	0.394043	0.22	5.683227

Flight Test #3 Dutch Roll Mode (MTPR Method)

t		r	Δr	Δr/Δr	
1121.7		-74.98			
1122.1	0.4	56.92	131.9		
1122.6	0.5	-17.11	-74.03	0.295151	
1123.05	0.45	4.74	21.85	0.338215	
1123.75	0.7	-2.65	-7.39		

Tavg/2	Period	ω_d	Δxavg	ζ	ω_n
0.55	1.1	5.711987	0.316683	0.26	5.915426

ζ_{avg}	ω_{navg}
0.236667	5.883803

Appendix O: Bank Angle Control Flight Test Dance Card

Test Card # 3: Bank Angle Control Validation Dance Card

1. Take-off
2. Climb to approximate altitude of 200 ft AGL
3. Remain in the pattern.
4. Perform one full revolution of a left hand "race track" pattern
5. Perform one full revolution of a right hand "race track" pattern
    i. Verify 3-D GPS solution
    ii. Verify airspeed
    iii. Verify attitude and rate data
    iv. Verify control surface telemetry
    v. Verify altitude
6. Continue with "race track" patterns until pilot is satisfied that he understands the handling characteristics of the aircraft

7. Place aircraft into steady level flight for trim capture, call **"TRIMMED"** on completion
8. Allow the aircraft to fly freely for at least 5 seconds
    i. Check to make sure that the aircraft holds 1 knot and 20 ft for 5 seconds
    ii. Capture control surface trim values

9. Enter the traffic pattern
    i. Disable all control loops except bank angle control
    ii. Set the bank angle command to **ON** and set the command value to **0.0 deg**

10. Fly the aircraft to comfortable upwind starting position
11. Engage autopilot on **"READY"** for 5 seconds and disengage
12. Return to the traffic pattern

13. Fly the aircraft to a comfortable upwind starting position for a right 10 deg bank angle
    i. Set the bank angle command to **ON** and set the command value to +**10.0 deg**
14. Engage autopilot on **"READY"**
15. On **"KNOCKOFF"** call disengage the autopilot
16. Return to the traffic pattern
    i. Check flight data and tune gains

17. Fly the aircraft to a comfortable upwind starting position for a left 10 deg bank angle
    i. Set the bank angle command to **ON** and set the command value to **-10.0 deg**
18. Engage autopilot on **"READY"**
19. On **"KNOCKOFF"** call disengage the autopilot
20. Return to the traffic pattern
    i. Check flight data and tune gains

21. Fly aircraft to a comfortable upwind starting position for 20 deg right bank angle
    i. Set the bank angle command to **ON** and set the command value to **+20.0 deg**
22. Engage autopilot on **"READY"**
23. On **"KNOCKOFF"** call disengage the autopilot
24. Return to the traffic pattern
    i. Check flight data and tune gains

25. Fly aircraft to a comfortable upwind starting position for 20 deg left bank angle
    i. Set the bank angle command to **ON** and set the command value to **-20.0 deg**
26. Engage autopilot on **"READY"**
27. On **"KNOCKOFF"** call disengage the autopilot
28. Return to the traffic pattern
    i. Check flight data and tune gains

29. Fly aircraft to a comfortable upwind starting position for 30 deg right bank angle
    i. Set the bank angle command to **ON** and set the command value to **+30.0 deg**
30. Engage autopilot on **"READY"**
31. On **"KNOCKOFF"** call disengage the autopilot
32. Return to the traffic pattern
    i. Check flight data and tune gains

33. Fly aircraft to a comfortable upwind starting position for 30 deg left bank angle
    i. Set the bank angle command to **ON** and set the command value to **-30.0 deg**
34. Engage autopilot on **"READY"**
35. On **"KNOCKOFF"** call disengage the autopilot
36. Return to the traffic pattern
    i. Check flight data and tune gains

37. Land

Appendix P: Heading Angle Control Flight Test Dance Card

Test Card #4: Heading Control Validation Dance Card

1. Take-off
2. Climb to approximate altitude of 200 ft AGL
3. Remain in the pattern.
4. Perform one full revolution of a left hand "race track" pattern
5. Perform one full revolution of a right hand "race track" pattern
    - Verify 3-D GPS solution
    - Verify airspeed
    - Verify attitude and rate data
    - Verify control surface telemetry
    - Verify altitude
6. Continue with "race track" patterns until pilot is satisfied that he understands the handling characteristics of the aircraft

7. Place aircraft into steady level flight for trim capture, call **"TRIMMED"** on completion
8. Allow the aircraft to fly freely for at least 5 seconds
    - Check to make sure that the aircraft holds 1 knot and 20 ft for 5 seconds
    - Capture control surface trim values

9. Enter steady level flight
    i. Disable all control loops except the bank angle and heading control loop
    ii. Set bank angle command to **AUTO**
    iii. Set the heading command to the **upwind trim heading**

10. Fly the aircraft to a comfortable starting position
11. Engage the autopilot on **"READY"** command from test engineer
12. On **"KNOCKOFF"** command from the test engineer disengage the autopilot
13. Return to the traffic pattern
    i. Check flight data and tune gains

14. Fly the aircraft to a comfortable starting position for a 45 degree right heading change
    i. Set the heading command to +45 degrees from trim
15. Engage the autopilot on **"READY"**
16. On **"KNOCKOFF"** call disengage the autopilot
17. Return to the traffic pattern

i. Check flight data and tune gains

18. Fly the aircraft to a comfortable starting position for a 45 degree left heading change
    i. Set the heading command to -45 degrees from trim
19. Engage the autopilot on **"READY"**
20. On **"KNOCKOFF"** call disengage the autopilot
21. Return to the traffic pattern
    i. Check flight data and tune gains

22. Fly the aircraft to a comfortable starting position for a 90 degree right heading change
    i. Set the heading command to +90 degrees from trim
23. Engage the autopilot on **"READY"**
24. On **"KNOCKOFF"** command from the test engineer disengage the autopilot
25. Return to the traffic pattern
    i. Check flight data and tune gains

26. Fly the aircraft to a comfortable starting position for a 90 degree left heading change
    i. Set the heading command to -90 degrees from trim
27. Engage the autopilot on **"READY"**
28. On **"KNOCKOFF"** command from the test engineer disengage the autopilot
29. Return to the traffic pattern
    i. Check flight data and tune gains

30. Fly the aircraft to a comfortable starting position for a 150 degree right heading change
    i. Set the heading command to +150 degrees from trim
31. Engage the autopilot on **"READY"**
32. On **"KNOCKOFF"** call disengage the autopilot
33. Return to the traffic pattern
    i. Check flight data and tune gains

34. Fly the aircraft to a comfortable starting position for a 150 degree left heading change
    i. Set the heading command to -150 degrees from trim
35. Engage the autopilot on **"READY"**
36. On **"KNOCKOFF"** call disengage the autopilot
37. Return to the traffic pattern
    i. Check flight data and tune gains

38. Return to manual mode

Appendix Q: Airspeed Control Flight Test Dance Card

Test Card #5: Airspeed Control Validation Dance Card

1. Take-off
2. Climb to approximate altitude of 200 ft AGL
3. Remain in the pattern.
4. Perform one full revolution of a left hand "race track" pattern
5. Perform one full revolution of a right hand "race track" pattern
    i. Verify 3-D GPS solution
    ii. Verify airspeed
    iii. Verify attitude and rate data
    iv. Verify control surface telemetry
    v. Verify altitude
6. Continue with "race track" patterns until pilot is satisfied that he understands the handling characteristics of the aircraft

7. Place aircraft into steady level flight for trim capture, call **"TRIMMED"** on completion
8. Allow the aircraft to fly freely for at least 5 seconds
    i. Check to make sure that the aircraft holds 1 knot and 20 ft for 5 seconds
    ii. Capture control surface trim values

9. Enter the traffic pattern
    i. Set all control loops except waypoint tracking to **ON**
    ii. Set the bank angle command to **AUTO**
    iii. Set the heading command to the **upwind trim heading**
    iv. Set the altitude command to **ON** and command **200 ft AGL**
    v. Set the IAS threshold to **-1 knots**
    vi. Set the airspeed command to the **trim airspeed**

10. Fly aircraft to comfortable upwind starting position
11. Engage the autopilot on **"READY"** command from test engineer
12. After **5 seconds** disengage autopilot
13. Return to the traffic pattern

14. Fly aircraft to comfortable upwind starting position
15. Engage the autopilot on **"READY"**
    i. Increase airspeed command to **+5 knots from trim**
16. On **"KNOCKOFF"** call disengage the autopilot
17. Return to the traffic pattern
    i. Check flight data and tune gains

18. Fly aircraft to comfortable upwind starting position
19. Engage the autopilot on **"READY"**
    i. Increase airspeed command to **-5 knots from trim**
20. On **"KNOCKOFF"** call disengage the autopilot
21. Return to the traffic pattern
    i. Check flight data and tune gains

22. Fly aircraft to comfortable upwind starting position
23. Engage the autopilot on **"READY"**
    i. Increase airspeed command to **+10 knots from trim**
24. On **"KNOCKOFF"** call disengage the autopilot
25. Return to the traffic pattern
    i. Check flight data and tune gains

26. Fly aircraft to comfortable upwind starting position
27. Engage the autopilot on **"READY"**
    i. Increase airspeed command to **-10 knots from trim**
28. On **"KNOCKOFF"** call disengage the autopilot
29. Return to the traffic pattern
    i. Check flight data and tune gains

Appendix R: Longitudinal Gain Change Log Sheet

Piccolo Flight Control System Longitudinal Gain Change Log Sheet

Date: 9:20 Aircraft: Yak-54 Test: Airspeed Control Data Processing Engineer: Edmond Leong

		Elevator Inner Loop		Pitch Damper		Airspeed Outer Loop		Throttle Inner Loop		Altitude Outer Loop	
	Time	Elevator Prediction Trust (K_{E_trust})	Z Acceleration Error Integral to Elevator (K_i)	Pitch Error to Elevator (K_θ)	Pitch Rate Error to Elevator (K_q)	TAS Error to TAS Rate (K_v)	TAS Rate Error to Z Acceleration (K_{av})	Throttle Prediction Trust (K_P)	Energy Rate Error Integral to Throttle (K_i)	Altitude Error to Altitude Rate Command (K_h)	Altitude Error to Z Acceleration Cmd (K_{ah})
Initial		0.50	1.50	0.10	0.10	0.60	1.00	0.50	1.80	0.40	1.20
Change 1	9:24	0.40									
Change 2	9:25	0.30									
Change 3	9:28					0.70					
Change 4	9:29						1.10				
Change 5	9:30						1.20				
Change 6	9:32						1.10				
Change 7	9:33						1.00				
Change 8	10:00			1.50							
Change 9	10:02			1.60							
Change 10	10:06			1.70							
Change 11	10:07			1.65							
Change 12											
Change 13											
Change 14											
Change 15											